QUANTITATIVE CHARACTERIZATION AND PEDOGENIC DEVELOPMENT OF SOIL STRUCTURE

By
© 2018
Aoesta Khalid Mohammed
M.A., University of Sulaimani, 2009
B.S., University of Sulaimani, 2004

Submitted to the graduate degree program in Geography and Atmospheric Science and the Graduate Faculty of the University of Kansas in partial fulfillment of the requirements for the degree of Doctor of Philosophy.

_____
Chair: Dr. Daniel R. Hirmas

_____
Dr. Stephen L. Egbert

_____
Dr. William C. Johnson

_____
Dr. Rolfe D. Mandel

_____
Dr. Terry A. Slocum

Date Defended: 4 May 2018

The dissertation committee for Aoesta K. Mohammed
certifies that this is the approved version of the following dissertation:

QUANTITATIVE CHARACTERIZATION AND PEDOGENIC DEVELOPMENT OF SOIL STRUCTURE

_____
Chair: Dr. Daniel R. Hirmas

Date Defended: 4 May 2018

ABSTRACT

Soil particles are often arranged into repeating patterns of aggregates with similar shapes, sizes, and degrees of expression. These repeating aggregates, known as 'peds,' are currently described using qualitative and subjective categories for type, size, and grade as follows. Peds are assigned a type class (e.g., platy, granular, prismatic, etc.) based on overall ped shape. Peds are classified into size categories (e.g., fine, medium, and coarse) based on quantitative ped width and thickness criteria. Peds are assigned a grade class (e.g., weak, moderate, or strong) which describes the degree of expression.

Soil structure develops as a result of complex interactions with climate, organisms, relief, parent material, and time. However, our understanding of these interactions is limited by the categorical and subjective nature of ped descriptions and the lack of datasets that include a wide range of variability in the factors responsible for the development of soil structure. Therefore, the first objective of this dissertation was to develop a method to quantify soil structure using morphometric indices for ped shape by analyzing previously published digital photographs of soil profiles and structural specimens. The second objective of this dissertation was to assemble an easily-accessible, two-dimensional data matrix containing laboratory and field-based measurements of soil properties across the USA and integrate topographic, climatological, and ecological data to, ultimately, explore the response of soil structure to exogenous and endogenous factors in both surface A horizons and subsurface B horizons. To those ends, we assembled two databases: the Ped Shape Digital Morphometric (PSDM) database and the University of Kansas Research Dataset of Soils (KURDS).

The PSDM database was used to develop new morphometric indices of ped silhouettes quantitatively describing ped shape. These morphometric indices were applied to a subset of

KURDS and used in conjunction with multinomial logistic regression and decision tree analyses of qualitative ped data to explore endogenous and exogenous controls on the development of soil structure. We found that the exogenous factor, climate, exhibited the greatest control over ped shape and size whereas clay content (endogenous) was the most important factor predicting ped grade. The finding that climate exhibits control over the evolution of soil structure represents an unexplored avenue for understanding how global climate change will affect morphological properties that control soil hydrology. Overall, this dissertation demonstrates the possibilities of describing peds in terms of quantitative variables and analyzing continental-scale databases of soil structure.

ACKNOWLEDGEMENT

I would like to thank Dr. Hirmas for his thoughtful guidance and instruction, as well as his continuous encouragement while researching and writing this dissertation. Without his support, this study could not have been possible. Many thanks to Drs. Terry Slocum, Rolfe Mandel, Steven Egbert, and Bill Johnson for their work as committee members and for their help and insightful conversations over the years. I sincerely thank Henry Ferguson for his assistance with assembling soil data. I would also like to thank the Department of Geography and Atmospheric Sciences for the opportunity to work as a graduate teaching assistant to support my studies. I thank the Higher Committee For Education Development (HCED) in Iraq for their financial support. I would like to thank my daughter Kaziwa, whose patience, encouragement and laughter keeps me going, and my dear friends Kim Hirmas and Arica Mauerer, whose invaluable friendship, support and love I can always count on. I am also grateful for Aaron my good colleague Koop, with whom I can talk all things pedological.

TABLE OF CONTENTS

CHAPTER 1. INTRODUCTION

Soils develop as a result of complex interactions between exogenous (external) factors such as, climate, relief, and time, and endogenous (internal) factors such as parent material and organisms, giving rise to soil morphological properties (Jenny, 1941). Examples of such morphological properties are soil structure, particle-size distribution, rupture resistance, root quantity, organic matter content, and color. For this study, we focus on the morphological property, soil structure, which can be defined as the arrangement of soil particles into repeating patterns of structural units within morphological horizons; these structural units (aka peds) typically have similar shapes, sizes, orientations, and degrees of expression (Nikiforoff, 1941; Hillel, 1998; Díaz-Zorita et al., 2002; Warrick, 2002).

Soil structure is important because it has considerable influence over biological, physical, and chemical soil processes, such as water retention, infiltration, erosion, root penetration, and aquifer recharge (Warrick, 2002). In addition, soil structure is shaped by these processes. For example, soil organisms that act to develop or modify soil structure (e.g., earthworms), are affected by the distribution of soil air and water, which, in turn, are affected by the presence of soil structure (Rabot et al., 2018). Thus, the processes that form soil structure and the processes controlled by presence of structure are coupled.

Despite its importance, our understanding of soil structure and the interactions between exogenous and endogenous factors in developing soil structure is limited by traditional categorical, subjective descriptions of peds. Such descriptions are more qualitative in nature than quantitative and, thus, suffer from investigator bias. That is, investigators must currently assign shape classes to peds using idealized diagrams or cognitive conceptualizations of ped shape, which many not conform to 'real-world' conditions. Researchers are, therefore, at risk of

assigning ped shape based on expectations rather than reliable and objective criteria. Because of the categorical nature of ped shape, subtle differences or variations remain unnoticed, unmeasured, and, ultimately, unaccounted for in pedological studies. Thus, basic questions such as, "How do prismatic and columnar peds compare in shape to platy and granular structure?," cannot be answered at present using current descriptions of soil structure. In addition, the influence that soil structure has on exogenous and other endogenous variables, or what influence these variables have on the development of soil structure *per se*, is currently unknown, which is due, in part, to the limitations associated with these descriptions. Therefore, soil forming processes will remain poorly understood until soil structure can be quantitatively characterized and analyzed. For these reasons, studies examining the evolution of soil structure over time or across broad continental scales are currently limited.

This dissertation aims to investigate soil structure and its relationship to exogenous and endogenous factors using *quantitative* methods developed as part of this project. Soil structure specimens were digitized from photographs and analyzed to obtain morphometric indices of ped shape; these indices were then applied to a large dataset of soils assembled in this dissertation. This dataset (approximately 95,000 observations and over 1,000 variables) was compiled from a database of field-based and laboratory soil properties from samples taken across the USA maintained by the USDA-Natural Resources Conservation Services (NRCS). We used a variety of statistical approaches to understand, over a wide range of environments and regions, the relationships between soil structure and exogenous and endogenous factors.

Chapter 2 describes how we developed an approach to quantify ped shape using morphometric indices—including circularity, roundness, aspect ratio, angle, width to height ratio, and solidity—created from non-published and published digital photographs of soil profiles

and structural specimens (Aandahl, 1982). We examined ped types from heuristic diagrams, three-dimensional (3-D) scans of peds and high resolution photographs. The heuristic diagrams were quantified to assess ped shapes derived from common conceptualizations of soil structure. The 3--D scans were quantified to assess the effect of ped orientation on shape measurements from ped silhouettes. Peds were outlined manually by identifying distinct (i.e., clearly visible) examples in photographs and diagrams resulting in silhouettes that were used in image analysis software to calculate the morphometric indices in this study. A survey was designed to poll expert judgment in order to properly classify the shape of these peds (see Appendix A). The results were compiled into the Ped Shape Digital Morphometric (PSDM) dataset. We analyzed this dataset using several multivariate statistical approaches, including classification trees and random forest analysis. In addition, an unlikeability coefficient was used to examine variation among the survey responses for each ped shape and each shape parameter. This coefficient calculates the degree of disagreement among survey participants with respect to each ped. The morphometric indices used in this study represent continuous variables that allow differences between ped shapes to be detected and examined.

Our goal in Chapter 3 was to understand how endogenous and exogenous factors influence the development of soil structure—specifically, the structural properties of ped shape, size, and grade over a continental scale. We assembled existing data into a single dataset known as the University of Kansas Research Dataset of Soils (KURDS). This dataset is the result of merging and cleaning more than 94,000 samples from the National Cooperative Soil Survey (NCSS) Soil Characterization database. Developed in the U.S. beginning in 1928, the NCSS database contains laboratory data and field-derived information such as depths, structure, rock fragments, pores, root distributions and landform properties for each soil sample from throughout

the US (all 50 states). Unfortunately, the complexity of the files in their original state precluded in-depth analysis of the data in their raw form. To reduce this complexity, we combined, cleaned, and filtered both field and laboratory soil data. Structural information from categorical descriptions was converted to quantitative ratio scales using values in the PSDM database for each of the common ped type classes. Ped size was calculated using the geometric mean diameter of the structure size class recorded for each horizon, and grade was placed on an ordinal scale ranging from structureless to strongly structured conditions. In addition, the dataset was combined with the USFS Ecoregions of the US and the Parameter-Elevation Regressions on Independent Slopes Model (PRISM) to add both climatological and ecological information. Finally, we put the data into a single two-dimensional data matrix to facilitate analysis.

We examined the development of soil structure over a wide range of exogenous and endogenous factors. We calculated the probability of soil structural variables such as ped type, size, and grade classes for all individual endogenous and exogenous variables and used decision trees (DTs) to evaluate the relative importance of these variables in the prediction of soil structure. The DTs also allowed us to incorporate both categorical and continuous variables into the analysis.

Chapter 4 concludes with a summary of the results of our analysis. Morphometric indices of ped shape, size, and grade can now be consistently assigned to structure class, regardless of depth or environment. Chapter 4 shows that quantitative descriptions and rigorous statistical analyses, even on qualitative descriptions, can open the door for investigations into endogenous and exogenous influences on the development of soil structure.

REFERENCES

Aandahl, A.R. 1982. Soils of the Great Plains: Land Use, Crops, and Grasses. University of Nebraska Press, Lincoln.

Díaz-Zorita, M., E. Perfect, and J. Grove. 2002. Disruptive methods for assessing soil structure. Soil and Tillage Research 64:3-22.

Hillel, D. 1998. Environmental Soil Physics. Academic Press, San Diego, CA.

Jenny, H. 1941. Factors of Soil Formation: A System of Quantitative Pedology. 1st ed. McGraw-Hill, New York.

Nikiforoff, C.C. 1941. Morphological classification of soil structure. Soil Science 52:193-212.

Rabot E., M. Wiesmeier, S. Schlüter, and H.J. Vogel. 2018. Soil structure as an indicator of soil functions: A review. Geoderma 314:122-137.

Warrick, A.W. 2002. Soil Physics Companion. CRC press, Boca Raton, FL.

CHAPTER 2. A DIGITAL MORPHOMETRIC APPROACH FOR QUANTIFYING PED SHAPE

ABSTRACT

Ped shape is an important property with considerable influence over soil processes, such as root penetration, water infiltration, and solute transport. Despite the host of methods employed to quantify other soil morphological properties, ped shape quantification remains elusive. Existing methods attempting to quantify soil structure utilize laboratory techniques that have limitations on sample size and resolution. Our goal was to overcome these limitations by developing an approach to quantify ped shape using morphometrics created from published digital photographs of soil profiles and structure specimens. In addition, ped shapes from heuristic diagrams and three-dimensional (3D) scans of peds were examined. The heuristic diagrams were quantified to assess ped shapes derived from common conceptualizations of soil structure, while the 3-D scans were quantified to assess the effect of ped orientation on shape measurements. Ped shape was quantified by manually outlining distinct examples of soil peds from high-resolution photographs and heuristic diagrams, and then calculating several morphometrics from the resulting silhouettes using image analysis software. A survey was designed to poll expert judgment in order to properly classify the shape of these peds. Using this method, we were able to transform typical categorical and subjective descriptions of peds into continuous quantitative shape data. The shape metrics, circularity and width to height ratio, exemplify the type of continuous variables that allow significant differences between ped shapes to be detected. This approach opens the door to analyzing soil structure at regional and continental scales through the analysis of existing photographs without the need to resample.

INTRODUCTION

Soil structure is the arrangement of soil particles into repeating patterns of aggregates with similar shape, size, orientation, and degree of expression that occur within morphological horizons (Nikiforoff, 1941; Arshad et al., 1996; Hillel, 1998; Díaz-Zorita et al., 2002; Kay and Angers, 2002). When these aggregates are large enough to be visible to the naked eye, they are known as 'peds' and their shapes have traditionally been described using qualitative shape classes such as platy, granular, blocky, or prismatic (Soil Survey Division Staff, 1993).

Ped shape (also referred to in the literature as ped type) both responds to and exhibits influence over several important soil biological, physical, and chemical processes such as plant root extension, water infiltration, and solute transport (Kay and Angers, 2002). The shape of peds provides clues in reconstructing paleoenvironments and for understanding soil genesis (Schaetzl and Anderson, 2005). Granular (i.e., small spherical) peds, for instance, often indicate current or previous bioturbation by earthworms (Jouquet et al., 2011). Ped shape can also provide evidence for the age of a soil and the stability of a landform (Harden, 1982); an example of this is the growth and coalescence of vesicular pores which result in platy structure in arid V horizons (i.e., surface and near surface horizons characterized by the dominance of vesicular porosity; Soil Survey Staff, 2015, which indicates land surface stability and strong soil development (Turk and Graham, 2011). Given sufficient pedogenic energy inputs, parent material at subsurface depths that are characterized by structureless conditions and lithogenic fabrics develop into morphological horizons that contain peds (Lin, 2011) exhibiting blocky and/or prismatic shapes, and, under sodic conditions, columnar shapes (Harden, 1982; Schaetzl and Anderson, 2005). Ped shapes tend to have more edges (angular) in younger soils than in older soils where peds are often more rounded and have larger numbers of faces (Dexter, 1985; Hartge et al., 1999).

Ped shape, through its effects on pore geometry, influences the rate of water movement into and through soil (Eck et al., 2016). Granular peds permit downward water movement, whereas platy peds act as a barrier to flow by concentrating percolating water in longer and more tortuous interpedal macropores (e.g., Arshad et al., 1996; Pagliai et al., 2004; Sasal et al., 2006). Ped (and aggregate) shape also affects porosity and tensile strength through its effect on aggregate packing arrangements (Dexter and Kroesbergen, 1985; Brown et al., 1996; Seben et al., 2013; Munkholm et al., 2016).

Despite what is known about the importance of soil structure, the usefulness of ped shape descriptions is limited by both the categorical and subjective nature of shape classes. This limitation arises for the following reasons. First, the absence of objective, consistent, and measurable shape criteria increases the uncertainty in assigning true shape class membership. Field soil scientists routinely assign peds to shape classes by comparing peds retrieved from excavation walls against idealized diagrams or cognitive conceptualizations of ped shape. The latter is likely influenced by experience and training and may give rise to considerable variability—both among soil scientists and over the course of a single career—in assigning ped shape. Second, the lack of definable shape criteria makes it difficult to assign structure classes on the basis of ped shape alone. Thus, in practice, ped shapes are often assigned after assessing other information, such as position in the profile, ped size, and/or soil color. This lack of independence may preclude accurate identification of ped shapes where they are not expected in the soil profile. Third and, perhaps, most importantly, the qualitative nature of the classification prevents the resulting nominal ped shape data from being compared on a quantitative scale and prohibits the detection of subtle differences in ped shapes that fall within a single class. For

instance, a question such as 'how different are prismatic and columnar peds compared to granular and platy peds?' cannot be answered with the current ped shape classification.

Several imaging methods such as photography, thin-section microphotography, and X-ray computed tomography have been applied to quantify either ped shape or corresponding pores (e.g., Dexter, 1985; Holden, 1992; Holden, 1993; Jangorzo et al., 2013; 2014). One drawback to these methods is sample size limitations. For example, aggregates and corresponding pore structures typically on the order of micrometers to centimeters are analyzed (e.g., Pagliai et al., 2004; Zucca et al., 2013; Martinez et al., 2015), although a single ped might be several orders of magnitude larger. Image resolution also has a considerable influence on the quantification of ped shape. Relatively high image resolution (e.g., 70 μm pixel^{-1}) is critical for accurately recording correct geometric ped shapes and can restrict the minimum size of peds used in studies of ped shape expression (Holden, 2001). A recently-developed method uses laser scanning to overcome these size limitations and shows promise in quantifying and linking macroscale soil structure in the field to hydraulic properties (Eck et al., 2013). This technique, however, is currently not widely used. Ped shape quantification, therefore, remains elusive (Hartemink and Minasny, 2014), despite the host of modern methods routinely employed to quantify other soil morphological properties such as color and texture.

The digitized images of peds and aggregates obtained in previous studies have been quantified with various metrics such as circularity and roundness that describe the geometry of the objects. As such, these metrics are described herein as 'digital morphometrics' since they quantitatively characterize shape from digitized images. This is a slight variation of the recently proposed term 'digital soil morphometrics' which is defined, in part, as the measurement and quantification of soil profile properties (Hartemink and Minasny, 2014). The application of

digital morphometrics to high-resolution photographs of soil profiles may allow the quantification of ped shape. Given the many collections of photographs of soil profiles (e.g., Aandahl, 1982; McDaniel et al., 1993) that exist for soils around the world, this approach may open up the opportunity for analyzing ped shapes at broader geographic scales than were previously possible and for reanalyzing existing photographs without the need to resample.

In this work, we developed a method to quantify ped shape using digital morphometrics by analyzing digitized photographs of soil profiles, heuristic structure diagrams, and three-dimensional (3-D) scans of peds. A secondary goal of this study was to assess to what degree years of experience and level of training influence the ability to identify ped shapes. To achieve these goals, we have assembled a database for quantifying ped shape referred to hereafter as the ped shape digital morphometrics (PSDM) database. The database consists of a collection of (1) photographs of individual peds (aka specimen photographs) and soil profiles (aka profile photographs) showing examples of soil structure from across the contiguous US; (2) multistripe laser triangulation (MLT) scans of individual peds, and (3) heuristic ped diagrams. We also solicited feedback from students, professionals, and faculty within the pedology community via an online survey in order to correctly classify digitized peds from the soil profile photographs (Fig. 1). Ultimately, our approach should allow typical categorical and subjective descriptions of ped shape to be transformed into continuous quantitative data.

Although structure size and grade are also described in the field using categorical classes (e.g., Schoeneberger et al., 2012), these data are transitive. That is, size and grade can be ranked in order from smallest to largest or weakest to strongest, respectively. Since current field description data of ped shape are non-transitive, our objective was to improve the characterization of this structural parameter.

METHODS AND MATERIALS

Digitizing Ped Shape

Many of the photographs in the PSDM database were obtained from previously published 35-mm film slides. A large fraction of the photographs (~62%) were taken from a photograph slide set by Aandahl (1982) of soils in the Great Plains (Fig. 2). These slides were scanned at extremely high resolution (3000 ppi). In addition to these, multiple photographs of individual ped specimens were obtained from published sources and Natural Resources Conservation Service (NRCS) field offices (Table 1); those obtained from published sources were digitally scanned and those obtained from field offices were already digitized. Heuristic diagrams from a variety of published sources illustrating idealized ped shapes were also identified and scanned. Easily recognizable ped specimens from the digitized color slides, individual specimen photographs, and scanned heuristic diagrams were outlined in Adobe® Illustrator® by hand using the pen tool to create a solid polygon (Fig. 3). Silhouettes of each ped type were created from these outlines. In addition, 3-D MLT scans of individual peds were imported into ObjViewer (http://people.eecs.ku.edu/~miller/NSF_TUES/NSF_TUES.html), rotated to multiple viewing angles, and saved as jpeg files in order to assess the effect of viewing angle on the morphometrics calculated from the 2-D ped silhouettes (Table 2). Figure 4 shows examples of MLT scans of subangular blocky, angular blocky, prismatic, wedge, platy, and granular peds.

In order to outline the ped specimens from each photograph or diagram accurately, the images were digitally magnified approximately 15 times. Peds in cross section that had easily definable boundaries on all sides and appeared to represent a repeating pattern of soil structure were chosen as candidates for digitization. Soil structure types were digitized following a similar

logic to Holden (2001); pixels with similar colors were considered to be part of the soil aggregate whereas pixels that fell between two distinguishable colors were considered to be interpedal pores (i.e., spaces between soil structures). All digitized silhouettes that were derived from photographs, diagrams, and 3-D MLT scans were subsequently analyzed using ImageJ (version 1.48; http://imagej.nih.gov) to calculate morphometrics for each ped including circularity, roundness, major-axis ellipse angle, aspect ratio, solidity, and width to height ratio (Ferreira and Rasband, 2012; Eck et al., 2013).

Circularity, C, is the ratio between object area, A, and the area of a perfect circle with circumference equivalent to the perimeter of the object, P, calculated as:

$$C = 4\pi A / P^2 \quad [1]$$

Circularity values range between 0 and 1, with values near 1 indicating a smooth circular shape and values near 0 indicating a rougher and/or elongated shape. Thus, circularity is both a gross and fine-scale shape measurement (Stoyan and Stoyan, 1992; Ferreira and Rasband, 2012; Russ, 2011; Rodriguez et al., 2012). Roundness, R, is calculated from the area of an object and the length of the major axis of an ellipse fit to the object, E_{maj}, as:

$$R = \frac{4A}{\pi E_{\text{maj}}^2} \quad [2]$$

Roundness (angularity) varies between 0 and 1; 1 indicates a perfect circle and lower values indicate angular shapes. Aspect ratio, AR, is the ratio of major to minor axes lengths of an ellipse fit to an object calculated as:

$$AR = E_{\text{maj}} / E_{\text{min}} \quad [3]$$

where E_{min} is the length of the minor axis of the ellipse. Values for aspect ratio are equivalent to the inverse of roundness and range between 1 and ∞. Both roundness and aspect ratio were

calculated since they are commonly used morphometrics. Solidity, S, is the ratio between the area of an object and its convex area, V:

$$S = A/V \quad [4]$$

where, the convex area is defined as the area of the convex hull (i.e., the polygon created by connecting outward vertices and all interior angles less than 180°). Solidity is a measurement of overall convexity (i.e., a measurement of the particle edge roughness) for a given object where an object becomes more solid when the area of the object and area of the convex hull are close to each other. Solidity is a proxy for roughness of the surface, with values close to 1 indicating a smooth surface and values less than 1 indicating an increase in surface roughness. Width to height ratio (WH_{ratio}) is the ratio between width (W_{box}) and height (H_{box}) of the bounding box or enclosing rectangle around a silhouette. This bounding box is oriented relative to the coordinate system of the image instead of the silhouette. As such it is both a gross shape and orientation measurement, which is measured as:

$$WH_{ratio} = W_{box} \Big/ H_{box} \quad [6]$$

In addition, ped orientation was investigated using the angle of the major ellipse axis, which is the angle between the major axis of an ellipse fit to the ped silhouette and a line parallel to the x-axis of the image.

Survey

In order to ensure that each ped from the profile photographs in the PSDM database was classified correctly with respect to ped shape, a survey was designed containing the original photograph of the profile from which each ped was digitized along with associated silhouettes (Fig. 3). Participants (N = 78) were given the following choices to categorize ped shape: platy,

granular, subangular blocky, angular blocky, wedge, prismatic, columnar or N/A if the shape did not fall into one of these ped shape categories. A total of 53 soil profile photographs yielding 262 silhouettes was included in the survey. The heuristic diagrams ($N = 145$), MLT scans ($N = 14$), specimen photographs ($N = 44$), and soil profile photographs ($N = 32$) were not included in the survey because the peds from these sources were previously classified by their authors (e.g., Soil Survey Division Staff, 1993). Survey participants were asked to classify each photograph and silhouette pair into one of the 7 structure types (i.e., ped shape) listed above. In order to properly classify the shape of each ped in these photographs, the survey was distributed online using SurveyMonkey (http://www.surveymonkey.com) and advertised to the pedology community via the Soil Science Society of America Pedology Division list-serve as well as individual email solicitations to several NRCS soil scientists and university faculty currently teaching pedology.

Participant responses were organized in a frequency table. The mode (i.e., the measure of central tendency for nominally-scaled data) was calculated for each ped to assess the most frequent shape class reported by the participants (Burt et al., 2009). Shape metrics (e.g., circularity, roundness, etc.) were plotted against the unalikeability coefficient (u_2)—a measure of disagreement among the survey participants—in order to evaluate the effect of uncertainty on the value of each shape metric. Further details for the calculation and interpretation of u_2 are given in the Statistical Analyses section below.

Ped Shape Digital Morphometrics Database

The results from the survey and the image analyses were combined and organized into the PSDM database. The PSDM database contains information for each ped (e.g., the source of the photograph, soil order, and ped type) and numeric morphometric values including:

circularity, roundness, major-axis ellipse angle, aspect ratio, solidity, and width to height ratio. A total of 294 profile photographs, 44 specimen photographs, 145 diagrams, and 14 MLT scans were collected and collated yielding a total of 497 digitized peds (Table 2; Fig. 5).

Statistical Analyses

All statistical analyses in this study were conducted using the R statistical language Ver. 3.1.2 (R Core Team, 2014). Permutation tests as opposed to pairwise *t*-tests were conducted using a randomization *t*-test procedure to separate the means of each ped shape parameter at an α-level of 0.05 following Logan (Logan, 2010). These tests were used when the parametric assumptions of homoscedasticity and normality were not met even after attempting multiple transformations of the data.

A permutation test was also used in evaluating the effect of viewing angle on the shape parameters calculated from the 2-D silhouettes. Peds digitized by MLT were rotated in 3-D as follows. Equidimensional peds (i.e., angular blocky, subangular blocky, and granular) were rotated to nine different angles corresponding to nine possible viewing angles (i.e., 3 faces, 4 edges, and 2 corners) from which peds can be observed in silhouette from a cleaned soil profile (Fig. 6c). Anisotropic peds (e.g., prismatic and platy) were rotated to four different angles (2 faces and 2 edges; Fig. 6a,b). Because there was no obvious orientation for anisotropic wedge-shaped peds, these were treated as equidimensional with respect to viewing angle. For each viewing angle (i.e., orientation), 2-D silhouettes were screen captured and shape parameters analyzed. A total of 14 MLT scans were used in this study: granular (3), subangular blocky (2), angular blocky (3), wedge (2), prismatic (2), and platy (2). For each shape class and shape parameter, one orientation from each ped was randomly chosen and used to compare to the other shape classes using a *t*-test. The permutation test was conducted 500 times to generate a population of *P*-values that resulted from each *t*-test. We calculated the proportion of *P*-values

that were less than 0.05 to assess the sensitivity in detecting differences between shape classes from 2-D silhouettes that arise from different possible orientations in the soil profile photographs.

An unalikeability coefficient was calculated to examine the variation among the survey responses for each ped shape and each shape parameter. The unalikeability coefficient is a statistic that represents the variation in categorical data and was calculated for each silhouette following Kader and Perry (2007) as:

$$u_2 = 1 - \sum_i p_i^2 \qquad [5]$$

where p_i is the proportion of the total responses for the i^{th} ped shape category (e.g., granular, subangular blocky, prismatic, etc.). Values of u_2 near zero indicate that there was a high agreement among the survey participants in classifying a particular specimen; values near 0.8 indicate low agreement among the participants.

A random forest was used to determine the importance or prediction strength of the morphometrics in identifying ped shape class (Hastie et al., 2009). The technique generated multiple random classification trees (i.e., a forest; $N = 500$); each tree calculated the best predictor variable for each ped shape class. Random forests compare the results of each tree in the forest to calculate the most important predictor variables (Breiman, 2001; Liaw and Wiener, 2002). Importance is assessed by examining the mean decrease in accuracy as a result of randomly permuting each variable separately in each classification tree. In other words, importance records the amount of prediction error that results when removing the effect of each variable separately while leaving the other predictors unchanged (Breiman, 2001; Liaw and Wiener, 2002; Hastie et al., 2009). Variables with large decreases in accuracy are taken to be more important for the classification of respective ped shapes than others with lower decreases in

accuracy since the accuracy of the classification is sensitive to changes in that variable.

The results of the random forest were tabulated into a confusion matrix to evaluate the overall performance of the classification of ped shape using the morphometrics in this study. A confusion matrix compares the observed number of objects (counts) of each class to the number of predictions for those classes; class error rates are calculated from incorrect predictions by the model.

RESULTS AND DISCUSSION

Identifying Ped Shape

The mode class and the proportion of survey participants were calculated for each ped shape. Mean relative frequency (i.e., the average proportion of survey participants that agreed with the mode class) was calculated to assess how level of training (i.e., education) and years of experience influenced the ability of the participants to correctly identify ped shape (Fig. 7). Bars associated with identical letters in Fig. 7, indicate means that were not significantly different from each other. Educational level (i.e., bachelors, masters, and doctorate degree) was a significant factor in identifying prismatic peds. Prisms were more accurately recognized by participants holding doctorate degrees and less accurately identified by those with bachelors degrees. Other structure types, however, such as angular blocky, subangular blocky, and columnar, were more frequently identified by those with bachelors degrees, although these differences were not significant ($P > 0.05$). Similar to educational level, years of experience describing soil in the field also impacted participant ability to identify prisms, but did not appear to significantly affect the ability of participants to detect other structure types. In particular, participants who had more than 10 years of field experience more frequently described prismatic

structures correctly as determined by the mode class. These results suggest that the correct identification of prisms require more training and experience.

Ped Silhouettes Morphometrics

Silhouette morphometrics were obtained from profile and individual ped photographs (N = 338) in the PSDM database and analyzed to compare their values by shape class. Figure 8 shows the distribution of values for each shape parameter and the results of the permutation tests that were used to compare the means of the seven ped shapes (Fig. 8). Identical letters above the boxes indicate means that are not significantly different ($P > 0.05$) from each other. Platy structure significantly differs from the other ped shapes for each of the morphometrics calculated, whereas subangular and angular blocky structures are not significantly different ($P > 0.05$) from each other with respect to any morphometric except circularity. Similarly, prismatic and columnar peds are not significantly different ($P > 0.05$) from each other except with respect to circularity.

Circularity is the only shape parameter that distinguishes both equidimensional ped shapes (e.g., subangular and angular blocky, and granular) and anisotropic ped shapes (e.g., prismatic and columnar). Peds with small silhouette areas and high numbers of corners and edges will have low circularity values.

Equidimensional shapes were easily distinguished from each other based on their circularity values. Granular structure has a high circularity mean value of (0.83) due to its small perimeter to area ratio that distinguishes it from other equidimensional peds. Subangular blocky, angular blocky, and wedge structures have mean circularity values of 0.68, 0.63, and 0.48 (Fig. 8). Subangular blocky structure has a slightly lower perimeter to area ratio reflected in the higher

mean circularity value because its shape has fewer corners and edges and smoother boundaries compared to angular blocky.

Anisotropic ped shapes are also separated by circularity values. A prismatic structure has a mean circularity value of 0.48, while the value for columnar is 0.56. Columnar has a higher mean circularity value than prismatic because it has a slightly smaller perimeter to area ratio due to its rounded tops which increases circularity compared to prismatic peds. Circularity values for prismatic and wedge structures, however, were not significantly different ($P > 0.05$) from each other. Although these structures have similar perimeter to area ratios yielding similar circularity values, circularity does not consider the orientation of the peds. Width to height ratios, which incorporate silhouette orientation, however, show significant differences between prismatic and wedge structures (Fig. 8).

Using width to height ratio, we were able to distinguish equidimensional and anisotropic shapes with respect to ped orientation. Platy structure defined by flat, elongated and horizontally oriented shapes have a high width to height ratio mean value (4.6) compared to other anisotropic ped shapes, such as those vertically elongated (i.e., prismatic and columnar) that have lower width to high ratios. In addition, wedges can be separated from equidimensional ped shapes on the basis of width to height ratios due to orientations that create larger widths compared to subangular blocks, angular blocks, and granular. As mentioned above, the width to height ratios allowed wedges and prismatic structures to be distinguished from each other, which was not possible with circularity.

The major-axis ellipse angle measures the orientations of peds, and as previously noted, is the angle between the major axis of an ellipse fit to a ped silhouette and the x-axis of the image (i.e., parallel to the land surface). The major-axis ellipse angle for equidimensional peds (i.e.,

subangular blocky, angular blocky, and granular) ranges between 0 and 90° (Fig. 8). When the major axis angles of these peds are plotted as a histogram, granular structure shows a uniform distribution between 0 and 90° whereas subangular and angular blocky structures display bimodal distributions with central tendencies of the modes near 0 or 90° (data not shown). Wedge orientation ranges between 3 and approximately 30°, which distinguishes those structures from most equidimensional peds and other anisotropic peds (Fig. 8). As expected, prismatic and columnar peds are easily distinguishable from platy on the basis of ped orientation due to elongation in either the vertical (for columns and prisms) or horizontal (for platy) dimensions.

Roundness and aspect ratio, as opposed to circularity, are measures of gross ped shape. Roundness and aspect ratio values close to one refer to peds that are rounded whereas roundness values less than one or aspect ratio values greater than one refer to peds that are more elongated. Granular structures are significantly ($P < 0.05$) more equidimensional (i.e., more round) than angular and subangular blocky structures (Fig. 8). An interesting consequence of this difference is that, as discussed above, the distribution of equidimensional ped orientations tends to be more strongly bimodal in angular blocky peds and more uniform in granular peds (data not shown). Subangular blocky peds display a bimodal distribution that is slightly less pronounced than angular blocky. The shape of blocky structure creates a preference for the ellipse fit to the silhouettes such that the orientation of the major axis tends to be either vertical (~ 90°) or horizontal (~0°), thereby yielding a bimodal distribution of ped orientations. Since angular blocky structures have sharper and better-defined edges than subangular blocky structures as evidenced by the lower circularity values, the effect of blocky shape on ped orientation is stronger with angular blocky peds. By contrast, the higher roundness of granular structures does not influence the orientation of the ellipse fit to the silhouette, thus yielding a uniform

distribution of ped orientations. With the exception of platy structure, anisotropic peds are similarly elongated, with mean roundness values of 0.41, 0.36, and 0.42, and mean aspect ratio values of 2.79, 3.22, and 2.64 for columnar, prismatic, and wedge structures, respectively (Fig. 8).

Solidity describes the fine-scale surface roughness (Rodriguez et al., 2012) of ped silhouettes. Most of the ped shapes were indistinguishable with respect to solidity (Fig. 8). However, platy structure appeared to be more sensitive to solidity (platy was significantly different from other ped shapes) likely due to their thin, elongated shapes.

In addition to analyzing ped silhouettes digitized from profile photographs, we also analyzed the differences between ped shapes derived from several idealized ped diagrams (Table 1). Nearly all the shape morphometrics from the idealized diagrams follow the same distribution as the silhouettes derived from profile photographs, but with less variability among ped shapes (Fig. 9). Results of the permutation test (i.e., mean differences) show few significant differences between ped shapes compared with silhouettes derived from profile photographs (compare Fig. 9 with Fig. 8). Using shape parameters such as circularity, major-axis ellipse angle, and width to height ratio we were able to separate platy structure from other ped shapes. We were unable, however, to distinguish most of the other ped shapes using these parameters as was possible with the soil profile silhouettes (again, compare Figs. 8 and 9). The lack of irregular ped silhouette boundaries compared to field photographs of soil profiles is likely responsible for both the lower variability and difficulty in distinguishing ped shapes from each other in the diagram silhouettes. For example, while angular blocky is significantly ($P < 0.05$) lower than subangular blocky with respect to circularity in the silhouettes obtained from profile photographs (Fig. 8), circularity values are not significantly ($P > 0.05$) different from subangular blocky (Fig. 9). This lack of

variability is attributed to the fact that many of the diagrams represent angular blocky peds more smoothly than they appear in the field, thereby inflating their circularity values as the perimeter to area ratio decrease. This finding suggests that more careful attention to the geometric shape parameters that distinguish ped shape is needed when designing future heuristic ped shape diagrams.

Converting 3-D Ped Shapes to 2-D Silhouettes

As described above, the consequences of superimposing the 3-D nature of soil peds on 2-D soil profile silhouettes was examined using permutation tests. High-resolution (120 μm) 3-D digital (MLT) models of several peds were used to create 2-D silhouettes. The results of the permutation tests are given in Table 3. These values represent the proportion of times that randomly-selected 2-D silhouettes of contrasting peds were determined to be significantly ($P < 0.05$) different from each other. Values close to 1 indicate a high probability that significant differences will be detected between ped types regardless of the orientation of the 3-D scan when the 2-D silhouette was captured. We used an arbitrary critical value of 0.5 (i.e., 50%) as a breakpoint to separate peds whose results tend to be influenced by the conversion of 3-D to 2-D (< 0.5) from those that were robust to this conversion (> 0.5). Contrasting ped shapes that were not significantly different in Fig. 8 were not examined for the influences of 3-D ped orientation on 2-D silhouettes.

Anisotropic peds (i.e., prismatic and platy peds) tended to show more frequent differences than equidimensional peds, although the most frequent differences were observed between platy and angular blocky, platy and granular, and prismatic and angular blocky (0.5).

Wedges appeared to be sensitive to the orientation at which the 2-D silhouettes were taken, as differences between contrasting peds were seldom observed (≤ 0.25).

Prismatic peds show frequent differences (> 0.5) with all equidimensional ped shapes (i.e., angular blocky, subangular blocky, and granular) for the aspect ratio shape parameter. No other ped shape was observed to be frequently different (≤ 0.25) with respect to aspect ratio. These results suggest that aspect ratio may be sensitive to ped orientation for all but prismatic peds.

For major-axis ellipse angle, platy and prismatic are consistently different from each other (1.0). Thus, for any viewing angle, these ped shapes are always different for the samples used in this study. Angle appears to be more robust than other shape parameters in distinguishing platy from prismatic despite orientation of the 2-D silhouette. In addition, platy and wedge shapes were frequently different (~ 0.7) regardless of the orientation of the 3-D peds when the 2-D silhouettes were captured.

Roundness appears to be the least sensitive to ped orientation. Significant differences were frequently observed between angular blocky and platy, angular blocky and prismatic, prismatic and platy, granular and prismatic, and prismatic and subangular blocky (≥ 0.5). Width to height ratios were only frequently different between platy and angular blocky (0.53). Solidity appeared to be sensitive to ped orientation when the 2-D silhouette was captured, given that low significant difference frequencies were observed for all contrasts (≤ 0.13). Our approach to evaluating the conversion of 3-D ped shapes to 2-D silhouettes was not successful in frequently detecting differences between ped shapes, especially between equidimensional and anisotropic peds, likely due to the limited sample size (degrees of freedom) of the 3-D models (14 MLT-scans samples) used in the permutation tests.

Evaluating Ped Silhouette Morphometrics

We evaluated the quality of peds digitized from soil profile photographs using an unalikeability coefficient (Fig. 10). As discussed above, the unalikeability coefficient is a statistic that calculates variability among categorical data such as survey responses. In this work, the unalikeability coefficient represents the variability in assigning ped shapes in our survey. The unalikeability coefficient allows for the quality of peds delineated in the digitization process to be evaluated by quantifying the level of disagreement between participants in assigning a ped shape category to each silhouette. Figure 10 illustrates a range of high quality ($u_2 = 0$) to low quality ($u_2 = 0.8$) peds, from left to right on the x-axis.

The results showed that a majority of the survey participants agreed ($0.09 \leq u_2 \leq 0.52$) on the designation of granular structure indicating granular peds chosen in this study were of high quality and easily recognized. Columnar structure ($0.09 \leq u_2 \leq 0.67$) also showed relatively high agreement among the participants, probably because these shapes are easily distinguished from other peds based on morphological properties unrelated to geometric shape; for instance the bleached tops common to columns. Similarly, there is relatively high agreement for granular structure because the size of the ped and its depth position within the profile likely influenced the judgment of the participants. There was slightly less agreement among participants when assigning platy, prismatic, subangular blocky, and angular blocky shapes; the values of u_2 ranged from $0.23 \leq u_2 \leq 0.49$, $0.27 \leq u_2 \leq 0.66$, $0.12 \leq u_2 \leq 0.74$, $0.29 \leq u_2 \leq 0.74$, respectively. The higher amount of disagreement of these peds compared to granular or columnar may reflect the continuum of real world ped shapes that adds error to participant judgment when comparing profile photographs of peds to mental conceptualizations of soil structure. Another reason for

disagreement could be associated with inherent difficulties in recognizing these ped shapes from 2-D photographs and silhouettes.

Wedges have relatively high unalikeability coefficient values ($0.57 \leq u_2 \leq 0.71$) compared to other ped shapes and were, thus, clustered on the right side of the x-axes in Fig. 10. A possible reason for this is the difficulty in recognizing a wedge from 2-D photos. It is interesting to note that we had identified 23 wedges when the survey was first constructed. That number, however, declined to 8 based on participant responses. Thus, wedge structure appears to be inherently difficult to classify. This is also observed in the low frequency responses that indicated wedge structures in Figure 7. Among those peds that we had initially identified as wedges but were changed after the survey, 27% were identified as subangular blocky and 73% were angular blocky. This indicates that certain features of wedge-shaped peds, such as sharpness of the boundaries, may have more in common with angular blocky than other structures, adding to the difficulty of recognizing these peds correctly.

By quantifying the level of disagreement between survey responses we were able to distinguish individual peds within a shape class in terms of the ease by which the ped was recognized. As u_2 tended toward zero in Fig. 10, the shapes were recognized by a higher percentage of the participants, likely because the quality of the peds improved. By fitting a line to the data in Fig. 10, the y-intercept was determined and interpreted as the predicted value of the true metric if 100% of the participants agreed on the shape class of the ped. This provides an alternative to using the central tendency of the shape distribution when calculating the representative metrics since central tendency (e.g., mean or median) does not account for the quality of each specimen. Table 4 presents the predicted y-intercepts for the significant ($P < 0.05$) linear and non-linear fits shown in Fig. 10. Linear regressions were used for most of the

data, except where y-intercept values would be predicted to fall outside the range of possible values for the metric (e.g., > 90° major–axis ellipse angles or aspect ratio < 1). In these cases, either logistic or exponential regressions were used to match the shape of the data. The y-intercept values are probably more meaningful for peds that had a range of quality, including high-quality peds as indicated by the unalikeability coefficient. In this study, wedges did not have low u_2 values and, therefore, y-intercept values for those peds are unlikely to be reliable.

Predicted y-intercept values for major–axis ellipse angles show that angular blocky peds were taller than they were wide, which caused these peds to be vertically oriented (~90°), making them distinguishable from other equidimensional peds. This difference can also be seen with the predicted width to height ratio shape parameter (0.21), indicating that angular blocky peds in this database were relatively thinner and taller than other equidimensional peds.

Similar slopes for the regression line illustrated in Fig. 10 for prismatic and columnar peds were observed for most of the shape parameters in this study (e.g., circularity, roundness, aspect ratio, and width to height ratio) over similar ranges of shape metric quality (i.e., u_2 values). For example, both peds showed increasing circularity values as their quality decreased (Fig. 10).

Relative Importance of Morphometrics in Distinguishing Ped Shape

In order to evaluate the importance of each morphometric in distinguishing ped shape, a random forest was run using all measured shape parameters (i.e., circularity, roundness, etc.). Figure 11 shows the ordered relative importance or prediction strength of each variable for each ped shape (Liaw and Wiener, 2002). The results show that circularity is the most important variable for distinguishing equidimensional ped shapes (i.e., angular blocky, subangular blocky, and granular) (Fig. 11). The second most important shape metric after circularity is width to

height ratio for angular blocky and granular, and major-axis ellipse angle for subangular blocky. For prismatic, platy, and wedge shaped peds, width to height ratio was the most important shape parameter, followed by circularity for both prismatic and wedge shaped peds and aspect ratio for platy peds. Aspect ratio is the most important morphometric for describing columns; however, the width to height ratio is also important for identifying these peds.

Subangular blocky, angular blocky, and granular (equidimensional) peds have relatively equal major to minor axis ellipse lengths of the peds. Those peds can best be identified based on their circularity values. As addressed in the methodology section, circularity is both a gross shape and fine-scale shape measurement (i.e., edges around ped). For subangular blocky, angular blocky, and granular peds, circularity is the most important shape parameter since circularity is a measurement of equidimensionality (area is equivalent or close to their perimeter) that also accounts for edges and corners around the ped. By contrast, platy, prismatic, columnar, and wedge (anisotropic) peds have relatively larger differences between major to minor axes ellipse lengths. In particular, prismatic, wedge, and platy are best distinguished by their width to height ratio; these peds are significantly elongated in their vertical dimension. Aspect ratio (i.e., aspect ratio is the ratio of major to minor axis ellipse lengths) was an important shape parameter for identifying columnar structure.

We calculated a confusion matrix to assess the overall accuracy of the classification trees in the random forest (Table 5). High frequencies in the same modeled and observed categories refer to accurate predictions from the random forest using the five variables shown in the Fig. 11. The highest-class error rates were observed in columnar (0.87), wedge (0.75), and angular blocky (0.73), indicating these shapes are difficult to distinguish with these variables. In particular, angular blocky was most frequently misclassified as subangular blocky, columnar as

prismatic, and wedge as angular blocky. These types of soil structures may be sensitive to other soil morphological factors, such as color and/or depth within the profile.

CONCLUSIONS

This study presents a method for quantifying ped shape using a variety of morphometrics. Results show that our method was able to transform typical categorical descriptions of soil structure into continuous quantitative data. Shape metrics such as circularity and width to height ratio are continuous variables that allow differences between ped shapes to be detected. By contrast, assigning categorical classes to ped shapes precludes the ability to observe morphological differences in soil structure. Digital shape metrics from this study can also be used to convert morphological descriptions of soil structure into numeric shape indices.

Central tendency measures (i.e., mean and median) of shape metrics derived from populations of representative peds such as those used in this study can be used to quantitatively describe ped shape; however, these measures do not account for the quality or representativeness of each ped. Thus, we used the predicted shape metrics at a zero unalikeability coefficient, which accounts for the quality of each ped, to quantitatively describe ped shape. Numeric values from this study may open up the opportunity to study soil genesis and model hydrologic processes at regional and continental scales without the need to resample (i.e., using photographs of previously sampled soil pits).

The results from our survey showed that participant ability to recognize prismatic structure was positively influenced by education and expertise suggesting that the correct identification of prisms requires more training and experience. Besides prismatic structures,

however, higher levels of education and more years of field experience did not make considerable differences in identifying ped shapes.

For future studies that examine ped shape, we recommend removing a subset of peds from each horizon and taking photographs of these specimens to capture their silhouettes during a typical soil profile description. These specimens can be digitized more accurately and objectively when photographed as individual samples. Also, we recommend that photographs obtained by NRCS field offices be made accessible to examine structure on previously excavated profiles.

REFERENCES

Aandahl, A.R. 1982. Soils of the great plains: Land use, crops, and grasses. University of Nebraska Press, Lincoln.

Arshad, M.A., B. Lowery, and B. Grossman. 1996. Physical tests for monitoring soil quality. p. 123-141. *In* J.W. Doran and A.J. Jones (ed.) Methods for assessing soil quality. Soil Science Society of America, Madison, WI.

Brady, N.C., and R. Weil. 2009. Elements of the nature and properties of soil. 3rd ed. Prentice Hall, Upper Saddle River, NJ.

Breiman, L. 2001. Random forest. Machine Learning 45:5-32.

Brown, A.D., A.R. Dexter, W.C.T. Chamen, and G. Spoor. 1996. Effect of soil macroporosity and aggregate size on seed-soil contact. Soil & Tillage Research 38:203-2016.

Burt, J.E., G.M. Barber, and D.I. Rigby. 2009. Elementary statistics for geography. 3rd ed. The Guilford Press, New York.

Dexter, A.R. 1985. Shapes of aggregates from tilled layers of some Dutch and Australian soils. Geoderma 35:91-107.

Dexter, A.R., and B. Kroesbergen. 1985. Methodology for determination of tensile strength of soil aggregates. Journal of Agricultural Engineering Research 31:139-147.

Díaz-Zorita, M., E. Perfect, and J.H. Grove. 2002. Disruptive methods for assessing soil structure. Soil & Tillage Research 64:3-22.

Eck, D.V., D.R. Hirmas, and D. Giménez. 2013. Quantifying soil structure from field excavation walls using multistripe laser triangulation scanning. Soil Science Society of America Journal 77:1319-1328. doi: 10.2136/sssaj2012.0421

Eck, D.V., M. Qin, D.R. Hirmas, D. Giménez, and N.A. Brunsell. 2016. Relating quantitative soil structure metrics to saturated hydraulic conductivity. Vadose Zone Journal 15.

Ferreira, T., and W. Rasband. 2012. ImageJ User Guide [Online]. IJ 1.46r revised ed. Available online at https://imagej.nih.gov/ij/docs/guide/user-guide.pdf (verified 2 June 2016).

Harden, J.W.1982. A quantitative index of soil development from field descriptions: Examples from a chronosequence in central California. Geoderma 28:1-28.

Hartemink, A.E., and B. Minasny. 2014. Towards digital soil morphometrics. Geoderma 230-231:305-317. doi: http://dx.doi.org/10.1016/j.geoderma.2014.03.008

Hartge, K.H., J. Bachmann, and N. Pesci. 1999. Morphological analysis of aggregate shape. Soil Science Society of America Journal 63:930–933.

Hastie, T., R. Tibshirani, and J. Friedman. 2009. The elements of statistical learning: Data mining, inference, and predition. 2nd ed. Springer, New York.

Hillel, D. 1998. Environmental soil physics. Academic Press, San Diego, CA.

Holden, N.M. 1992. A rapid two-dimensional quantification of soil ped shape. Ph.D. diss. National University of Ireland, University College, Dublin, Ireland.

Holden, N.M. 1993. A two-dimensional quantification of soil ped shape. Journal of Soil Science 44:209-219. doi: 10.1111/j.1365-2389.1993.tb00446.x

Holden, N.M. 2001. Description and classification of soil structure using distance transform data. European Journal of Soil Science 52:529-545.

Jangorzo, N.S., F. Watteau, and C. Schwartz. 2013. Evolution of the pore structure of constructed technosols during early pedogenesis quantified by image analysis. Geoderma 207-208:180-192.

Jangorzo, N.S., F. Watteau, and C. Schwartz. 2014. Image analysis of soil thin sections for a non-destructive quantification of aggregation in the early stages of pedogenesis. European Journal of Soil Science 65:485-498.

Jouquet, P., G. Huchet, N. Bottinelli, and T.D. Thu. 2011. What are the limits of the drilosphere? An incubation experiment using metaphire posthuma. Pedobiologia 54:S113-S117.

Jury, W.A., and R. Horton. 2004. Soil physics. 6th ed. John Wiley & Sons, Inc., Hoboken, NJ.

Kader, G.D., and M. Perry. 2007. Variability for categorical variables. Journal of Statistics Education 15:0-16.

Kay, B.D., and D.A. Angers. 2002. Soil structure. p. 249-295. *In* A.W. Warrick (ed.) Soil physics companion. CRC press, Boca Raton, FL.

Kubiena, W.L. 1954. Atlas of soil profiles. Thomas Murby and Company, London.

Liaw, A., and M. Wiener. 2002. Classification and regression by randomForest. R News 2:18-22.

Lin, H. 2011. Three principles of soil change and pedogenesis in time and space. Soil Science Society of America Journal 75:2049-2070.

Logan, M. 2010. Biostatistical design and analysis using R: A practical guide. Wiley-Blackwell, Oxford, UK.

Martinez, F.S.J., F.J. Muñoz Ortega, F.J. Caniego Monreal, A.N. Kravchenko, and W. Wang. 2015. Soil aggregate geometry: Measurements and morphology. Geoderma 237-238:36-48.

McDaniel, P.A, R.J. Ahrens, and M.E. Timpson. (ed.) 1993. The Marbut Memorial Slides. Soil Science Society of America, Madison, WI.

Munkholm, L.J., R.J. Heck, B. Deen, and T. Zidar. 2016. Relationshiop between soil aggregate strength, shape and porosity for soils under different long-term management. Geoderma 268:52-59.

Nikiforoff, C.C. 1941. Morphological classification of soil structure. Soil Science 52:193-212.

Pagliai, M., N. Vignozzi, and S. Pellegrini. 2004. Soil structure and the effect of management practices. Soil & Tillage Research 79:131-143.

R Core Team. 2014. R: A language and environment for statistical computing. R Foundation for Statistical Computing, Vienna, Austria.

Rodriguez, J.M., J.M.A. Johansson, and T. Edeskär. 2012. Particle shape determination by two-dimensional image inalysis in geotechnical engineering. p. 207-218. Proc. Nordic Geotechnical Meeting, 16th, Copenhagen, Denmark. 9-12 May 2012. Danish Geotechnical Society, Dgf-Bulletin 27, Copenhagen, Denmark.

Russ, J.C. 2011. The image processing handbook. 6th ed. CRC Press, Boca Raton, FL.

Sasal, M.C., A.E. Andriulo, and M.A. Taboad. 2006. Soil porosity characteristics and water movement under zero tillage in silty soils in argentinian pampas. Soil & Tillage Research 87:9-18.

Schaetzl, R.J., and S. Anderson. 2005. Soils: Genesis and geomorphology. Cambridge University Press, Cambridge, UK.

Schoeneberger, P.J., D.A. Wysocki, E.C. Benham, and Soil Survey Staff. 2012. Field book for describing and sampling soils. Ver. 3.0. Natural Resources Conservation Service, National Soil Survey Center, Lincoln, NE.

Seben, G.d.F., Jr., J.E. Corá, C. Fernandes, and R. Lal. 2013. Aggregate shape and tensile strength measurment. Soil Science 178:301-307.

Soil Survey Division Staff. 1993. Soil survey manual. Department of Agriculture Handbook 18. Soil Conservation Service, U.S. Government Printing Office, Washington, DC.

Soil Survey Staff. 2015. Illustrated guide to soil taxonomy. Version 2. USDA-NRSC National Soil Survey Center. USDA-NRCS, Lincoln, NE.

Stoyan, D., and H. Stoyan. 1992. Fractals, random shapes, and point fields: Methods of geometrical statistics. John Wiley & Sons, New York.

Turk, J.K., and R.C. Graham. 2011. Distribution and properties of vesicular horizons in the western United States. Soil Science Society of America Journal 75:1449-1461.

Zucca, C. N. Vignozzi, S. Madrau, M. Dingil, F. Previtali, and S. Kapur. 2013. Shape and intraporosity of topsoil aggregates under maquis and pasture in the Mediteranean region. Journal of Plant Nutrition and Soil Science. 176:529-539. doi: 10.1002/jpln.201200144

Table 1. Summary of photographs and sources used to create the PSDM database.

Media	Sources†	Ped Shape	Number
Profile photographs	Aandahl, Nikiforoff, Soil Survey, Marbut, This study	Subangular blocky, angular block, granular, wedges, platy, prismatic, columnar	294
Specimen photographs	Nikiforoff, Soil Survey, NRCS	Subangular blocky, angular blocky, granular, prismatic, columnar, platy	44
MLT scans	KU	Subangular blocky, angular block, granular, wedges, platy, prismatic, columnar	14
Ped diagrams	Hillel, Jury, Kubiena, Fieldbook, Brady	Subangular blocky, angular block, granular, wedges, platy, prismatic, columnar	145

† Aandahl = Aandahl (1982); Marbut = McDaniel et al. (1993); Nikiforoff = Nikiforoff (1941); KU = University of Kansas; NRCS = NRCS field office photographs; Soil Survey = Soil Survey Division Staff (1993); Hillel = Hillel (1998); Jury = Jury and Horton (2004); Fieldbook = Schoeneberger et al. (2012); Kubiena = Kubiena (1954); Brady = Brady and Weil (2009).

Table 2. Summary of digitized peds from profile photographs, specimen photographs, diagrams, and multistripe laser triangulation (MLT) scans in the PSDM database.

Ped Type	Abbreviation	Profile	Specimen	Diagram	MLT	Total
Angular blocky	abk	35	5	14	3	57
Columnar	col	19	4	6	0	29
Granular	gr	8	21	72	3	104
Platy	pl	25	1	23	2	51
Prismatic	pr	55	6	8	2	71
Subangular blocky	sbk	87	7	20	2	116
Wedges	wg	65	0	2	2	69
Total		294	44	145	14	497

Table 3. The proportion of *P*-values that were less than an α-level of 0.05 out of a population of 500 *P*-values reflecting the results of *t*-tests that compared silhouttes from randomly selected ped orientations derived from 3-D models digitized using MLT. Values close to unity can be interpreted as a high probability of finding a significant difference despite the orientation of the 3-D ped when the 2-D silhoutte is captured. Mean differences that were not significantly different ($P > 0.05$) in Fig. 8 were not examined for the influences of 3-D ped orientation on 2-D silhouette-derived morphometrics and are left blank.

	Ped Type				
Ped Type	abk	gr	pl	pr	sbk
			Circularity		
gr	0.052				
pl	0.850	0.842			
pr	0.536	0.354	0.042		
sbk	0.020	0.098	0.484	0.428	
wg	0.216	0.140	0.098		0.194
			Aspect ratio		
gr	0.084				
pl	0.124	0.102			
pr	0.648	0.692	0.000		
sbk		0.072	0.000	0.508	
wg			0.000		
			Major-Axis Ellipse Angle		
gr					
pl	0.252	0.044			
pr	0.182	0.156	1.000		
sbk			0.098	0.312	
wg		0.096	0.712	0.116	0.178
			Roundness		
gr	0.066				
pl	0.532	0.670			
pr	0.534	0.598	0.000		
sbk		0.060	0.144	0.496	
wg	0.234	0.206	0.016		0.168
			Solidity		
gr					
pl	0.006	0.028			
pr	0.004	0.004	0.000		
sbk		0.132	0.024	0.020	
wg		0.050	0.002		
			Width to Height Ratio		
gr					
pl	0.530	0.430			
pr	0.454	0.266	0.326		
sbk			0.034	0.400	
wg	0.150	0.112	0.174	0.144	0.148

Table 4. Intercept values for the regression models shown in Fig. 10 representing perfect theoretical agreement among survey participants (i.e., $u_2 = 0$). Values following a ± symbol represent 1 standard error.

Ped Type	Circularity	Major-Axis Ellipse Angle	Width to Height Ratio	Aspect Ratio	Roundness	Solidity
abk	0.91 ± 0.06	88.1 †	0.21 ± 0.08	1.00 ± 0.29	0.97 †	0.90 ± 0.01
col	0.35 ± 0.08	84.0 ± 1.82	0.19 ± 0.14	4.37 ± 0.75	0.07 ± 0.12	0.82 ± 0.03
gr	1.01 ± 0.02	35.0 ± 3.32	1.13 ± 0.03	1.34 ± 0.03	0.76 ± 0.01	0.93 ± 0.01
pl	0.27 ± 0.03	5.73 ± 1.07	4.21 ± 0.46	6.77 ± 0.84	0.08 ± 0.10	0.74 ± 0.03
pr	0.27 ± 0.05	82.2 ± 0.90	0.14 ± 0.08	5.87 ± 0.72	0.04 ± 0.07	0.87 ± 0.01
sbk	0.75 ± 0.03	40.1 ± 2.94	1.13 ± 0.04	0.97 ± 0.16	0.82 ± 0.05	0.90 ± 0.00
wg	0.48 ± 0.02	15.4 ± 2.87	1.94 ± 0.13	1.00 ± 1.62	1.00 †	0.89 ± 0.01

† Since the asymptotes of the logistic model were fixed, no standard errors are associated with these intercept values.

Table 5. Confusion matrix for the random forest prediction. Rows represent ped type determined from survey responses; columns represent ped type predicted from the random forest. Counts along the diagonal indicate number of correct predictions.

Observed	Modeled							Class error
	abk	col	gr	pl	pr	sbk	wg	
abk	11	0	1	1	0	26	1	0.725
col	1	3	0	0	16	3	0	0.870
gr	0	0	71	0	0	15	0	0.174
pl	0	0	0	25	0	0	1	0.038
pr	1	4	0	0	50	6	0	0.180
sbk	9	1	13	1	5	63	2	0.330
wg	3	0	0	1	0	2	2	0.750
Error rate								0.334

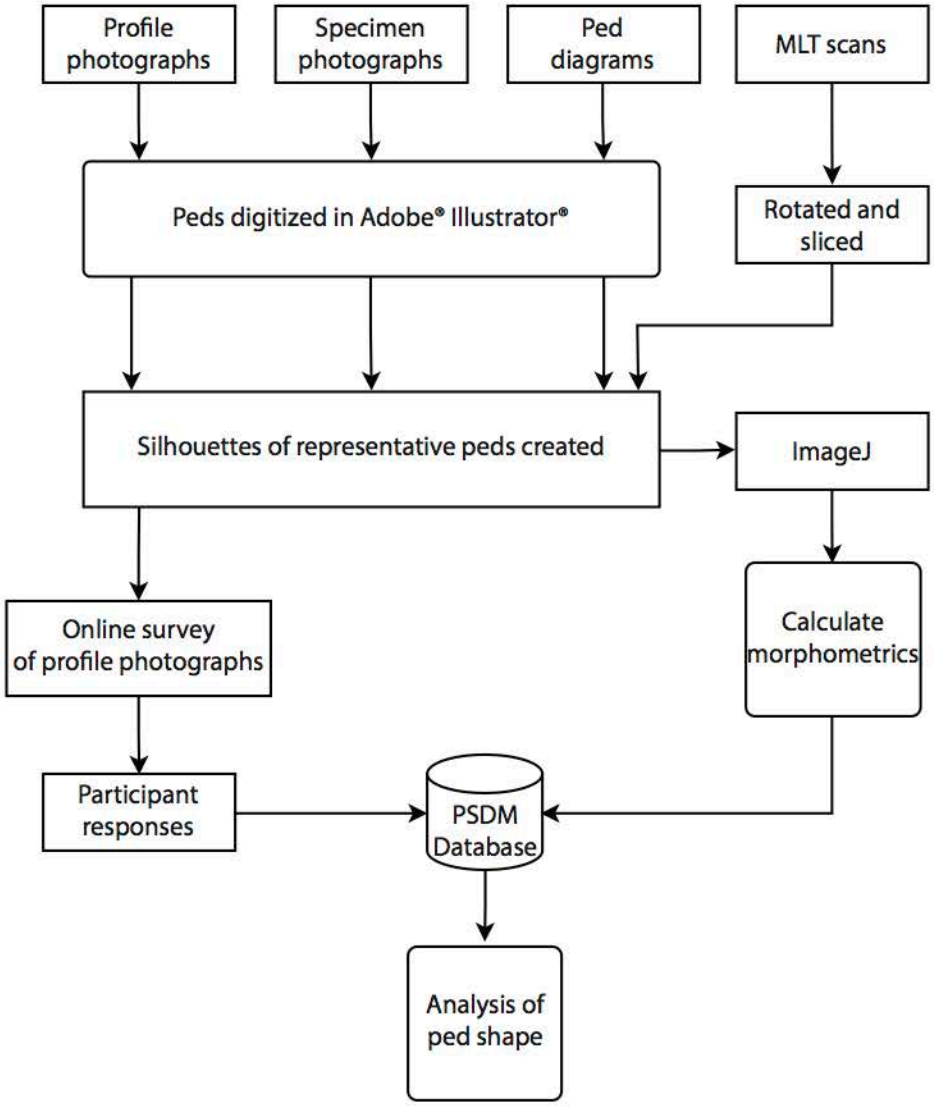

Fig. 1. Flow diagram illustrating the procedure used in this study for developing the ped shape digital morphometrics (PSDM) database.

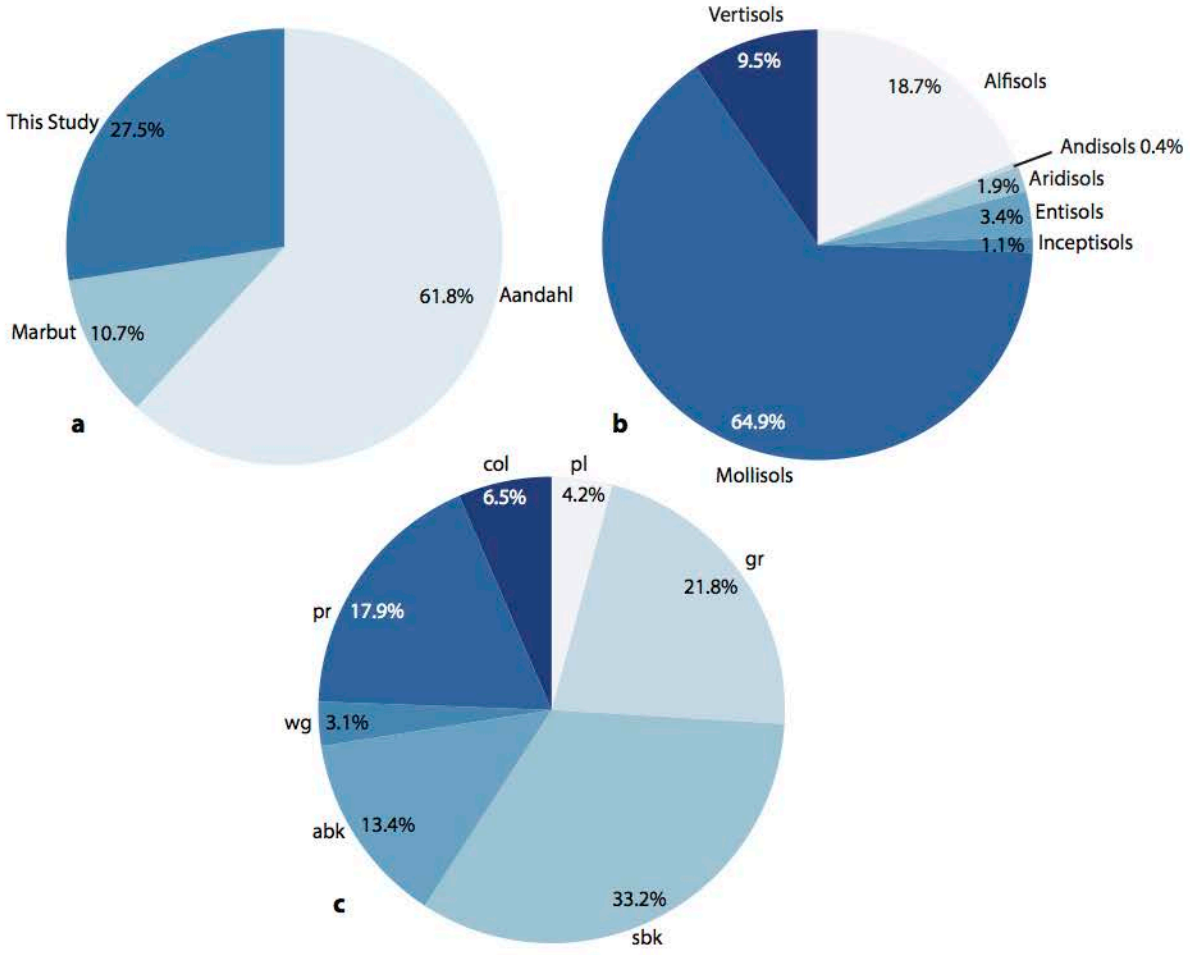

Fig. 2. Relative proportions of (a) photo sources, (b) soil taxa, and (c) ped types represented in the survey. Soil structure: abk = angular blocky; col = columnar; gr = granular; sbk = subangular blocky; pl = platy; pr = prismatic; and wg = wedge.

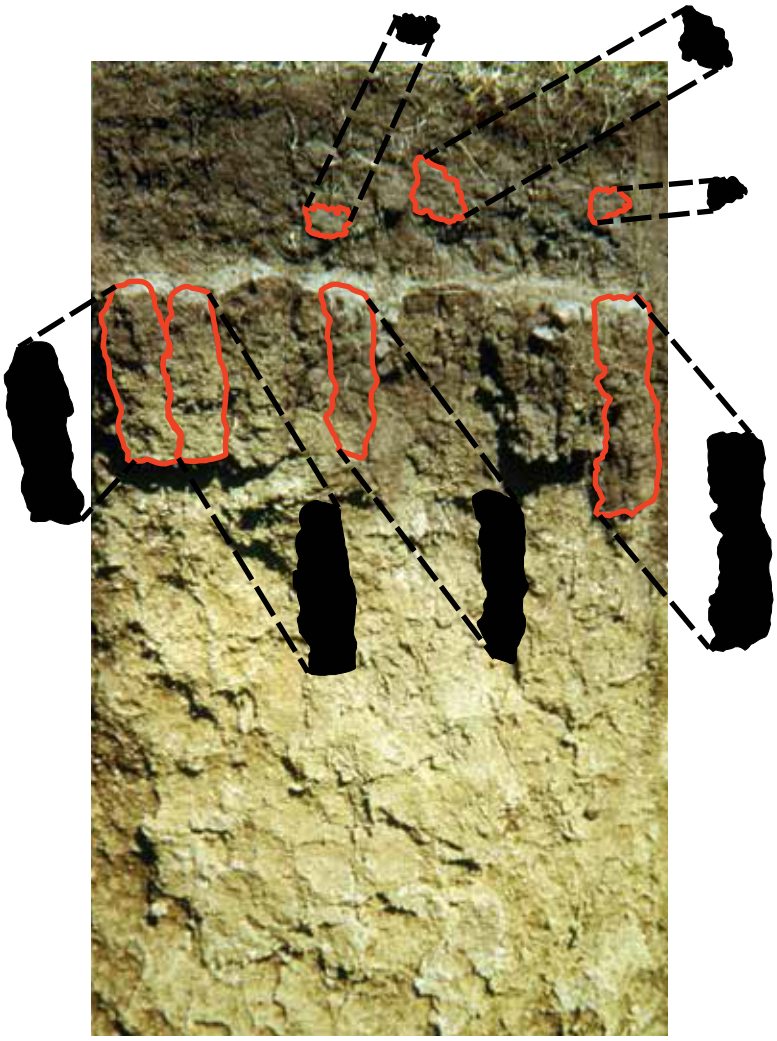

Fig. 3. Digitized peds from a profile photograph of the Cavour series (modified from Aandhal, 1982). Red lines in the photograph indicate outlined edges of each digitized ped. Dashed black lines show the location of the solid black silhouette representing each ped on the excavation wall. Silhouettes were analyzed through ImageJ to calculate various morphometrics. A modified version of this figure was used in the survey which contained everything except the red outlines.

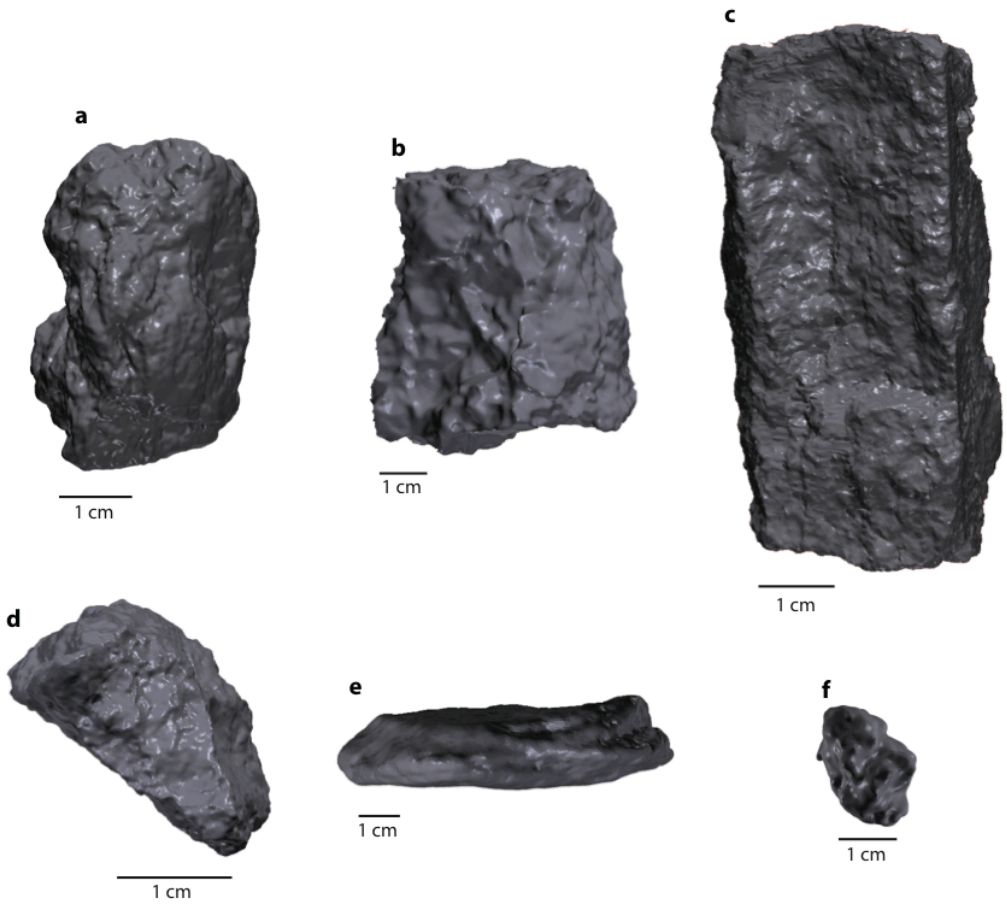

Fig. 4. Representative 3-D ped models digitized by MLT scanning for: (a) subangular blocky structure, (b) angular blocky structure, (c) prismatic structure, (d) wedge structure, (e) platy structure, and (f) granular structure.

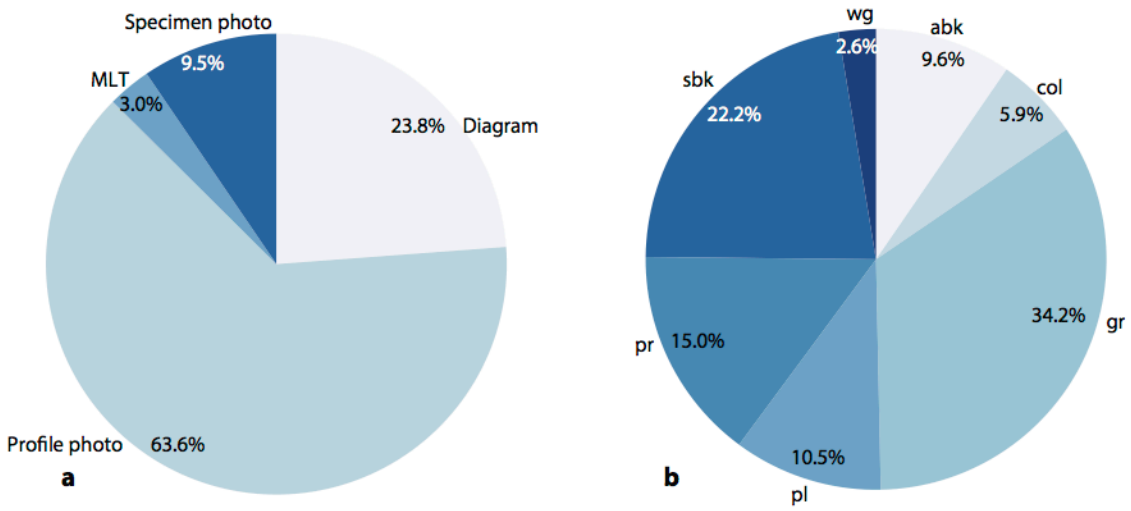

Fig. 5. Relative proportions of (a) media sources used to create the PSDM database as well as the proportions of (b) ped types in the database. Media source: MLT = multistripe laser triangulation scans. Soil structure: abk = angular blocky; col = columnar; gr = granular; sbk = subangular blocky; pl = platy; pr = prismatic; and wg = wedge.

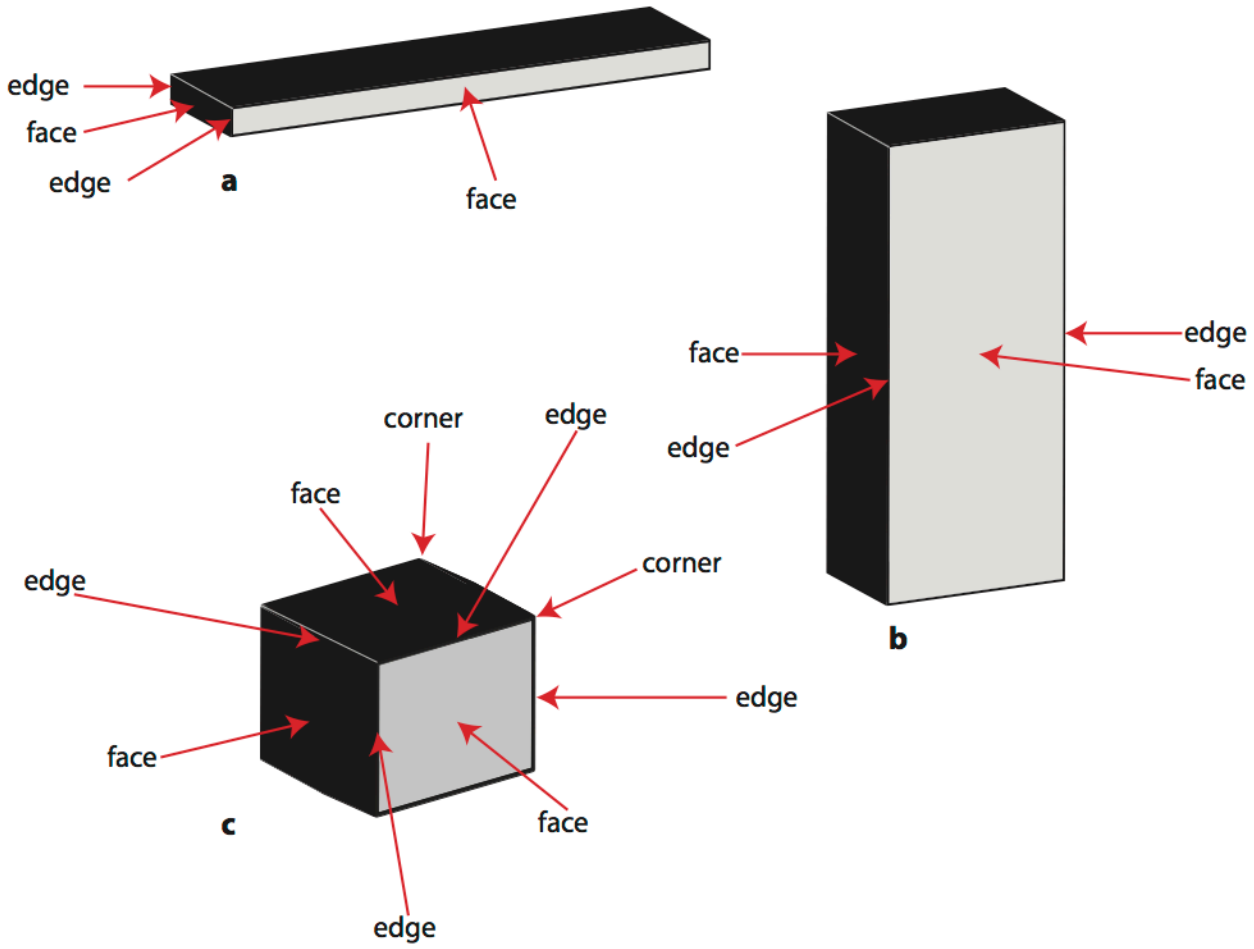

Fig. 6. Illustration showing how peds were digitized from MLT scans. Anisotropic peds (a,b) were rotated to four different angles corresponding to two faces, and two edges. Equidimensional peds (c) were rotated to nine different angles corresponding to three faces, four edges, and two corners.

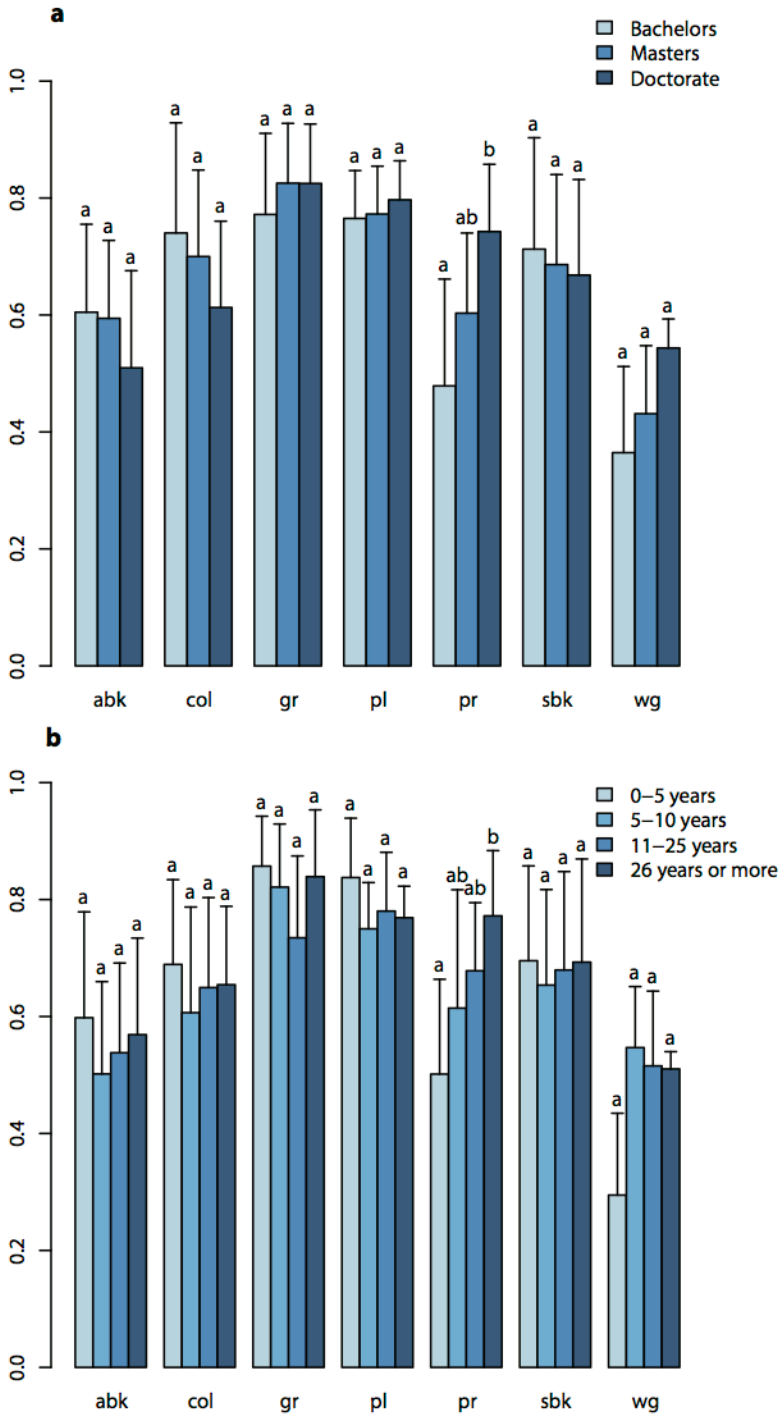

Fig. 7. Mean relative frequency of survey participant responses (y-axis) for (a) educational level and (b) years of experience describing soil. Error bars show 1 standard deviation above the mean frequency values. Soil structure: abk = angular blocky; col = columnar; gr = granular; sbk = subangular blocky; pl = platy; pr = prismatic; and wg = wedge. Identical letters above the bars indicate means of participant responses that are not significantly different within ped types at an α-level of 0.05.

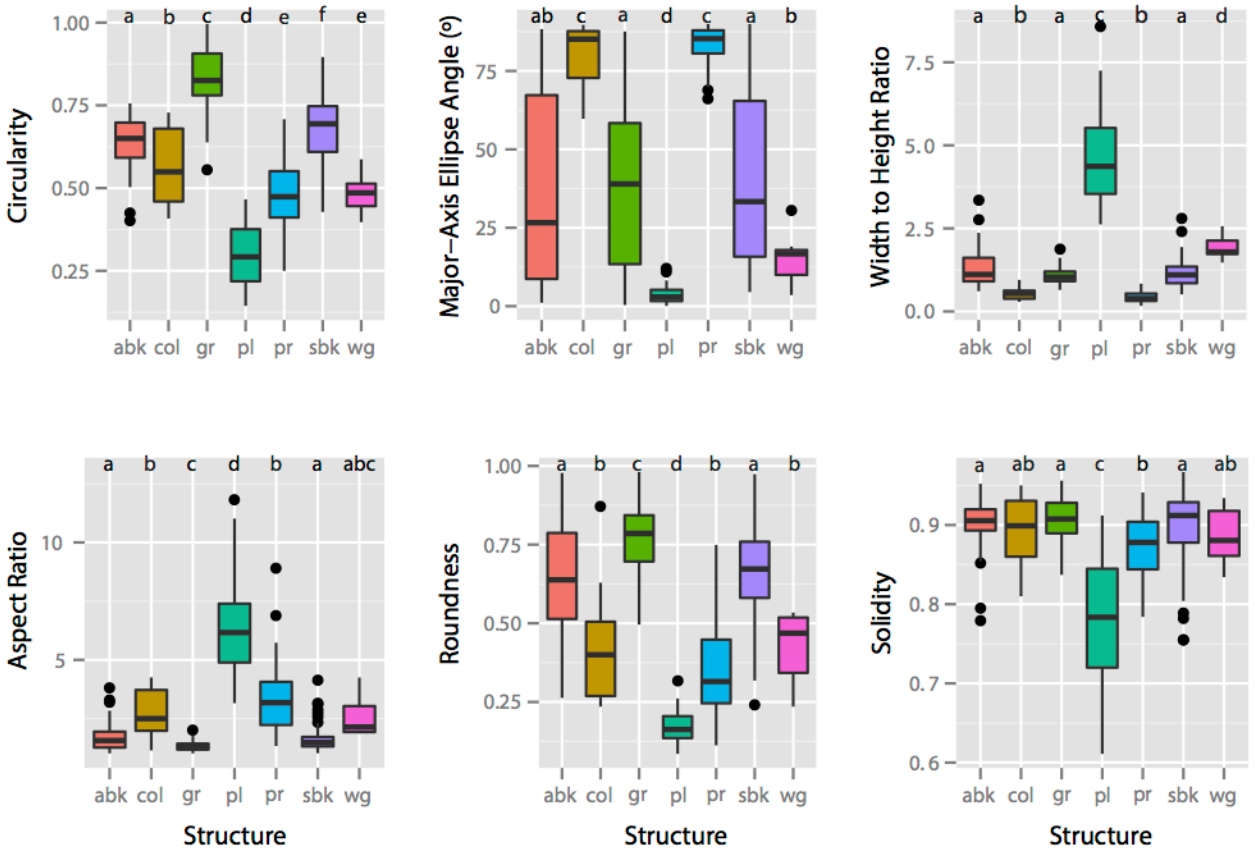

Fig. 8. Boxplots of each shape parameter measured in this study from silhouettes derived from profile and individual specimen photos in the PSDM database. Identical letters above the boxplots indicate means that are not significantly different at an α-level of 0.05. Boxes show the upper and lower quartiles, center bars show median values, whiskers extend to extreme data values, and points show very extreme values (greater than 1.5 times the interquartile range). Soil structure: abk = angular blocky; col = columnar; gr = granular; sbk = subangular blocky; pl = platy; pr = prismatic; and wg = wedge.

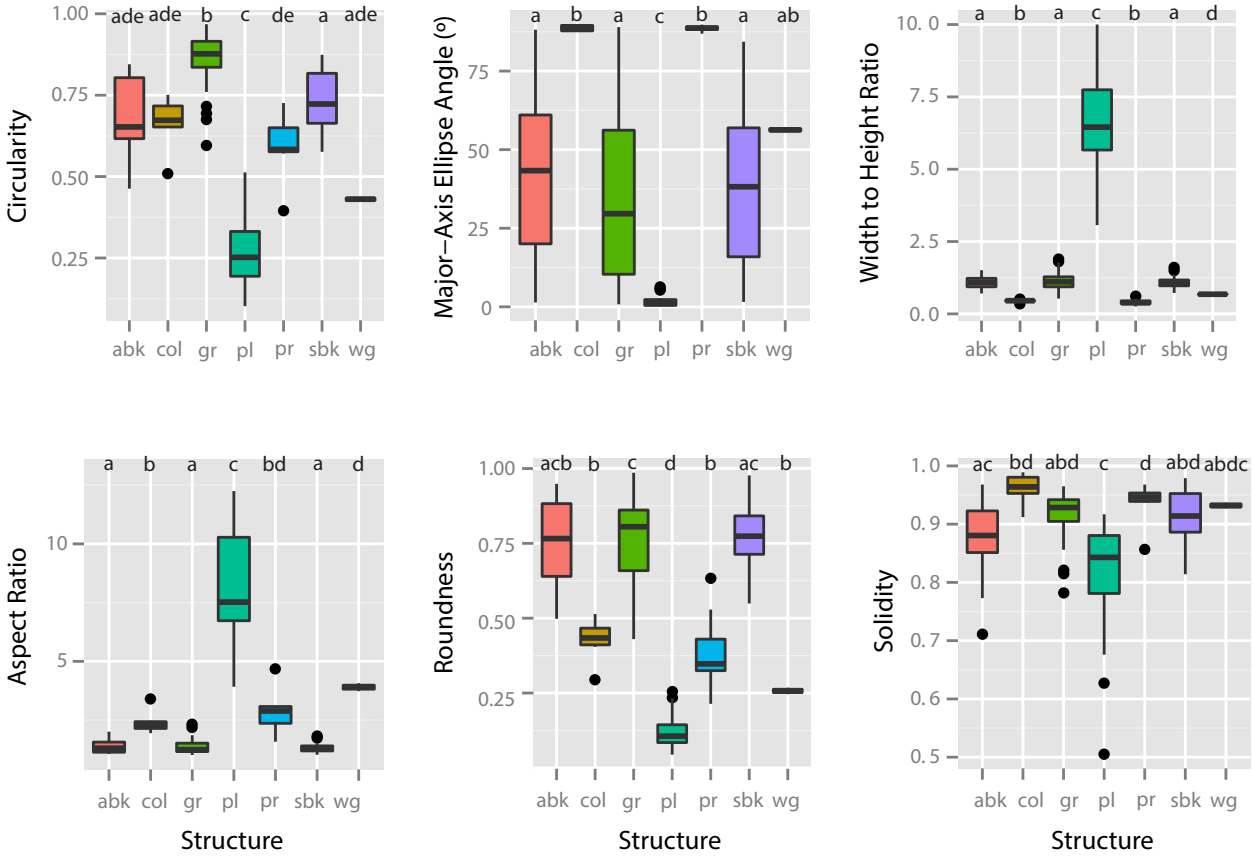

Fig. 9. Boxplots of each shape parameter used in this study measured from silhouettes of ped diagrams in the PSDM database. Identical letters above the boxplots indicate means that are not significantly different at an α-level of 0.05. Boxes show the upper and lower quartiles, center bars show median values, whiskers extend to extreme data values, and points show very extreme values (greater than 1.5 times the interquartile range). Soil structure: abk = angular blocky; col = columnar; gr = granular; sbk = subangular blocky; pl = platy; pr = prismatic; and wg = wedge.

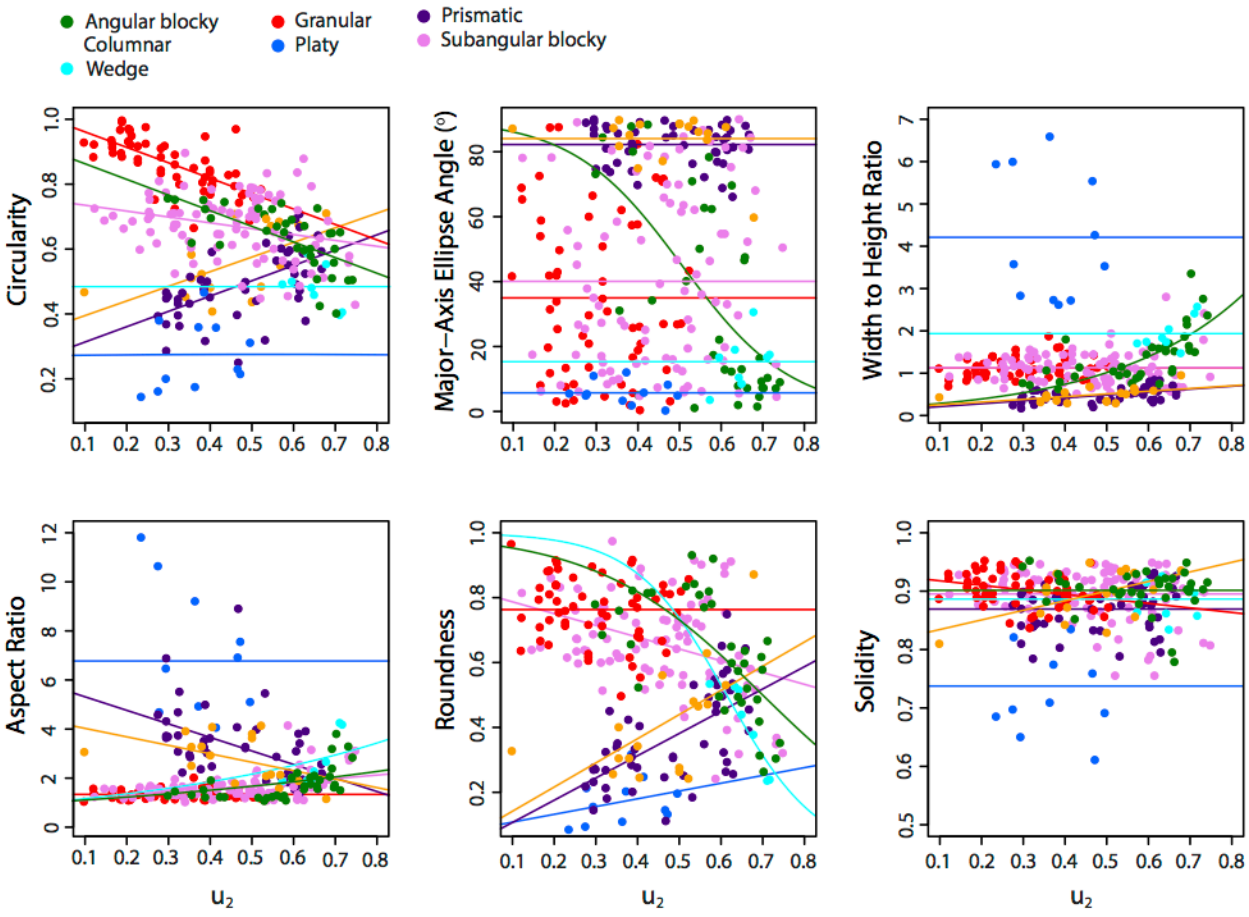

Fig. 10. Plots of shape parameters used in this study against unalikeability coefficient (u_2) for all peds in the survey (n = 262). Values of u_2 (i.e., x-axis) close to zero refer to high agreement among the survey participants when assigning ped type; values of 0.8 refer to high disagreement when assigning ped type to a digitized ped. Regression models were chosen to match the shape of the data and included linear, exponential, and logistc regressions. Where regression models were not significant, horizontal lines that indicate the means of the shape parameter were ploted. y-Intercept values for the regressions indicate predicted shape metrics for perfect agreement among the survey participants.

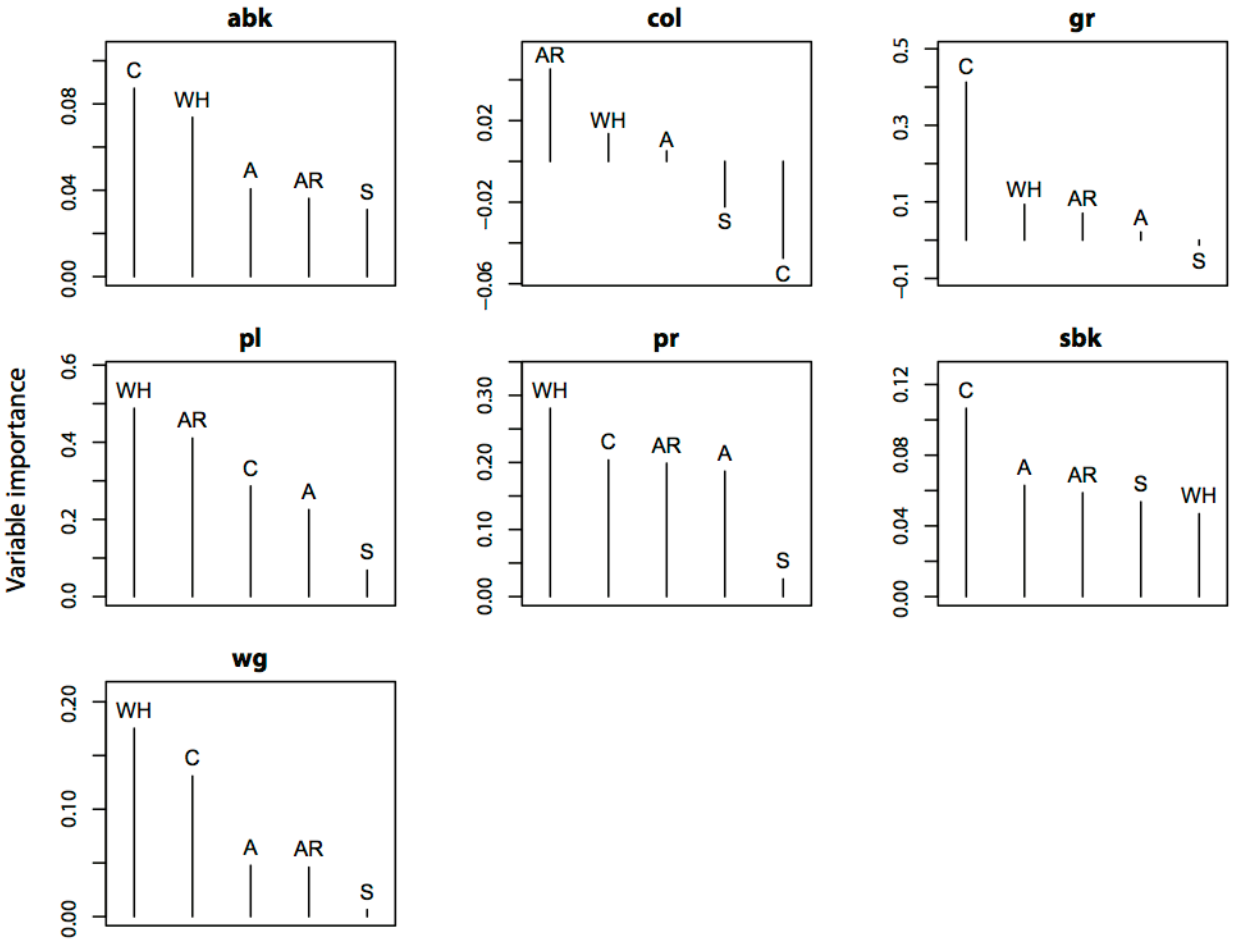

Fig. 11. Shape metric importance measured from random forest predictions for each ped type. Soil structure: abk = angular blocky; col = columnar; gr = granular; sbk = subangular blocky; pl = platy; pr = prismatic; and wg = wedge. Shape metric: C = circularity; WH = width to height ratio; AR = aspect ratio; A = major axis ellipse angle; and S = solidity.

CHAPTER 3. EXOGENOUS AND ENDOGENOUS CONTROLS ON THE DEVELOPMENT OF SOIL STRUCTURE

ABSTRACT

The roles played by exogenous and endogenous factors in the development of soil structure (ped type, size, and grade) are poorly understood. Exogenous factors are those external to soil, such as climate and slope, whereas endogenous factors are internal, such as soil organic carbon and clay content. Unfortunately, the categorical and qualitative nature of currently available soil structural data along with the lack of a broad scale dataset containing wide ranges in the values of exogenous and endogenous factors, have impeded our understanding of the development of soil structure. In this study, we assembled a soil, climate, and ecological dataset for the USA, and used it to analyze relationships between soil structure and exogenous and endogenous variables. We simplified the format of the National Cooperative Soil Survey (NCSS) Soil Characterization database, which contains laboratory data and field-derived information, and analyzed a subset of the data after merging this information with climatological and ecological data. Additionally, we used a recently-developed method to quantify the description of ped shape. Quantitative ped sizes were calculated using the geometric mean diameter of the structure size class recorded for each horizon, and numerical values of ped grade were calculated using an ordinal scale ranging from structureless to strongly structured conditions. The merged and cleaned dataset is termed the University of Kansas Research Dataset of Soils (KURDS) and contains more than 94,000 observations from approximately 20,000 pedons. We found that the exogenous factor, climate, was the most important predictor for ped shape and size. Cold and/or dry climates promoted the development of larger anisotropic peds with rougher surfaces whereas

warmer, more humid climates promoted the development of finer equidimensional peds with smoother surfaces. These findings suggest that climate influences the development of soil structure through its control on mechanisms affecting soil aggregation. We argue that climate promotes the development of soil structure along either separation or aggregation pathways characterized, respectively, by largely mechanical mechanisms in cold, dry environments and predominately biological and chemical mechanisms in warmer, wet environments. This connection between climate and the development of soil structure represents a potentially important effect of climate on a morphological property strongly linked to soil hydrology. Overall, this study demonstrates the potential of utilizing continental-scale datasets in pedological research.

INTRODUCTION

Soil structure denotes the arrangement of soil particles, which are often arranged into repeating patterns of aggregates that occur within morphological horizons; these aggregates typically have similar shapes, sizes, orientations, and degrees of expression (Nikiforoff, 1941; Hillel, 1998; Díaz-Zorita et al., 2002; Warrick, 2002). When these repeating aggregates are large enough to be visible to the naked eye, they are known as 'peds' and their shapes have traditionally been described using qualitative and subjective categories for shape, size, and grade, although several studies have described peds in terms of quantifiable properties (Dexter, 1985; Mohammed et al., 2016; Hirmas and Giménez, 2017).

Soil structure is an important property because it has considerable influence over biological, physical, and chemical soil processes, such as water retention, infiltration, erosion, root penetration, and aquifer recharge (Warrick, 2002). For example, Lin et al. (1999) showed

that ped shape can significantly affect steady-state infiltration rates, although these effects depended on initial moisture conditions and particle-size distribution. Structure also influences soil climate through its effects on soil water evaporation, respiration, and the exchange of gases with the atmosphere (Davidson and Janssens, 2006). In general, the influence of soil structure on these processes occurs through modifications of soil macropores (Kutílek, 2004).

Although numerous studies have investigated the effects of soil structure on physical or biogeochemical soil processes, few studies have focused on either the development of soil structure or the response of ped shape, size, and grade to either external (i.e., exogenous) and internal (i.e., endogenous) factors. Exceptions include the work of Dexter (1985), Hartge (1993), and Holden (1993; 1995). For example, Dexter (1985) found that soil aggregates sampled from the upper 10 to 20 cm became less round with increasing clay content and more round with soil organic matter (SOM) and time since reclamation. In contrast, Holden (1993) found that seasonal variation observed in ped shape was not significantly associated with either gross ped or soil physical properties.

The limitations of these studies, however, were that samples were either taken only from surface layers of the soil profile (which restrict their representation of the whole profile), samples were composed only of fine peds/aggregates (less than a few centimeters), and/or these studies used only relatively small sample sizes ($N \approx 10$) even in cases where quantitative approaches were used (Rabot et al., 2018). Thus, despite several previous studies and reviews (e.g., Bronick and Lal, 2005; Rabot et al., 2018), little is known about the role of exogenous factors (e.g., climate) or endogenous soil properties (e.g., clay content or SOM) on the expression of soil structure. In order to understand these roles, investigations should include a wide range of values of relevant exogenous and endogenous variables and examine their individual and combined

effects on soil structure development and expression. Utilizing a wide range of values, especially with exogenous variables, requires that studies be conducted over broad scales (e.g., continental scales) where this range of values would be realized. We argue that large, broad-scale datasets containing soil structural information could be used to overcome this limitation and allow investigations to be conducted at these broad scales.

In fact, such broad-scale datasets do exist that contain either field-based morphological data, laboratory measurements, climatological information, topography, or ecological data (i.e., representing various exogenous and endogenous information). For example, the USDA-Natural Resources Conservation Service (USDA-NRCS) maintains a large, continental-scale, quality-controlled database that contains both laboratory and field-based soil data covering much of the conterminous USA. To date, however, this information has not been integrated with other relevant data sources into a single, readily accessible dataset for investigation of soil structure.

The overall goal of this study, therefore, was to understand how endogenous and exogenous factors influence the development of soil structure—specifically, the structural properties: ped shape, size, and grade. The key objectives of this work were to (1) assemble an easily-accessible, two-dimensional data matrix that contains laboratory and field-based measurements across the USA and integrates topographic, climatological, and ecological data useful for understanding soil structure; and (2) use these data to explore the response of soil structure to exogenous and endogenous factors in both surface and subsurface horizons.

METHODS AND MATERIALS

Data

We used the National Cooperative Soil Survey (NCSS) Soil Characterization Database maintained by the USDA-NRCS. This dataset contains information on soil properties from samples excavated mostly by NRCS personnel and measured at the Kellogg Soil Survey Laboratory (KSSL) in Lincoln, NE, as well as cooperative university laboratories. Notably, the dataset provides the geographic extent necessary to cover the range of exogenous and endogenous variables relevant to studying soil structure. The dataset also serves as the foundation for the national Soil Survey Geographic Database (SSURGO). These data are stored in 119 tables within two large Microsoft ACCESS database files—one for laboratory characterization data (577 MB) and one for field-based pedon data (648 MB; e.g., depths, structure, rock fragments, redoximorphic features, pores, root distributions, and landform properties). Because the structure of these data files is complex, we pre-processed the files to put them into an easily accessible format for further analysis as follows (Fig. 1).

First, a query was performed to select the relevant soil chemical, physical, and mineralogical properties from the laboratory data. We also, separately, selected the relevant soil morphological, geographic, taxonomic, and site information from the pedon data files. Second, both the laboratory and pedon data files were read into R (R Core Team, 2017) as two separate R data.frame objects and the geographic coordinates for the laboratory samples were converted from a degrees-minutes-seconds format to decimal degrees to match the format in the pedon data. In addition, categorical pedon data were cleaned by tagging missing data as "NA" and inconsistencies in spelling or capitalization were fixed. For example, the dataset contained different entries for the same soil order such as "Mollisols" and "mollisols" which were

corrected to just “Mollisols.”

A major drawback to the structure of the original pedon data files is how multiple values that describe a single soil horizon or pedon property are represented. In these cases, whole rows in the ACCESS data tables are duplicated as many times as there are values for that property. For instance, if a horizon was described as having weak, medium prismatic structure parting to strong, fine, angular blocky structure, the horizon would be represented by 2 rows in the ACCESS data table—one for each description of structure. If the same horizon was also described as having both many fine and common medium roots, then the horizon would be represented by 4 rows. We found that this data structure overrepresented the number of soil horizons in the original pedon data by more than a factor of 5 (i.e., 121,095 unique soil horizons were represented by 679,521 rows) and thus complicated the analysis. In order to simplify this structure and facilitate analysis, multiple values of the same variable described for a single horizon were moved into additional columns to keep each horizon represented by a single row. For example, multiple values of ped type (e.g., prismatic and angular blocky) were placed in additional ped type columns (e.g., ped type 2, ped type 3, etc.).

The pedon and laboratory R data.frame objects were joined into a single data.frame using the unique pedon and horizon identifiers appropriate to each data table found in the original database (Fig. 1). The geographic coordinates provided separately in the pedon and laboratory data were checked via regression to independently verify the join process. The new, merged data.frame object was further cleaned by removing the variable-specific identifiers while retaining the unique pedon and horizon-level identifiers, removing duplicate columns (i.e., ones that contained the same information but occurred in both the laboratory and pedon datasets separately), resetting the levels of each column of R factor class in the data.frame, and renaming

several columns to facilitate analysis and clarity (e.g., "NCSS_Pedon_Taxonomy_latitude_decimal_degrees" was changed to "lat").

We then added several new columns to the dataset. We used the quantified ped shape values reported by Mohammed et al. (2016) to calculate new ped shape variables in the dataset. These variables included roundness, which measures bulk shape roundness between 1 (perfectly circular) and 0 (perfectly angular), and solidity, which measures surface roughness with values less than 1 indicating increasing roughness (Mohammed et al., 2016). We also transformed ped size from discrete classes into continuous quantitative data using the geometric midpoint of the appropriate size class recorded for each horizon following the definition of size classes provided by Schoeneberger et al. (2012). The ped size for the largest category (defined separately for each ped type) was assigned the lower boundary of that class since the upper boundary is undefined (Schoeneberger et al., 2012). In order to facilitate analysis of ped size, we used a standardized size class nomenclature by changing occurrences of "thin" or "thick" (used to describe platy peds; Schoeneberger et al., 2012) to "fine" or "coarse," respectively. Structural grade values were transformed to an ordinal scale ranging from structureless (0) to strongly structured conditions (3). In cases of compound soil structure (i.e., structure characterized by nested peds), quantitative values of ped shape, size, and grade for each structural unit present were combined into a single numerical description using an approach developed by Hirmas and Giménez (2017).

Quantitative values were also calculated for roots and added as new variables in the dataset. For each root size class recorded (i.e., very fine, fine, medium, coarse, or very coarse), the corresponding root quantity value (i.e., average number of roots recorded within the assessment area) was converted to root density, RD, following Eq. [1]:

$$RD_i = f_i q_i \quad [1]$$

where q_i is the root quantity value for the ith root size class, and f_i is the fraction of the assessment area occupied by the cross-sectional area of a single root of size i assuming the assessment area bisects the root. This assumption makes the quantity a conservative estimate. The ith fraction is calculated as:

$$f_i = \frac{d_i^2 \pi}{4 A_i} \quad [2]$$

where d_i is the root diameter calculated as the geometric midpoint of the ith root size class and A_i is the assessment area assigned to the ith size class following Schoeneberger et al. (2012). For very fine and fine root size classes, A_i is 0.0001 m^2; for medium and coarse size classes, A_i is 0.01 m^2. Very coarse roots are assigned A_i values of 1 m^2. Root diameters were calculated for each root size as 0.00032 m (very fine), 0.00141 m (fine), 0.00316 m (medium), and 0.00707 m (coarse). Because the upper bound is undefined for the very coarse size class, we assigned the d_i for that class to be equal to its lower bound (0.01 m), further making these estimates conservative. The combined cross-sectional areal density of all roots was calculated as the sum of the RD values across all size classes recorded for each horizon. Because the cross-sectional profile (the 2-D structure) is assumed to represent the morphological properties of the pedon (the 3-D structure), the RD values can be taken as volumetric estimates of root density (i.e., volume of roots per volume of soil; $m^3\ m^{-3}$).

In addition to quantitative metrics for soil structure and roots, several climatological variables including mean annual precipitation (MAP) and mean annual temperature (MAT) from the Parameter-Elevation Regressions on Independent Slopes Model (PRISM Climate Group, 2016), were added to the dataset. The PRISM data comprised 30 years of gridded data at a 4-km resolution across the conterminous USA. These data were used to calculate a relative proxy metric (effective energy and mass transfer, EEMT) representing the energy available for

pedogenesis in units of MJ m^{-2} y^{-1} following Rasmussen and Tabor (2007). Because this pedogenic energy proxy relies on both MAP and MAT in its calculation, we used it in this study as a convenient climatological parameter that integrates both precipitation and temperature into a single numerical value.

Next, we used ArcGIS (ArcGIS Desktop ver. 10.2, ESRI, Redlands, CA) to assign individual samples in the dataset to US Forest Service (USFS) ecoregions of the USA (https://www.fs.fed.us/rm/ecoregions/products/map-ecoregions-united-states/) and Köppen-Geiger climate classes (Peel et al., 2007) to add further ecological and climatological information (Table 1; Fig. 2). The USFS ecoregions data used in this study contains three hierarchical ecosystem levels. The largest ecosystem levels are domains, which represent groups of related climates differentiated on the basis of MAP and MAT. Domains are divided into divisions differentiated by seasonal patterns of precipitation and temperature. Divisions are further subdivided into provinces differentiated by natural land cover (Baily, 1989). The Köppen-Geiger climate classification divides climate into five main climate groups: A (tropical), B (dry), C (temperate), D (cold), and E (polar) (Peel et al., 2007). The second letter (i.e., f, m, s, w, W, S, T and F) indicates the type of seasonal variability in precipitation, while the third letter (i.e., a, b, and c) indicates the type of seasonal variability in temperature.

Finally, the dataset was read back into R, saved as a final R data.frame object, and output as an RData file for analysis. This final 2-D data matrix is known as the University of Kansas Research Dataset of Soils (KURDS) and contains information on 1,035 variables measured on 94,189 unique horizons distributed across 19,732 pedons. These data include taxonomic, morphological, physical, chemical, mineralogical, geographical, geomorphological, climatological, and ecological information. After assembling the dataset, 30 pedons were

randomly selected within KURDS and compared to online records from the NRCS (https://ncsslabdatamart.sc.egov.usda.gov) to verify the consistency of the dataset. No inconsistencies were observed during this verification process.

In this study, we selected pedons (N = 1,602) and soil horizons (N = 4,431) in KURDS based on parent material, taxonomy, horizon nomenclature, depth, and drainage class (Table 2). We selected only the parent materials that were most common in the dataset (i.e., alluvium, residuum, till, and loess). Soil orders were selected to avoid young or poorly developed soils (i.e., Entisols and Inceptisols), limited geographical distributions within the US (i.e., Spodosols and Oxisols), highly-localized environmental settings (i.e., Histosols), or unique pedogenic pathways (i.e., Andisols, Gelisols, and Vertisols). Thus, only Ultisols, Mollisols, Alfisols, and Aridisols were selected. We also grouped soil samples by horizons into surface layers (A horizons) with midpoint depths between 0−25 cm and subsurface layers (B horizons) with midpoint depths <25 cm. We excluded plowed layers (e.g., Ap horizons) and horizons below lithologic discontinuities in order to minimize the influence of confounding factors. Soils with poor or very poor drainage classes were removed from the dataset to separate effects of exogenous climatological variables from site-specific hydrology. Figure 2 shows the geographic distribution of the pedons selected after filtering the data for this study.

Statistical Analyses

The distribution of each continuous variable used in this study was checked for normality by visually inspecting histograms of those variables. Because many of these variables violated assumptions of normality, they were transformed following Table 3. In this study, we analyzed many of the relationships with depth; however, we considered depth to be neither an exogenous

nor endogenous variable, but simply the vertical location with respect to the land surface where endogenous variables occurred.

We used multinomial logistic regression (MLR) to calculate the probability of categorical soil structure variables such as ped type, size, and grade classes across a range of values for the individual endogenous and exogenous variables listed in Table 3. Multinomial logistic regression is an extension of binary logistic regression that allows for more than two categories of the dependent or outcome variable and uses a maximum likelihood estimation to evaluate the probability of the categorical data (Borooah, 2002; Hosmer and Lemeshow, 2000, 2013; Malone et al., 2017). We analyzed the data with MLR using the nnet R package (Venables and Ripley, 2002).

In addition to MLR, decision trees (DTs) were utilized to evaluate the relative importance of the exogenous and endogenous variables in predicting soil structure. We used DTs in order to incorporate both categorical and continuous variables simultaneously in the analysis (Logan, 2010). In general, DTs are often used as an alternative to regression analysis in determining how a series of explanatory variables will impact a dependent variable (Lander, 2014). Trees were created using the rpart R package (Therneau et al., 2017). In order to prevent overfitting, trees were pruned by selecting a minimum value of the complexity parameter that minimized the standard deviation of the errors calculated from cross-validation predictions generated from a set of cost-complexity prunings (Therneau et al., 2017).

In order to evaluate depth dependence in the relative importance of the endogenous variables in predicting soil structure, we examined the data using the following procedure. First, pedons were selected from the dataset (N = 1,086) that contained contiguous horizons (beginning with the surface horizon) meeting the criteria listed in Table 2. Second, an equal-area

spline function (Bishop et al., 1999) was applied to the quantified structure variables and endogenous soil variables indicated in Table 3 using the GSIF R package (Hengl et al., 2017) in order to predict the values of those variables at a 1-cm depth increment. The equal-area spline consists of a series of quadratic polynomials fitted piecewise through the sampling layer depths with a constraint that preserves the area under the curve (Odgers et al., 2012). Third, we predicted the quantified soil structure variables (i.e., ped roundness, solidity, etc.) using DTs for each 1-cm depth increment separately in order to calculate a normalized importance value representing an aggregated goodness of split measure of each independent variable, which was then scaled to sum to 100. The calculation of this importance value is described in detail by Therneau et al. (2018). Finally, we used a spline function to smooth the resulting depth functions with a moving 25-cm depth window in order to reduce high-frequency noise in the predicted soil variable importance and aid the visual interpretation of the trends.

RESULTS AND DISCUSSION

Ped Type, Size, and Grade Interactions

We examined the interactions between the qualitative soil structural variables in the dataset with mosaic plots (Fig. 3). These plots show the proportion (i.e., probability) of each class value of either ped size (Fig. 3a) or grade (Fig. 3b) occurring within each ped type (read from the box heights) as well as the relative proportions of horizons in the dataset that were contained in each ped type (read from the box widths). In order to eliminate the complexity associated with horizons where multiple ped types, sizes, or grades were recorded, these samples were removed from the MLR analysis. Medium was the most commonly recorded size class for

both angular blocky (71%) and prismatic (53%) peds. Granular peds occurred predominantly as fine sizes (65%) while subangular blocky occurred mostly as medium sizes (52%).

Although the data in Fig. 3 show the results across all depths used in this study, structures in the surface horizons (i.e., non-plowed, A horizons with midpoint depths ≤25 cm)—which made up 23% of these data—were largely characterized by fine (67%) granular and fine (51%) subangular blocky, with these two structures making up 60% and 30% of all surface ped types, respectively (Appendix B Fig. B1a). By contrast, subsurface horizons (i.e., B horizons with midpoint depths >25 cm), composing 77% of the data shown in Fig. 3, were predominantly characterized by medium (55%) subangular blocky structure, which alone made up 79% of all subsurface ped types (Appendix B Fig. B1b). Thus, the distribution of probabilities in Fig. 3a are more strongly weighted by the frequency of subangular blocky structure in the subsurface horizons and the coarser size classes of those peds compared to the finer granular and subangular blocky size classes of the surface horizons. Similarly, the distribution of medium angular blocky and prismatic size classes is due to the occurrence of these peds almost exclusively in subsurface horizons; only 0.2 and 1% of surface horizons in the dataset were characterized by prismatic and angular blocky structure, respectively, and less than 1 and 3% of angular blocky and prismatic peds, respectively, were observed in surface horizons.

The differences in ped size class between surface and subsurface horizons may be related to the relative position of these horizons with respect to the land surface. The mechanisms responsible for soil structural evolution are discussed below and include freezing and thawing, slaking, root growth, and organic bonding (Díaz-Zorita et al., 2002). These mechanisms are likely to have a stronger, more direct role in structural development in surface horizons, which are, comparatively, more exposed to atmospheric fluctuations than subsurface horizons, and may

explain the tendency toward finer ped sizes in these horizons as larger fluctuations in temperature and moisture from freeze/thaw or wet/dry cycles may induce weakness planes in soil structural units that can reduce ped size.

Size class for platy structure occurred with a somewhat bimodal distribution—that is, most platy peds fell within fine (30%) or coarse (37%) size classes with fewer occurring as medium (25%) (Fig. 3a). Platy structure was concentrated at shallow depths with 83% of these peds occurring in surface horizons (only 0.6% of all subsurface horizons in the dataset were characterized as platy) (Appendix B Fig. B1). In addition, the majority of pedons (76%) containing surface horizons with platy structure occurred in either the Great Basin, Mojave, or Sonoran deserts (sensu Laity, 2002) of the southwest USA, with 87% of these pedons occurring in desert, semi-desert, or steppe ecoregion provinces and 72% of them occurring in dry Köppen-Geiger climate classes (i.e., BSh, BSk, BWh, or BWk; see Table 1 for an explanation of these symbols) (Appendix B Table B2; B8).

Because samples in the dataset were removed that indicated disturbance by plowing, these platy peds are largely the result of natural processes such as the development of vesicular horizons. Vesicular horizons form in arid and semi-arid environments from the addition of eolian sediment, establishment of physical or biological surface seals, and exposure to wet/dry cycles that create and grow vesicular pores (i.e., bubble-like, isolated soil pores) (Turk and Graham, 2011). As the vesicular pores enlarge through this process, they ultimately coalesce and collapse to form platy structure (Anderson et al. 2002; Turk and Graham, 2014). Our finding that surface horizon platy structure occurs largely within dry environments is consistent with this formation process of vesicular horizons.

It is unclear what is driving the bimodal distribution in size classes for platy peds. However, we observed both physical and chemical differences between the medium compared to the fine and coarse sizes. For instance, mean silt content was lowest for horizons with medium platy peds at 30±5.0% (± standard error) with fine and coarse sizes containing 45±4.4% and 36±3.8%, respectively (data not shown). Mean $CaCO_3$ content was higher for medium platy peds (10.5±4.7%) compared to 7.0±2.6% for fine and 6.8±2.2% for coarse sizes while, interestingly, mean saturated-paste pH was lower for medium platy (7.24±0.41%) compared to 7.64±0.19% for fine and 7.76±0.26% for coarse sizes. Differences between the distribution of platy sizes may be linked to these physical and/or chemical differences although the link between these properties and vesicular horizon formation is unclear (Turk and Graham, 2011).

Ped grades showed a relatively similar distribution for granular, platy, prismatic, and subangular blocky peds (weak grades ranged from 38 to 56%, moderate grades from 38 to 58%, and strong from 4 to 12%) compared to angular blocky peds, which exhibited stronger grades (i.e., 13% weak, 64% moderate, and 23% strong) (Fig. 3b). One reason for the shift toward stronger grades is the association between angular blocky peds and higher clay content (36±0.8% compared to 25±0.3% for all other ped types). This association is further discussed below. However, another reason for these stronger grades is that angular blocky structures tend to be identified by describers more easily (Mohammed et al., 2016), suggesting that they may be described more frequently in higher grade classes when compared to other ped types.

Depth Distribution of Soil Structure

Figure 4 presents the MLR results for soil structure class data (i.e., ped type, size and grade) as a function of depth for the subset of KURDS used in this study. Granular structure was

the most frequently observed ped type (i.e., highest predicted probability) between the surface where it occurred in 67% of the samples and a depth of 14 cm (reaching a 43% occurrence rate at that depth) (Fig. 4a). Below 14 cm, granular structure continued to decrease to <5% below 40 cm. Platy structure was observed at a rate of 8.4% at the surface decreasing to <5% at a depth of 21 cm. The second most frequent ped type observed at the surface was subangular blocky (18%), which became the dominant structure type below 14 cm peaking at an occurrence rate of 82% at 48 cm. The frequency of subangular blocky structure decreased below that depth until being surpassed by prismatic structure (41%) at a depth of 224 cm. The occurrence of angular blocky increased from near zero to about 50 cm reaching a rate of 10% below which it flattened reaching its highest value of 16% at a depth of ~200 cm. Interestingly, the occurrence of prismatic structure increased relatively linearly from the surface to a depth of approximately 125 cm increasing its slope below that point until reaching 56% at a depth of 275 cm and becoming the most common ped type below 224 cm.

The depth distribution of size class frequency for angular and subangular blocky structure is shown in Fig. 4b. Medium angular and subangular blocky peds were observed on average at the highest rates throughout the soil profiles and ranged between 45% at the surface to a peak of 61% at 147 cm. However, the overall trend of the size class data for these ped types was toward a monotonic increase of size with depth. That is, very fine and fine peds decreased from their surface occurrence rates of 12 and 37%, respectively, while coarse and very coarse increased with depth reaching probability values of 42% for coarse sizes at the deepest sampling points in this dataset (275 cm) surpassing fine peds below 158 cm. No significant trends between grade class and soil depth were observed; moderate grades were the most frequently described (~57%) followed by weak (~37%) and strong (~6%) (Fig. 4c).

On average, the upper 25 cm of the soils examined in this dataset were dominated by granular and subangular blocky structure (Appendix B Fig. B1a) accounting for approximately 90% of the ped types occurring within that depth. The granular structure decreased exponentially with depth likely reflecting an association with the depth distribution of soil biota and SOM. For example, the creation of randomly-oriented cracking patterns driven by soil drying from high concentrations of fine roots near the surface has been linked to the distribution of granular structure (Oades, 1993). Similarly, concentrations of endogeic earthworms at shallow depths can produce soil fabrics characterized by spherical macroaggregates (i.e., granular peds) through the combined effects of compaction and egestion (Blanchart et al., 1997; 1999). Soil organic carbon (OC), which follows a similar exponential decrease with depth (Jobbágy and Jackson, 2000), also encourages the formation of granular structure by increasing soil cohesion (Schaetzl and Anderson, 2005).

The predominance of subangular blocky structure in subsurface horizons to an average depth of approximately 225 cm, may be due to a combination of concentration of silicate clays in B horizons through pedogenic translocational processes, which enhance cohesion of the soil material, and an increasing overburden pressure, which acts to consolidate and aggregate the primary particles with depth. As this pressure increases with depth through the weight of overlying material beyond the observed peak probability at approximately 50 cm, the formation of equidimensional peds, such as subangular blocky structure, becomes less favorable due to the asymmetrical development of weakness planes in response to soil shrinkage (Hartge and Horn, 2016). That is, anisotropic peds, such as prisms, are formed through the separation of laterally-adjacent structural units brought about by shrinkage-induced compression of drying soil material under conditions of increased vertical pressure with depth (Turk et al., 2012). This increase in

pressure with depth from the overlying soil material also explains the distribution of angular and subangular blocky ped sizes shown in Fig. 4b where the formation of larger peds are encouraged through the consolidation of soil material under this pressure. The rapid increase of subangular blocky structure in the upper 50 cm of the soil followed by a more gradual decline beyond that depth may also reflect the rate and/or frequency of drying of soil material; in general, rapid dewatering of the soil material tends to favor the formation of blocky structure (Turk et al., 2012).

Effects of Individual Exogenous and Endogenous Properties on Soil Structure

Ped Type Class

The MLR-predicted ped type probabilities for each exogenous and endogenous variable are shown in Fig. 5. In surface horizons, the probability of granular structure showed a positive association with OC content, root density, and EEMT (Fig. 5e,h,i). High EEMT values are associated with warm, wet climates and ecoregions with higher SOM and root densities that promote the formation of granular structure. Despite occurring with the highest probability over most of the sand range (i.e., $\lesssim$77% sand), granular structure was negatively correlated with sand content (Fig. 5b). This negative correlation may be due, perhaps, to the reduced shrinkage of coarse textured soils in response to drying by roots compared to fine-textured soils although granular structure did not show an obvious positive association with clay content (Fig. 5a). A negative association was observed between granular structure and high values of CEC/clay ratio (i.e., $\gtrsim$4.5) with a concomitant increase in angular blocky structure above that value (Fig. 5d) likely reflecting the effects of shrink-swell, high-CEC clay minerals which encourage higher angularity in ped shape.

The two soil chemical dispersion indices, ESP and Ca/Mg ratio, showed opposite effects on granular structure in surface horizons (Fig. 5f,g). Granular structure was negatively correlated to higher ESP—becoming less prominent than platy structure above ~3% and prismatic structure above ~12%—reflecting a decrease in vegetation and root density with increasing sodicity (RD and ESP were negatively correlated: Pearson product-moment correlation coefficient, $r = -0.24$—H_0: $\rho = 0$, $t = -7.50$, $P < 0.001$; data not shown) (Dye et al., 1980). By contrast, lower values of Ca/Mg ratio, which indicate greater potential for dispersion, were associated with a higher probability of granular structure with values above ~25 favoring the formation of subangular blocky structure (Fig. 5g). The mechanism for this trend is unclear. Higher values of Ca/Mg ratio tend to encourage flocculation of clays (Dontsova and Norton, 2002), which may serve to bind granular structure into larger equidimensional structural units recognized in the field as subangular blocky peds. However, the probability of finer granular ped size classes did not decrease with increasing Ca/Mg as expected (data not shown).

Platy structure showed several interesting trends in surface horizons. Drier and/or colder climates (EEMT $\lesssim$ 8 MJ m^{-2} y^{-1}) were negatively associated with increasing probabilities of platy structure as were larger values of OC and RD (Fig. 5e,h,i) owing partly to the positive correlation between these variables (i.e., OC and EEMT: $r = 0.32$—H_0: $\rho = 0$, $t = 7.21$, $P < 0.001$; RD and EEMT: $r = 0.22$—H_0: $\rho = 0$, $t = 5.61$, $P < 0.001$; data not shown). Sodicity was positively correlated with platy structure, with platy peds becoming dominant between ESP values of ~2.7 and ~12% (Fig. 5f). Thus, platy peds were favored under drier/colder climates in soils with greater potential for dispersion and lower densities of roots and SOM (Anderson et al. 2002; Schaefer and Dalrymple, 1995).

Compared with surface horizons (Fig. 5a-j), subsurface horizons (Fig. 5k-t) showed much less variability in the probability of most ped types, with subangular blocky structure dominating the majority of the range of the exogenous and endogenous variables examined (consistent with Figs. 4a and B1). The probability of subangular blocky structure decreased in soils with clay contents above ~25% with a corresponding increase in angular blocky structure, which became dominant above ~60% clay (Fig. 5k). Similar results were observed with CEC and CEC/clay ratio, with the former corresponding to an increase in angular blocky structure at CEC values above ~20 $cmol_c\ kg^{-1}$ and the latter corresponding to an increase in prismatic structure at CEC/clay ratios above ~1 (Fig. 5m, n). Subangular blocky and prismatic structures in subsurface horizons showed opposite trends below ~0.1% OC content (Fig. 5o); the probability of subangular blocky structure increased with larger OC values in that range while the probability of prismatic structure decreased. Increasing values of ESP above ~7.5% were associated with decreasing subangular blocky structure and increasing columnar structure probabilities (Fig. 5p). Warmer, wetter climates (increasing values of EEMT) were associated with increasingly common subangular blocky structure (Fig. 5s).

In general, these results indicate that the development of subangular blocky structure is favored under conditions of sufficient clay content provided that the clay is dominated by lower CEC minerals (Southard and Buol, 1988). Additionally, the subsurface development of angular blocky structure is favored by high clay content (≳60%) and high CEC, although the individual effects of these variables on the frequency of ped types is unclear given that clay content and CEC were strongly positively correlated (i.e., $r = 0.61$—H_0: $\rho = 0$, $t = 33.10$, $P < 0.001$; data not shown). Prismatic structure development appears to be encouraged by high CEC/clay ratios but this effect can be partly explained by the effect of depth or weight of the overlying material as

shown in Fig. 4a since CEC/clay and horizon midpoint depth were positively correlated (i.e., $r = 0.05$—H_0: $\rho = 0$, $t = 2.26$, $P = 0.012$; data not shown). A similar statement can be made for the relationship observed between OC and the ped types subangular blocky structure and prismatic (i.e., OC and depth: $r = -0.30$—H_0: $\rho = 0$, $t = -11.54$, $P < 0.001$; data not shown). The positive relationship between EEMT and subsurface subangular blocky structure likely reflects the influence of climate on clay formation and the production of SOM (clay content and EEMT: $r = 0.074$—H_0: $\rho = 0$, $t = 3.53$, $P < 0.001$; OC and EEMT: $r = -0.090$—H_0: $\rho = 0$, $t = -3.29$, $P < 0.001$; data not shown). As expected, high soil sodicity in the subsurface promotes the development of columnar structure through the dispersion of the tops of otherwise prismatic peds (Schaefer and Dalrymple, 1995) although actual morphological differences between prismatic and columnar structure due to the rounding of the ped tops is largely imperceptible (Mohammed et al., 2016).

Ped Size Class

The MLR-derived ped size class probabilities for only angular and subangular blocky structure is shown in Fig. 6. Surface horizons show a general trend toward increasing probability of coarser peds with increasing clay content—that is, fine (i.e., 5-10 mm) peds became more frequent with larger clay content at the expense of very fine (i.e., <5 mm) peds (Fig. 6a). A similar relationship was observed in subsurface horizons where medium (i.e., 10-20 mm) peds became more frequent at the expense of fine peds with increasing clay content (Fig. 6k). Increased frequencies of coarser ped sizes at the expense of finer peds were also observed for increasing sand content and sodicity in both surface and subsurface horizons (Fig. 6b,f,l,q). Root density, OC, and EEMT in surface horizons showed a positive trend with the probability of fine

structure at the expense of medium (Fig. 6e,h,i). Perhaps the most dramatic trends toward ped size fining were observed in Fig. 6d,n where ped size decreased with increasing CEC/clay ratio in surface and subsurface horizons.

Overall, increasing RD and biological activity reflected in the production of SOM and supported by increasingly warmer and wetter climates (i.e., increasing EEMT), promotes the separation of the soil groundmass into finer peds. This tendency toward the reduction of ped size may represent a combination of the creation of dense patterns of weakness planes by roots and subsequent soil drying (Oades, 1993), increased bioturbation processes such as the egestion of soil particles by earthworms or the enhanced creation of pore networks by ants (Jongmans et al., 2003; Leveque et al., 2014; Drager et al., 2016), and/or increased turnover of SOM through stimulation of the soil microflora by environments characterized as warmer and more humid (Carvalhais et al., 2014). The decrease in ped size is further promoted by 2:1 clays with higher CECs and, likely, higher propensity to shrink and swell as reported for soil aggregates (Fernández-Ugalde et al., 2013), especially in subsurface horizons where these clays are more abundant. By contrast, increased clay content in both surface and subsurface horizons promotes the aggregation of both soil particles and smaller structural units. The reason sand showed the same relationship as clay may be due to an overall reduction in the presence of shrink-swell clays with increasing sand content, which if present would tend to fragment the soil into smaller ped sizes. It is unclear why the potential for more dispersion represented by larger ESP values increased the probability of ped size nor why increased dispersion potential indicated by the Ca/Mg ratio showed the opposite trend (Fig. 6g). Adding to this confusion, the values of the two dispersion potential indices for surface horizons were negatively correlated (i.e., $r = -0.18$—H_0: $\rho = 0$, $t = -2.66$, $P = 0.004$; data not shown). However, surface horizons with ESP values > 3

were concentrated in deserts of the southwestern US while Ca/Mg ratios < 1 were concentrated east of the 100th meridian (data not shown) in the humid subtropical hot-summer (Cfa) Köppen-Geiger climate class (Table 1; Fig. 2) suggesting that different processes may be at work under conditions of high ESP compared to low Ca/Mg ratio.

Ped Grade Class

Structural grade class probabilities showed a positive relationship with clay and OC in surface horizons where moderate grades increased at the expense of weak grades (Fig. 7a,e). Although CEC showed a similar relationship (Fig. 7c), this is likely a reflection of both clay content and OC as opposed to a mineralogical effect since only a slight trend was observed with CEC/clay ratio and grade (Fig. 7d). As effective aggregating agents, clay content and OC are likely acting to form better defined structural units reflected in the higher-grade classes. This was true in subsurface horizons as well where clay content showed a similar positive relationship with grade (Fig. 7k) and CEC following a similar but somewhat muted pattern (Fig. 7m). Sand content was inversely related to grade likely reflecting a diluting effect of the increased sand on clay content (Fig. 7b,l).

The dispersion potential indices, ESP and CEC/clay ratio, were also negatively related to structure grade where increased dispersion (i.e., increasing ESP and decreasing CEC/clay) yielded weaker grades in surface horizons (Fig. 7f,g). A closer look at the data revealed that the trend with dispersion potential was entirely driven by angular and subangular blocky peds; no trend was detected between dispersion potential and grade for granular peds (data not shown). Because, the effects of increased dispersion potential near the land surface is concentrated on the outside of peds, soil particles at ped faces and edges tend to disperse and erode into interpedal

pore spaces likely reducing the visibility and, thus, the expression of individual structural units. However, grade probabilities and ESP were not associated in subsurface horizons (Fig. 7p) although increasing dispersion potential represented by decreasing Ca/Mg ratio in subsurface horizons corresponded to better ped expression (Fig. 7q). The reason for the reversal in the trend from that observed in surface horizons with Ca/Mg ratio is unclear.

Increasing CEC/clay ratio (corresponding to an increase in expansive clay minerals) showed a stronger effect of reducing ped grade in the subsurface than in surface horizons (Fig. 7d,n). However, the surface trend is somewhat obscured by the opposite effects of granular and combined angular and subangular blocky peds at that depth (data not shown). Granular peds showed an increasing tendency toward strengthening of structural grade with increasing CEC/clay ratio while angular and subangular blocky peds showed a weakening of grade. It is likely that the increased tendency toward fragmentation of soils at the surface characterized by high CEC/clay ratios helped strengthened the distinctness of individual granular peds while decreasing the stability of larger structural units (i.e., angular and subangular blocky peds; Fig. 6d,n) leading to an overall decrease in visual assessments of grade for those peds.

Surprisingly, no clear relationships between ped grade and the exogenous variables—EEMT and slope—were observed in surface horizons despite the relationship observed between OC and grade and the known relationship between climate and OC (Fig. 7i,j) (Rasmussen et al., 2018). In subsurface horizons, however, increasing EEMT corresponded to a tendency toward moderate grades at the expense of weaker and stronger grade classes whereas increasing surface slope corresponded to an increased probability of stronger grades (Fig. 7s,t). The relationship between EEMT and grade may reflect an accommodation between strengthening effects of increased clay content in the subsurface and weakening effects of increasing expansive clay

minerals (represented by the relationship with CEC/clay ratio) concentrated in the subsurface. The strengthening trend in grade with increasing surface slope is unclear but may be due to soil movement in response to increased gravitational potentials under increasing pressure from overlying soil horizons, which can fracture the soil groundmass leading to more visually distinct peds.

Influence of Parent Material on Soil Structure

We examined the relationships between qualitative soil structures (ped type, size and grade class) with parent materials for surface and subsurface horizons using MLR. Across all parent materials, the most dominant type of soil structure in surface horizons was granular. Loess exhibited the highest proportion of granular (84%), followed by till (75%) and residuum (68%) (Fig. 8a). The second most dominant structure type in surface horizons was subangular blocky, which accounted for 35% of alluvium and 30% of residuum parent materials. Platy structure accounted for 18% in alluvium.

The high probability of granular occurring in loess might be due to the high composition of silt in these soils (69.4%; data not shown) and the climate or ecoregions in which these soils are found. Pedons formed in loess parent material in KURDS tend to cluster mostly in the Prairie Parkland (Temperate) ecoprovince (Fig. 2) and contain root systems that are deep and extensive. As discussed above, these prairie rooting systems promote the development of granular structure to the depth of maximum root development (Oades, 1992).

Figure 8b shows the results of MLR for all parent materials in subsurface horizons. The most frequently observed soil structure was subangular blocky (82%) for both alluvium and residuum; subangular blocky also occurred at a rate of 75% for loess and 70% for till. The

second most common ped type observed was angular blocky, with a higher predicted value in till (23%) as compared to other parent materials. Prismatic structure was observed at a higher probability in both loess (17%) and till (5%) compared to alluvium and residuum. The reason for these higher percentages may be the combination of high clay content and slope in loess (28% clay and 21.6% slope) and till (32% clay and 17.9% slope) in subsurface horizons. The higher occurrence of prismatic structure in these parent materials might be explained by the increased effects of wet/dry or freeze/thaw cycles in soils with higher slopes and sufficient clay content. As slope increases, soils tend to move via gravitational processes induced by pedoturbation, which may form planes of weakness orthogonal to the land surface promoting the formation prismatic structures.

Fine peds were observed in surface horizons with the highest probability observed in loess (67%) compared to other parent materials (Fig. 9a). Medium ped sizes were observed at a rate of 38% in alluvium. Till showed the highest proportion of very fine ped sizes (39%) compared to other parent materials. Coarse ped sizes were observed with the highest frequency in loess (8%). Loess showed a bimodal distribution of ped sizes from fine to coarse with very few medium ped sizes recorded for these surface horizons. The high RD (0.03) observed in loess soils in our dataset might explain the high probability of very fine and fine ped sizes occurring in loess compared to other parent materials. This is because of the tendency for high fine RD to promote finer structures through the development of randomly oriented planes of weakness (e.g., Oades, 1992).

Medium ped sizes were the most common in subsurface horizons (Fig. 9b), occurring mostly in soils developed in residuum parent materials (69%). Fine peds occurred predominately

in loess (35%) and very coarse peds showed the highest occurrence in alluvium (1.1%). Overall, no clear trend in subsurface ped sizes of angular and subangular blocky structure was observed.

In addition to ped type and size, we also examined the relationships between ped grade and parent material (Fig. 10a,b) for both surface and subsurface using MLR. Weak and moderate ped grades occurred in high proportions across all parent materials. The proportion of strong ped grades in surface horizons was lower than in subsurface horizons. However, loess, compared to other parent materials, showed the highest proportion of strong ped grades (10.3%) and the lowest proportion of weak ped grades (34.5%) in surface horizons. Till had a higher proportion of weak grades (62.7%) in surface horizons compared to other parent materials. In subsurface horizons, a higher proportion of weak ped classes (38.2%) were observed in alluvium. With the exception of loess in surface horizons, as with ped sizes, no clear trend was observed in ped grade classes across the four parent materials examined in this study.

Relative Importance of Exogenous and Endogenous Variables on Soil Structure

Pruned DTs were used to assess the relative importance and effects of exogenous (including EEMT, slope, and parent material) and endogenous variables on the prediction of each categorical and quantitative description of soil structure (i.e., the response variables in Table 3). We included depth in these models as a categorical variable to indicate whether a sample was collected from a surface horizon or subsurface horizon.

Figure 11 presents the results of this analysis for ped type, roundness, and solidity. The first values displayed in the shaded boxes correspond to the central tendency (mode for categorical variables—Fig. 11a—and mean for continuous variables—Fig. 11b,c) of the data subset defined by the criteria given in the previous splits; the second values correspond to

percentages of all samples that fall in the respective subset. The only significant predictor of ped type in the dataset used in this study was depth (Fig. 11a). Granular peds were predicted from surface horizons and subangular blocky peds were predicted from subsurface horizons likely reflecting the abundance of these two ped types in surface and subsurface horizons, respectively (Appendix B Fig. B1). Ped type (on a nominal scale) was transformed into more meaningful continuous variables—ped roundness and solidity, both on a ratio scale—adding the property of transitivity (or "rankableness") and placing it on a metric scale such that the degree of difference between two ped types could be assessed (Kachigan, 1991). Climate (i.e., EEMT) was the most important predictor for ped roundness followed by slope, OC, and parent material (Fig. 11b). Values of EEMT ≥36 MJ m^{-2} y^{-1} (i.e., relatively warm and humid climates) produced ped shapes that were more round (0.80) whereas EEMT values <36 MJ m^{-2} y^{-1} (i.e., colder and/or drier climates) were associated with peds that were less round (0.64). For soils within climates characterized by EEMT values <36 MJ m^{-2} y^{-1}, gently sloping land surfaces (<13%) were associated with higher roundness (0.67) than more steeply sloping surfaces (0.47). Values of OC ≥0.64% corresponded to higher values of roundness (0.76) compared to OC values <0.64% (0.36) for steeply sloping soils under relatively cold and/or dry climates (EEMT < 36 MJ m^{-2} y^{-1}). For soils under these climates and slopes that were characterized by low OC, much lower values of ped roundness (0.25) were associated with loess and till parent materials compared to alluvium and residuum (0.75).

Climate was also the best predictor for solidity where dry climates (EEMT < 10 MJ m^{-2} y^{-1}) characterized by BSh, BWh, and BWk Köppen-Geiger climate classes were associated with slightly rougher peds with mean solidity values of 0.87 compared to 0.90 in more humid climates (Fig. 11c). Depth and OC were the second most important variables with rougher ped shapes

observed for soils with OC values <1.4% (0.89) and smoother peds observed in soils with higher OC (0.91) under climates characterized by EEMT values ≥10 MJ m^{-2} y^{-1}. Surface horizons, which were associated with slightly higher solidity values (0.85) than subsurface horizons (0.88), were partitioned by RD for soils under dry climates. In these soils, low RDs (<0.002) promoted the development of rougher peds (0.79) compared to higher RDs (0.87) likely reflecting the increased probability of platy structure in arid surface horizons with low RDs (Fig. 5; Appendix B Table B1 and B7) since platy peds are associated with lower solidity values (Mohammed et al., 2016).

Overall, exogenous variables (EEMT and/or slope) were more important in detecting differences in the quantitative ped shape metrics (roundness and solidity) than any of the other variables used in this analysis. Soils in warmer, more humid environments characterized by higher SOM content promoted the development of peds that were, in general, smoother and more equidimensional (i.e., represented by higher roundness values). By contrast, anisotropic peds with higher surface roughness are produced under warmer, drier environments. This tendency toward either smoother, equidimensional peds or rougher, anisotropic peds may reflect a forcing by climate toward one of two dominant pathways of soil structural evolution. According to the paradigm for soil structure proposed by Díaz-Zorita et al. (2002), soil structural units develop as a result of either (1) 'building up processes' by which soil particles and smaller aggregates agglomerate or (2) 'breaking down processes' by which unstructured, cohesive soil material or larger aggregates fracture into smaller units. Although it is likely that both of these processes are operating simultaneously (Díaz-Zoritz et al., 2002), the results in Fig. 11 suggest that one of these two types of processes may be dominant in a given environment. Using the idea of pedogenic pathways proposed by Johnson and Watson-Stegner (1987) and defined by Schaetzl

and Anderson (2005) as 'a set of pedogenic processes leading to a given soil morphology,' here we define two pedogenic pathways related to soil structure—aggregation and separation—that result, respectively, from either a dominance of building up processes (e.g., organic bonding, or enmeshing of soil particles/aggregates by roots or fungal hyphae) or a dominance of breaking down processes (e.g., freezing/thawing or shrinking/swelling). Because climate can strongly influence dominant weathering processes in a landscape (Peltier, 1950), in the absence of other strong forcings (e.g., land use), these pathways are likely controlled by prevailing climate such that soil structure evolves via either separation pathways through largely mechanical processes such as wet/dry or freeze/thaw cycles under colder/drier climates, or aggregation pathways through dominantly biological or chemical processes such as root growth or the precipitation and translocation of authigenic clays under warmer/wetter climates.

Pruned DTs for qualitative ped size class data of angular and subangular blocky structure and quantitative ped size data (i.e., geometric mean of each size class) for all ped types are shown in Fig. 12. Climate, represented by EEMT, was the only important variable for predicting ped size class (Fig. 12a). Fine angular and subangular blocky peds were predicted for environments characterized by EEMT values between approximately 33 and 50 MJ m^{-2} y^{-1}; medium peds were predicted outside that range. Although the reason for this tendency toward finer ped size classes in angular and subangular blocky structure under moderate climates is unclear, we note that the majority of the data (84%) were from samples with EEMT values less than 50 MJ m^{-2} y^{-1}. Thus, this finding might reflect more of a general tendency toward the development of finer peds in soils under warm, humid climates compared to cold, dry climates as (observed in Fig. 6i) instead of a tendency toward fine peds under moderate climates and coarse peds under more extreme climates. This finding appears to be consistent with Baver (1934) who

reported that the percentage of silt and clay particles in surface horizons that were aggregated in a given soil mass decreased with increasing precipitation along a constant isotherm. This was attributed to the loss of inorganic aggregating agents in surface horizons under increasing precipitation. However, temperature relationships with aggregation were more ambiguous in that study with a decrease in percent aggregation observed with increasing temperature under humid climates and an increase in aggregation observed for increasing temperature for semi-arid environments (Baver, 1934). The best predictor for quantitative ped size class was depth (Fig. 12b) where surface horizons were associated with smaller peds (4.6 mm) and subsurface horizons with larger peds (19 mm). This result is consistent with the results in Fig. 4 where an average continuous drop in ped size (albeit qualitative class data) was observed with depth from the surface to over 2.5 m. However, the results in Fig. 12b are likely driven by the predominance of subangular blocky peds in subsurface horizons, which represent considerably larger structural units compared to the granular peds at the surface (Appendix B Fig. B1).

The DTs in Fig. 13 show that clay was the only important variable for predicting both ped grade class (qualitative) and ped grade data (quantitative) where increasing values of clay were associated with stronger grade classes and larger numerical grade values. These results are consistent with Fig. 7a,k that show increasing frequencies of stronger classes with increasing clay content for both surface and subsurface horizons and likely reflect the effectiveness of clay as an aggregating agent strengthening ped expression.

We also used DTs for each 1-cm soil depth interval to examine the importance of various endogenous factors (i.e., clay content, sand content, OC, CEC, CEC/ clay ratio, RD, ESP, Ca/Mg ratio) on quantified soil structure properties. Figure 14 plots the normalized variable importance metrics calculated from the DTs against depth. Organic carbon was the most important variable

at the surface with respect to ped size, steeply dropping below other endogenous variables within approximately the upper 10 cm. Between approximately 10 cm to 30 cm, Ca/Mg ratio was the most important factor influencing ped size with clay content becoming important below 30 cm. Below approximately 80 cm, both CEC and clay content were the most important variables for predicting ped size likely reflecting combined effects of texture and clay mineralogy on the development of ped sizes.

Clay content was the most important factor for ped grade, which is consistent with the results presented in Fig. 13. Both roundness and solidity showed similar importance distributions with depth. Organic carbon was the most important predictor near the surface (0 to ~30 cm). Texture (i.e., clay and sand content) was the most important factor accounting for roundness and solidity between approximately 30 and 75 cm with CEC becoming important below that depth. We interpret this pattern as follows. Ped shape is controlled predominately by SOM near the surface with clay becoming important due to increased cohesiveness below approximately 30 cm. This finding is consistent with Dexter (1985) who found clay and SOM to be correlated with ped roundness and roughness. Clay mineralogy controls ped shape at deeper depths likely because of increased pressures of the overlying soil material as discussed previously. Surprisingly, plant roots were not distinguished from other variables influencing ped grade, size, or shape.

CONCLUSIONS

The most influential factors determining ped shape were the exogenous variables, climate and slope, along with depth. The most important endogenous variables for predicting ped shape were OC, clay content, and mineralogy. Platy, prismatic, and angular blocky peds decreased

under more humid conditions, whereas granular peds in surface horizons and subangular blocky peds in subsurface horizons increased with increasing EEMT (i.e., warmer, more humid climates). These changes were reflected in anisotropic (less round) peds with rougher surfaces in cold and/or dry climates and more equidimensional peds with smoother surfaces in warmer, wetter climates.

Overall, the exogenous variable, EEMT, played the most important role in the development of ped size in surface and subsurface horizons. Warmer, more humid climates (increasing EEMT) promoted the development of smaller ped sizes. In general, ped size was also a function of depth with smaller peds occurring in surface horizons (4.6 mm on average above 25 cm) and larger peds occurring in subsurface horizons (19 mm on average below 25 cm). Clay content was the only important variable affecting ped grade.

Given the importance of soil structure in controlling soil hydraulic properties, our findings suggest that the relationship between soil structure and exogeneous variables such as climate should be further investigated to predict the effect of global climate forcings on soil and near-surface hydrology. We have demonstrated that the development of the large soil dataset in this work (KURDS) opens the door to a rigorous analysis by combining both field- and laboratory-based observations and measurements with ecological and climatological information at a continental scale. Future work using KURDS should benefit from a combined qualitative and quantitative analysis approach similar to that used in this study.

REFERENCES

Anderson, K., S. Wells, and R. Graham. 2002. Pedogenesis of vesicular horizons, Cima Volcanic Field, Mojave desert, California. Soil Science Society of America Journal 66:878-887.

Bailey, R. 1989. Explanatory supplement to ecoregions map of the continents. Environmental Conservation 16:307-309.

Baver, L.D. 1934. A classification of soil structure and its relation to the main soil groups. Soil Science Society of America Journal B15:107-109.

Bishop, T.F.A., A.B. McBratney, and G.M. Laslett. 1999. Modelling soil attribute depth functions with equal-area quadratic smoothing splines. Geoderma 91:27-45.

Blanchart E., P. Lavelle, E. Braudeau, Y. Le Bissonnais, and C. Valentin. 1997. Regulation of soil structure by geophagous earthworm activities in humid savannas of cote d'ivoire. Soil Biol. Biochem. 29:431-439.

Borooah, V.K. 2001. Logit and Probit: Ordered and Multinomial Models. Sage University Papers Series on Quantitative Applications in the Social Sciences, Series No. 138, Sage Publications, Thousand Oaks, CA.

Bronick, C.J., and R. Lal. 2005. Soil structure and management: a review. Geoderma 124:3-22.

Carvalhais, N., M. Forkel, M. Khomik, J. Bellarby, M. Jung, M. Migliavacca, M. Mu, S. Saatchi, M. Santoro, M. Thurner, U. Weber, B. Ahrens, C. Beer, A. Cescatti, J.T. Randerson, and M. Reichstein. 2014. Global covariation of carbon turnover times with climate in terrestrial ecosystems. Nature 514:213-7.

Davidson, E.A., and I.A. Janssens. 2006. Temperature sensitivity of soil carbon decomposition and feedbacks to climate change. Nature 440:165-173.

Dexter, A.R. 1985. Shapes of aggregates from tilled layers of some Dutch and Australian soils. Geoderma 35:91-107.

Dexter, A.R., and B. Kroesbergen. 1985. Methodology for determination of tensile strength of soil aggregates. Journal of Agricultural Engineering Research 31:139-147.

Díaz-Zorita, M., E. Perfect, and J.H. Grove. 2002. Disruptive methods for assessing soil structure. Soil & Tillage Research 64:3-22.

Dontsova, K.M., and L.D. Norton. 2002. Clay dispersion, infiltration, and erosion as influenced by exchangeable Ca and Mg. Soil Sci. 167:184-193.

Drager, K.I., D.R. Hirmas, and S.T. Hasiotis. 2016. Effects of ant (*Formica subsericea*) nests on physical and hydrological properties of a fine-textured soil. Soil Science Society of America Journal 80:364-375.

Dye, P.J., and B.H. Walker. 1980. Vegetation-environment relations on sodic soils of Zimbabwe Rhodesia. J. Ecol. 68:589-606.

Fernández-Ugalde, O., P. Barré, F. Hubert, I. Virto, C. Girardin, E. Ferrage, L. Caner, and C. Chenu. 2013. Clay mineralogy differs qualitatively in aggregate-size classes: clay-mineral-based evidence for aggregate hierarchy in temperate soils. European Journal of Soil Science 64:410-422.

Ghezzehei, T.A. 2012. Soil structure. p. 2-1−2-14. *In* P.M. Huang et al. (Eds.) Handbook of Soil Sciences: Properties and Processes. 2nd ed. CRC Press, Boca Raton, FL.

Hartge, K.-H., and R. Horn. 2016. Essential Soil Physics: An Introduction to Soil Processes, Functions, Structure, and Mechanics. E. Schweizerbart'sche Berlagsbuchhandlung, Stuttgart, Germany.

Hartge, K.H., J. Bachmann, and N. Pesci. 1999. Morphological analysis of aggregate shape. Soil Science Society of America Journal 63:930–933.

Hengl, T., 2017. GSIF: Global Soil Information Facilities. R package version 0.5-4 [online]. Avilable at (https://CRAN.R-project.org/package=GSIF)

Hillel, D. 1998. Environmental Soil Physics. Academic Press, San Diego, CA.

Hirmas, D.R., D. Giménez. 2017. A geometric equation for representing morphological field information in horizons with compound structure. Soil Science Society of America Journal 81:863-867.

Holden, N.M. 1993. A two-dimensional quantification of soil ped shape. Journal of Soil Science 44:209-219.

Holden, N.M. 1995. Temporal variation in ped shape in an old pasture soil. Catena 24:1-11.

Hosmer, D.W., and S. Lemeshow. 2000. Applied Logistic Regression. 2nd ed. John Wiley & Sons Inc., New York.

Jobbágy, E.G., and R.B. Jackson. 2000. The vertical distribution of soil organic carbon and its relation to climate and vegetation. Ecological Application 10:423-436.

Johnson, D.L., and D. Watson-Stegner. 1987. Evolution model of pedogenesis. Soil Science 143:349-366.

Jongmans, A.G., M.M. Pulleman, M. Balabane, F. van Oort, and J.C.Y Marinissen. 2003. Soil structure and characteristics of organic matter in two orchards differing in earthworm activity. Applied Soil Ecology 24:219-232.

Kachigan, S.K. 1991. Multivariate Statistical Analysis: A Conceptual Introduction. 2nd ed. Radius Press, New York.

Kutílek M. 2004. Soil hydraulic properties as related to soil structure. Soil and Tillage Research 79:175-184.

Laity, J.E. 2002. Desert environments. p. 380-401. *In* A.R. Orme (ed.) The Physical Geography of North America. Oxford Univ. Press, New York.

Lander, J.P. 2014. R for Everyone: Advanced Analytics and Graphics. Addison-Wesley, Upper Saddle River, NJ.

Leveque T., Y. Capowiez, E. Schreck, T. Xiong, Y. Foucault, and C. Dumat. 2014. Earthworm bioturbation influences the phytoavailability of metals released by particles in cultivated soils. Environ Pollut 191:199-206.

Lin, H.S., K.J. McInnes, L.P. Wilding, and C.T. Hallmark. 1999. Effects of soil morphology on hydraulic properties: I. quantification of soil morphology. Soil Science Society of America Journal 63:948-954.

Logan, M. 2010. Biostatistical Design and Analysis using R: A Practical Guide. John Wiley & Sons Inc., Hoboken, NJ.

Malone, B.P., B. Minasny, and A. B. McBratney. 2017. Using R for Digital Soil Mapping. Springer, Basel, Switzerland.

Mohammed, A.K., D.R. Hirmas, D. Giménez, R.D. Mandel, and J.R. Miller. 2016. A digital morphometric approach for quantifying ped shape. Soil Science Society of America Journal 80:1604-1618.

Nikiforoff, C.C. 1941. Morphological classification of soil structure. Soil Science 52:193-212.

Oades, J.M. 1993. The role of biology in the formation, stabilization and degradation of soil structure. Geoderma 56:377-400.

Odgers, N.P., Z. Libohova, and J.A. Thompson. 2012. Equal-area spline functions applied to a legacy soil database to create weighted-means maps of soil organic carbon at a continental scale. Geoderma 189-190:153-163.

Peel, M.C., B.L. Finlayson, and T.A. McMahon. 2007. Updated world map of the Köppen-Geiger climate classification. Hydrol. Earth System. Sci. 11:1633–1644.

Peltier, L.C. 1950. The geographic cycle in periglacial regions as it is related to climatic geomorphology. Annals of the American Association of Geographers 40:214-236.

PRISM Climate Group, Oregon State University, http://prism.oregonstate.edu, downloaded 22 Jun 2016.

R Core Team, 2017. R: A language and environment for statistical computing, Ver. 3.4.1. R Foundation for statistical computing. Vienna, Austria.

Rabot, E., M. Wiesmeier, S. Schlüter, and H.J. Vogel. 2018. Soil structure as an indicator of soil functions: A review. Geoderma 314:122-137.

Rasmussen C., K. Heckman, W.R. Wieder, M. Keiluweit, C.R. Lawrence, A.A. Berhe, J.C. Blankinship, S.E. Crow, J.L. Druhan, C.E. Hicks Pries, E. Marin-Spiotta, A.F. Plante, C. Schädel, J.P. Schimel, C.A. Sierra, A. Thompson, and R. Wagai. 2018. Beyond clay: Towards an improved set of variables for predicting soil organic matter content. Biogeochemistry 137:297-306.

Rasmussen, C., and N.J. Tabor. 2007. Applying a quantitative pedogenic energy model across a range of environmental gradients. Soil Science Society of America Journal 71:1719-1729.

Schaefer, C.E.R., and J. Dalrymple. 1995. Pedogenesis and relict properties of soils with columnar structure from Roraima, north Amazonia. Geoderma 71:1-17.

Schaetzl, R.J., and S. Anderson. 2005. Soils: Genesis and Geomorphology. Cambridge Univ. Press, Cambridge.

Schoeneberger, P.J., D.A. Wysocki, E.C. Benham, and Soil Survey Staff. 2012. Field book for describing and sampling soils. Ver. 3.0. Natural Resources Conservation Service, National Soil Survey Center, Lincoln, NE.

Six, J., K. Paustian, E.T. Elliott, and C. Combrink. 2000. Soil structure and organic matter: I. Distribution of aggregate-size classes and aggregate-associated carbon. Soil Science Society of America Journal 64:681-689.

Southard, R.J., and S.W. Buol. 1988. Subsoil blocky structure formation in some North Carolina Paleudults and Paleaquults. Soil Science Society of America Journal 52:1069-1076.

Therneau T., B. Atkinson, and B. Ripley .2017. Rpart: Recursive Partitioning and Regression Trees. R package version 4.1-11 [online]. Available at (https://cran.r project.org/package=rpart)

Therneau, T.M., E.J. Atkinson, and Mayo Foundation. 2018. An Introduction to Recursive Partitioning using the RPART Routines. Available at (https://cran.r project.org/web/packages/rpart/vignettes/longintro.pdf)

Turk, J.K., and R.C. Graham. 2011. Distribution and properties of vesicular horizons in the western United States. Soil Science Society of America Journal 75:1449-1461.

Turk, J.K., and R.C. Graham. 2014. Analysis of vesicular porosity in soils using high resolution X-ray computed tomography. Soil Science Society of America Journal 78:868-880.

Turk, J.K., O.A. Chadwick, and R.C. Graham. 2012. Pedogenic processes. p. 30-1–30-29. P.M. Huang et al. (Eds.) Handbook of Soil Sciences: Properties and Processes. 2nd ed. CRC Press, Boca Raton, FL.

Venables, W.N., and B.D. Ripley. 2002. Modern Applied sSatistics with S. 4th ed. Springer, New York.

Warrick A.W. 2002. Soil Physics Compaion. CRC Press, Boca Raton, FL.

Table 1. Köppen-Geiger (KG) climate classification, mean effective energy and mass transfer (EEMT), mean annual precipitation (MAP), mean annual temperature (MAT), and the ecoregion province in each KG climate region of the USA that occurred the most frequently (mode) for the University of Kansas Research Dataset of Soils (KURDS).

KG Climate Region	Symbol	Mean EEMT [MJ m^{-2} y^{-1}]	Mean MAP [mm]	Mean MAT [ºC]	Ecoregion Province
Tropical Monsoon	Am	72.57	1435	24	Everglades
Tropical Savanna	Aw	67.49	1354	24	Everglades
Hot Low-Latitude Steppe	BSh	19.21	363	19	American Semi-Desert and Desert
Cold Midlatitude Steppe	BSk	11.83	372	11	California Dry Steppe
Hot Low-Latitude Desert	BWh	15.34	203	20	American Semi-Desert and Desert
Cold Midlatitude Desert	BWk	10.74	238	12	Intermountain Semi-Desert and Desert
Humid Subtropical Hot-Summer	Cfa	46.77	1174	15	Eastern Broadleaf Forest (Continental)
Marine West-Coast	Cfb	71.54	2035	11	Central Appalachian Broadleaf Forest – Coniferous Forest –
Mediterranean Dry-Summer Hot	Csa	31.66	907	14	Sierran Steppe – Mixed Forest – Coniferous Forest – Alpine
Mediterranean Dry-Summer warm	Csb	49.83	1406	12	Sierran Steppe – Mixed Forest – Coniferous Forest – Alpine
Humid Continental Hot-Summer	Dfa	30.87	1021	12	Eastern Broadleaf Forest (Continental)
Humid Continental Mild-Summer	Dfb	13.03	786	6	Laurentian Mixed Forest
Marine West-Coast Cool Summer	Dfc	6.70	738	3	Southern Rocky Mountains Steppe – Open Woodland – Coniferous Forest – Alpine
Warm Continental-Mediterranean Continenteal	Dsa	13.74	682	8	Northren Rocky Mountains Forest – Steppe – Coniferous Forest – Alpine Meadow
Temperate Continental-Mediterraneant Continental	Dsb	13.30	720	8	Sierran Steppe – Mixed Forest – Coniferous Forest – Alpine Meadow
Cool Continental	Dsc	14.27	841	6	Central Appalachian Broadleaf Forest – Coniferous Forest – Meadow
Humid Continental Hot-Summer	Dwa	9.97	639	7	Prairie Parkland (Temperate)
Subarctic	Dwb	7.10	520	5	Great Plains-Palouse Dry Steppe
Tundra	ET	5.58	812	2	Southern Rocky Mountains Steppe – Open Woodland – Coniferous Forest – Alpine Meadow

Table 2. Summary of the selection criteria used to create the dataset investigating soil structure in this study. The *N* column represents the total number of the respective feature in KURDS.

Selection Criteria	*N*	Notes
		Parent Material
Alluvium	26,352	Values of "slope alluvium", "valley side alluvium", and " alluvium" were selected
Residuum	15,774	Values of "residuum" were selected
Till	9,705	Values of "ablation till", "basal till", "flow till", "lodgement till", "melt-out till", "subglacial till", "supraglacial till", and "till" were selected
Loess	12,908	Values of "calcareous loess", "non-calcareous loess", and "loess" were selected
		Taxonomy
Alfisols	21,848	
Aridisols	2,097	
Mollisols	16,073	
Ultisols	1,905	
		Horizons
A horizon	5,857	Excluded buried horizons, lithologic discontinuities, and plowed layers; midpoint depth less than or equal to 25 cm of the mineral soil surface were selected
B horizon	1,609	Excluded buried horizons and lithologic discontinuities; midpoint depth greater than 25 cm of the mineral soil surface were selected
		Drainage Class
Somewhat poorly drained	10,454	
Moderately well drained	17,877	
Well drained	41,589	
Somewhat excessively drained	3,063	
Excessively drained	1,603	

Table 3. Summary of the variables, transformations, and statistical analyses used in this study. Response variables in this study are also endogenous variables.

Variables†	Variable Type	Cont. Data Trans.‡	Norm. Trans.§	Statistical Analyses¶
Ped type class	Response			MLR, DT
Ped roundess	Response	PSDM		DT
Ped solidity	Response	PSDM		DT
Ped size class	Response			MLR, DT
Ped size [mm]	Response	GM		DT
Ped grade class	Response			MLR, DT
Ped grade	Response	OV		DT
Clay [%]	Endogenous		$x^{1/2}$	MLR, DT
Sand [%]	Endogenous		$x^{1/2}$	MLR, DT
OC [%]	Endogenous		$\ln(x + 0.01)$	MLR, DT
CEC [$cmol_c\ kg^{-1}$]	Endogenous		$x^{1/2}$	MLR, DT
CEC/Clay	Endogenous		$\ln(x + 0.01)$	MLR, DT
ESP [%]	Endogenous		$\ln(x + 0.01)$	MLR, DT
Ca/Mg	Endogenous		$\ln(x + 0.01)$	MLR, DT
RD	Endogenous		$\ln(x + 0.00001)$	MLR, DT
Köppen-Gieger class	Exogenous			MLR#
EEMT [$MJ\ m^{-2}\ y^{-1}$]	Exogenous		$\ln(x + 0.01)$	MLR, DT
Ecoregion province	Exogenous			MLR#
Slope [%]	Exogenous		$\ln(x + 0.01)$	MLR, DT
Parent material	Exogenous			MLR, DT

† Clay, sand, and organic carbon (OC) percentages are given on a weight basis. Root density (RD) is given as a volumetric fraction. CEC, cation exchange capacity; ESP, exchangeable sodium percentage; EEMT, effective energy and mass transfer.

‡ Continuous data transformation. Ped shape data were converted from categorical variables to continuous using the predicted values presented in Mohammed et al. (2016) at an unalikeability coefficient equal to zero using the Ped Shape Digital Morphometric (PSDM) database. Size was converted to continuous data using the geometric mean (GM) of the size class for each size category. Grade values were assigned arbitrary ordinal values (OV) between 1 and 3 for weak and strong structure, respectively.

§ Normality transformation. Values of either 0.01 or 0.00001 were added to the respective variable (x) prior to taking the natural logarithm to avoid taking the logarithm of zero. Any normality transformations were used for both multinomial logistic regression and decision trees.

¶ MLR, multinomial logistic regression; DT, decision tree.

Results of these analyses are presented in Appendix B.

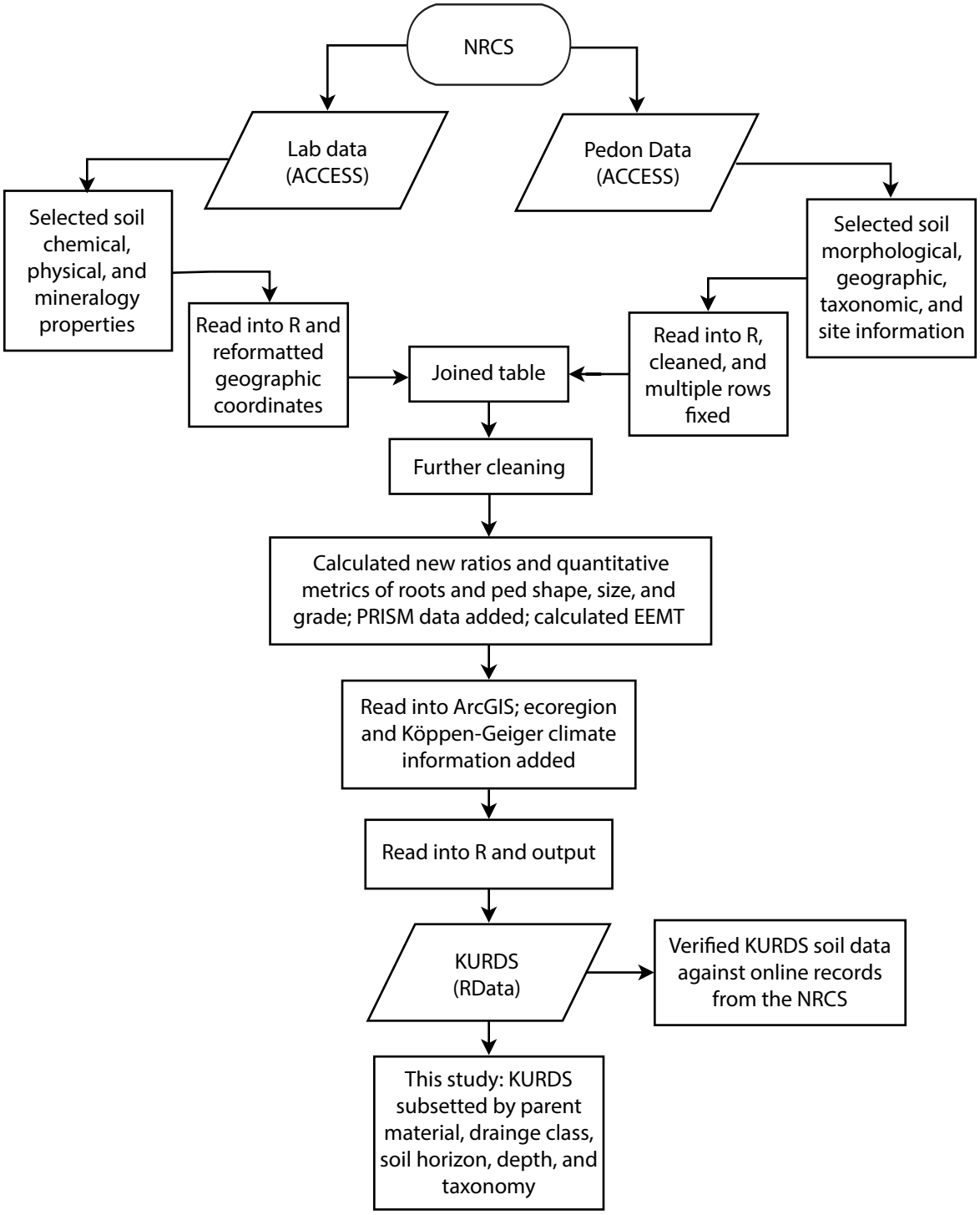

Fig. 1. Flowchart illustrating the procedure for assembling the University of Kansas Research Dataset of Soils (KURDS) and subset used in this study. See text for more explanation.

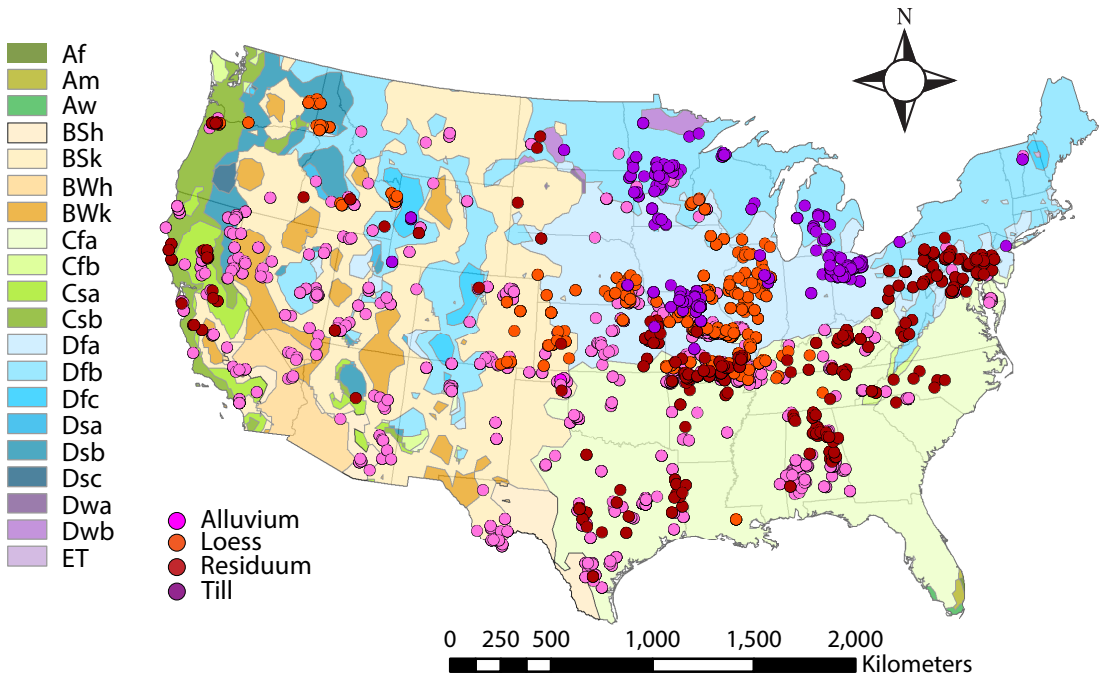

Fig. 2. Geographical distribution of the pedons (N = 1,602) used in this study (selected from KURDS) overlain on Köppen-Geiger climate regions in the conterminous USA. The color of points correspond to broad soil parent material classes. See Table 1 for an explanation of the Köppen-Geiger climate classes. For simplification, two pedons are omitted from this map that occurred in the Hawaii.

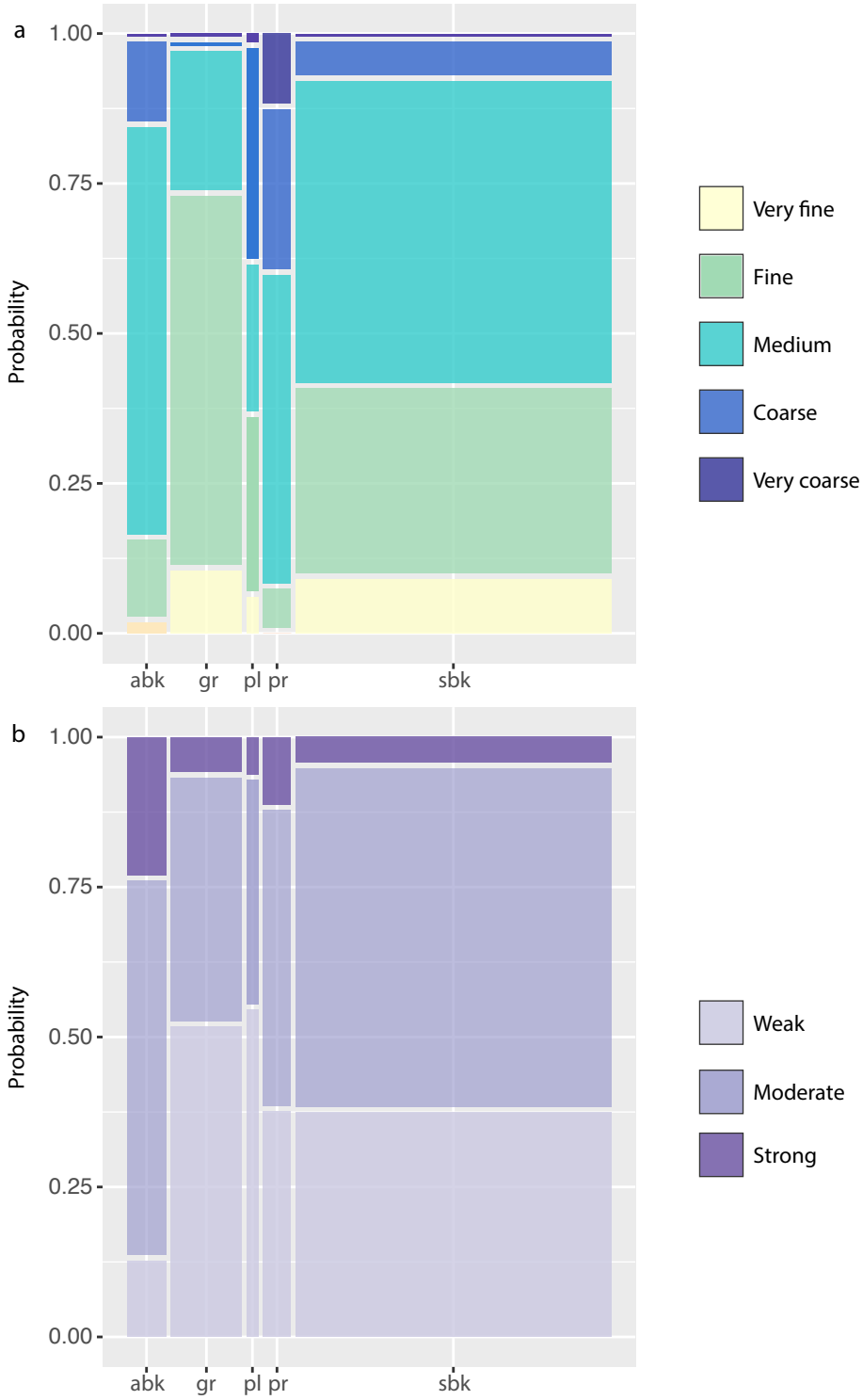

Fig. 3. Mosaic plots showing the multinomial logistic regression predicted probabilities of (a) ped size and (b) grade for each ped type (abk = angular blocky; gr = granular; pl = platy; pr = prismatic; sbk = subangular blocky). Intermediate ped size and grade classes were removed prior to analyzing the data with multinomial logistic regression. Width of the boxes corresponds to how many observations fall into the category.

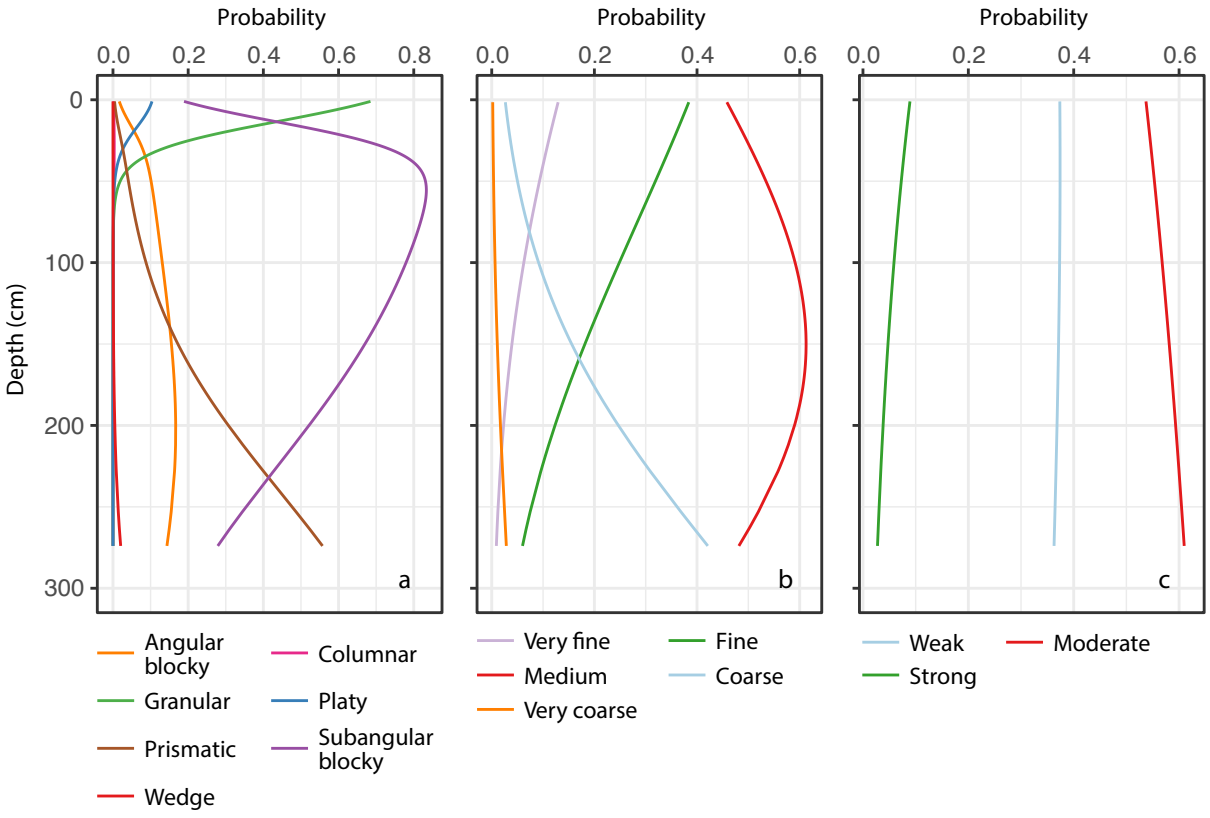

Fig. 4. Multinomial logistic regression predicted probabilities of (a) ped type class, (b) size class, and (c) grade class as a function of depth. Intermediate ped size and grade classes (e.g., very fine to fine or weak to moderate) were removed prior to multinomial logistic regression analysis. Only angular and subangular blocky peds are considered in (b).

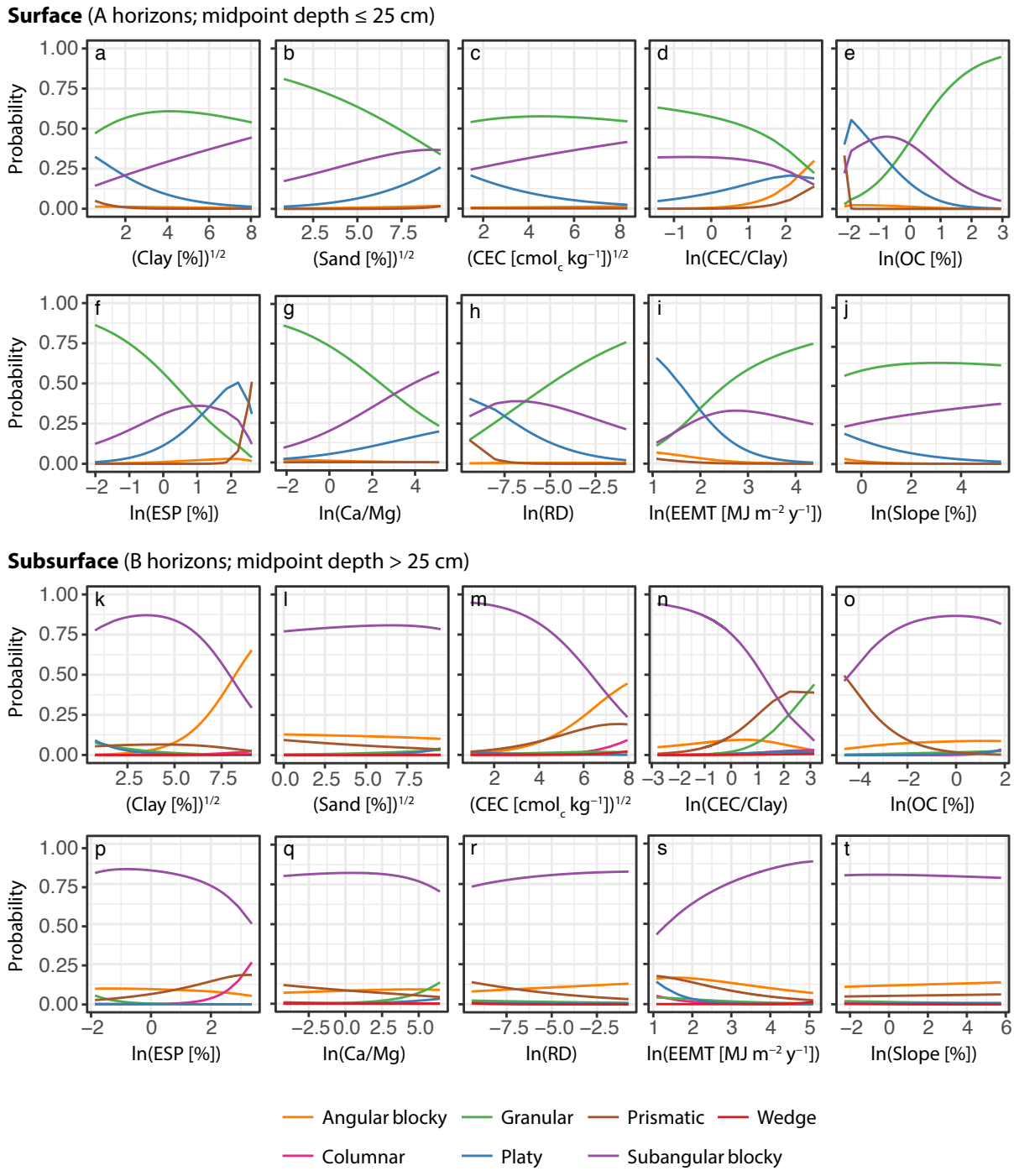

Fig. 5. Multinomial logistic regression plots showing the probability of predicting ped type given endogenous (a-h and k-r) and exogenous (i-j and s-t) variables for both surface (a-j) and subsurface (k-t) soil horizons.

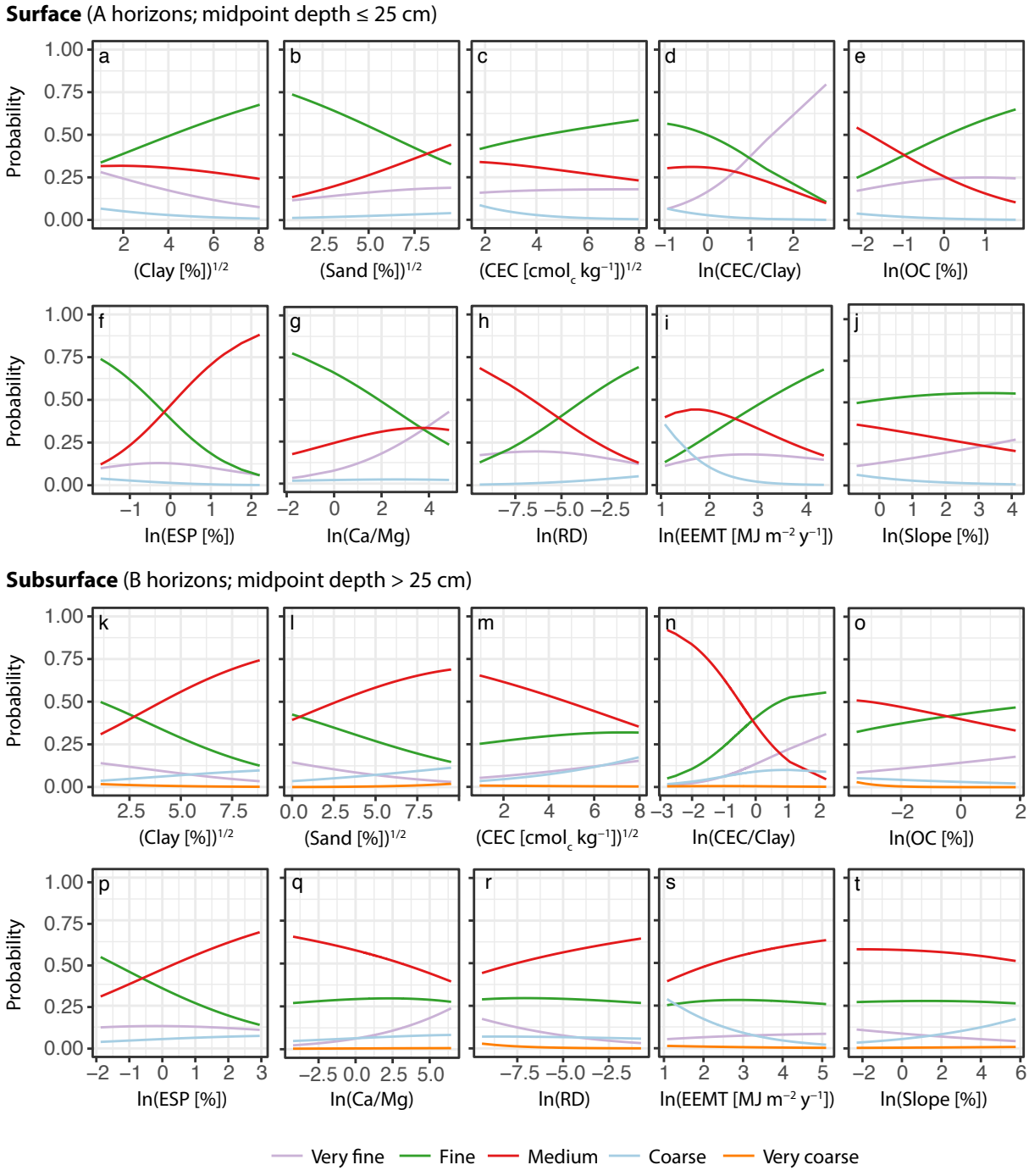

Fig. 6. Multinomial logistic regression plots showing the probability of predicting angular and subangular blocky ped sizes given endogenous (a-h and k-r) and exogenous (i-j and s-t) variables for both surface (a-j) and subsurface (from k-t) soil horizons. Intermediate size classes (e.g., very fine to fine) were removed prior to analyzing the data with multinomial logistic regression.

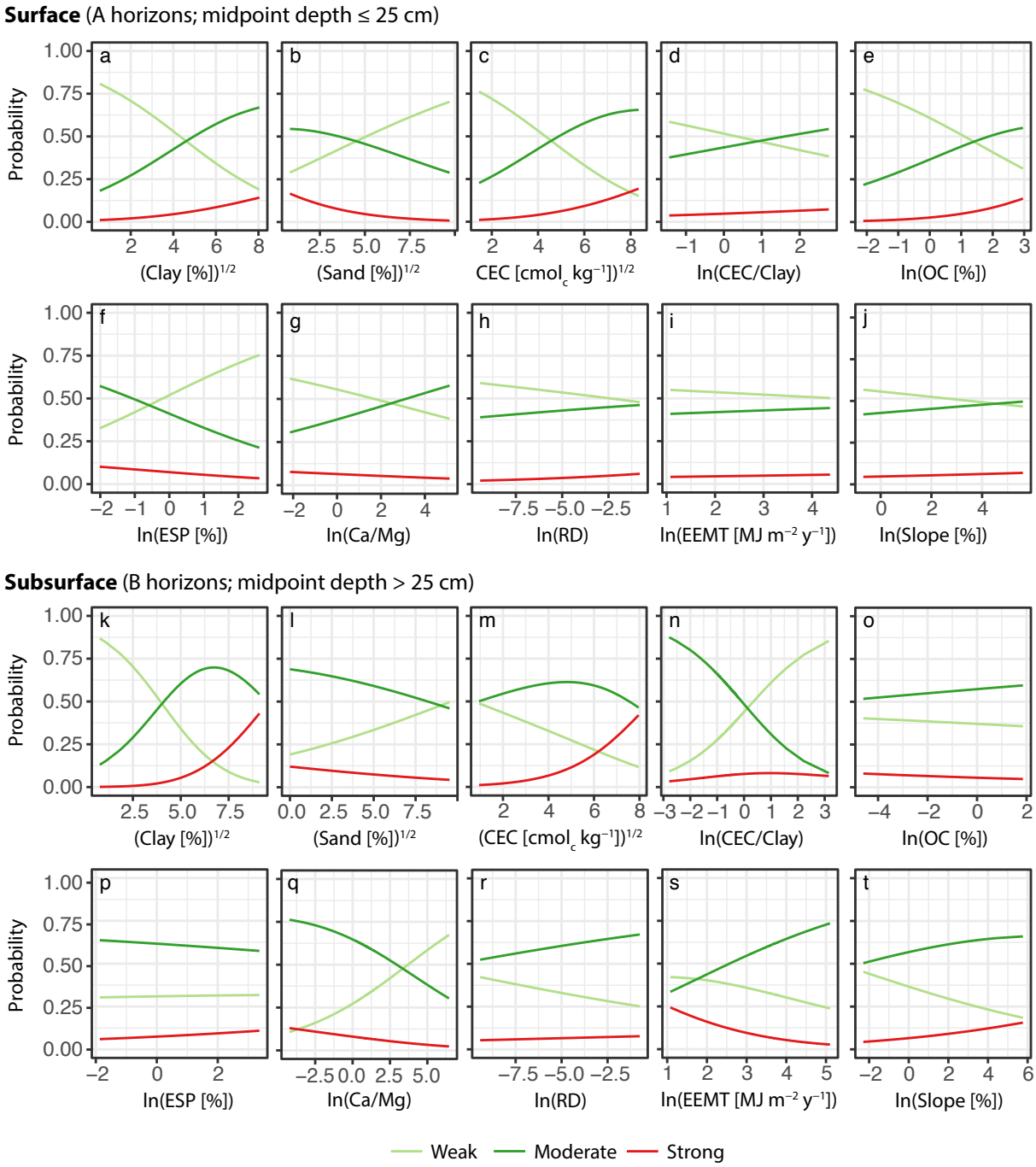

Fig. 7. Multinomial logistic regression plots showing the probability of predicting ped grade class given endogenous (a-h and k-r) and exogenous (i-j and s-t) variables for both surface (a-j) and subsurface (from k-t) soil horizons. Intermediate grade classes (e.g., weak to moderate) were removed prior to analyzing the data with mulinomial logistic regression.

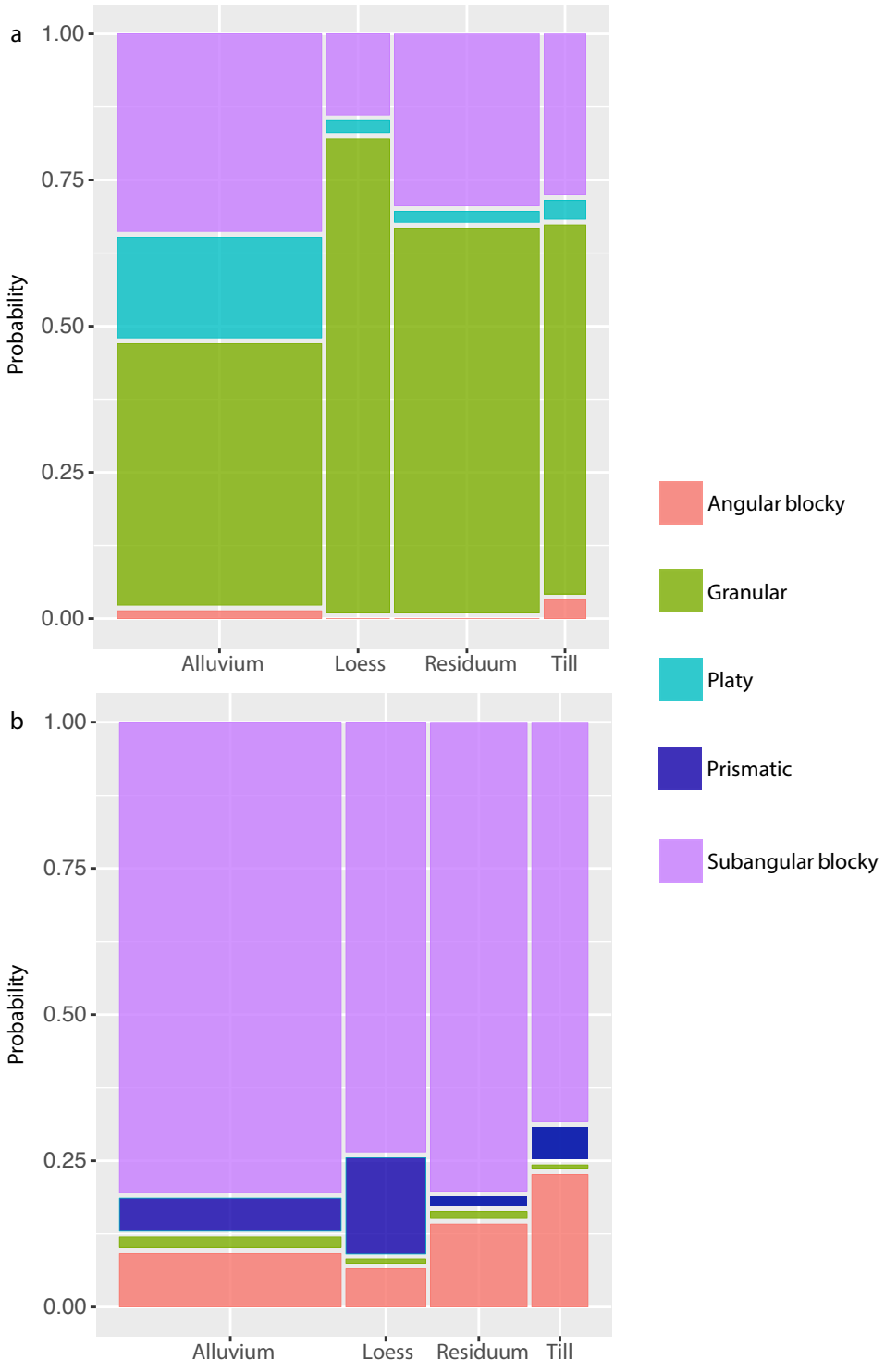

Fig. 8. Mosaic plots showing the multinomial logistic regression predicted probabilities of ped types for both (a) surface and (b) subsurface horizons for each parent material considered in this study. Width of the boxes corresponds to how many observations fall into the category.

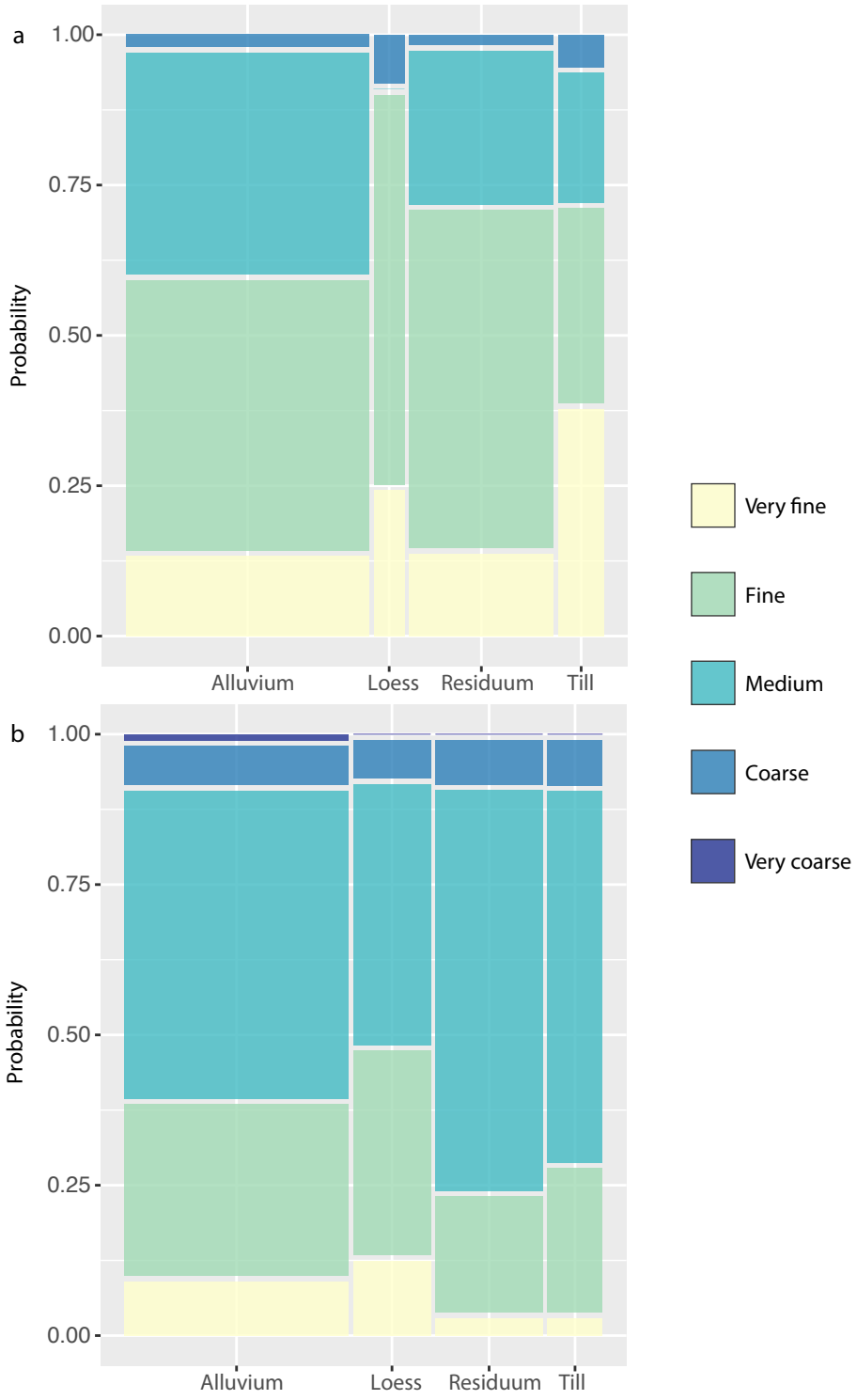

Fig. 9. Mosaic plots showing the multinomial logistic regression predicted probabilities of angular and subangular blocky ped sizes for both (a) surface and (b) subsurface horizons for each parent material considered in this study. Intermediate size classes (e.g., very fine to fine) were removed prior to analyzing the data with multinomial logistic regression. Width of the boxes corresponds to how many observations fall into the category.

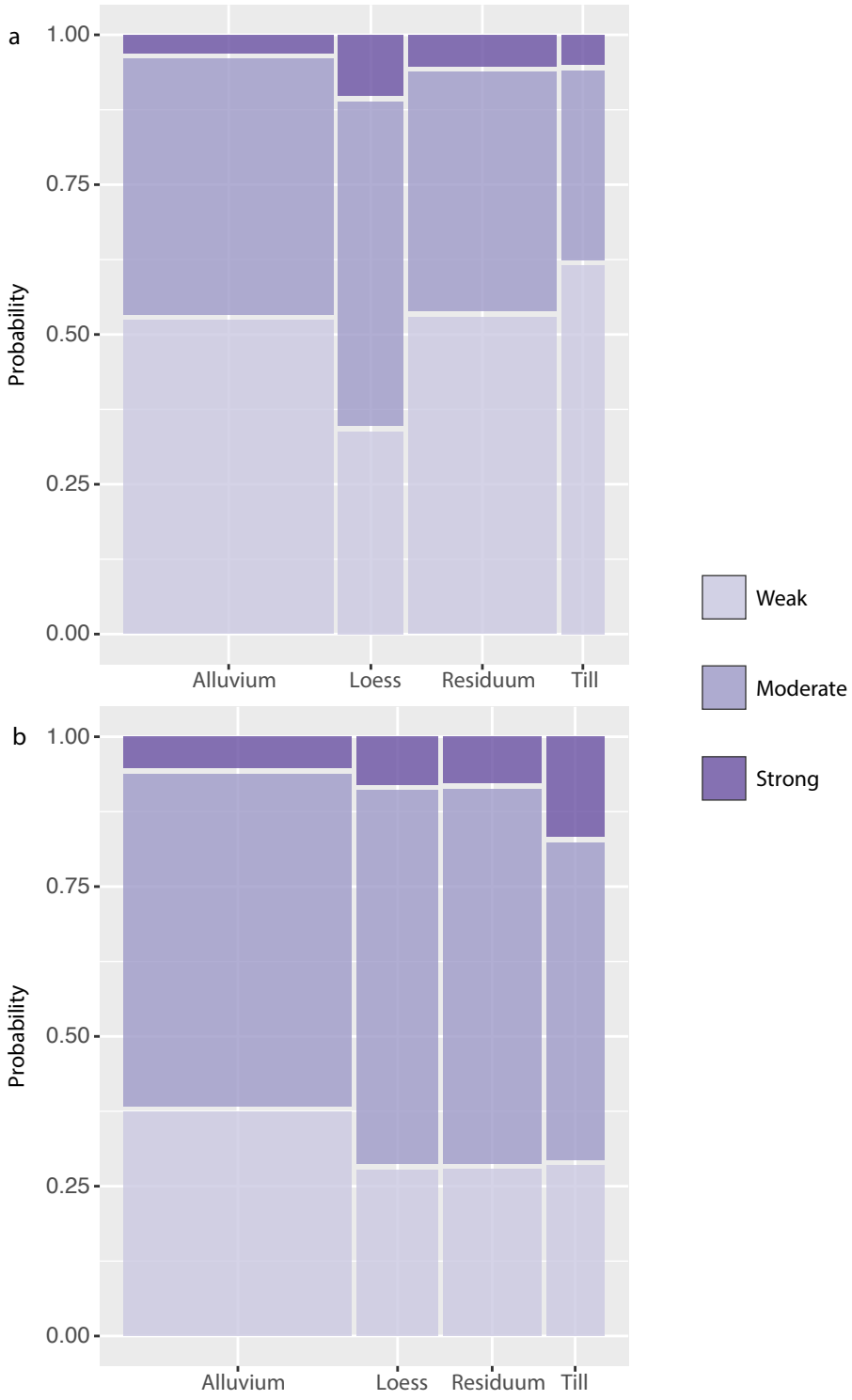

Fig. 10. Mosaic plots showing the multinomial logistic regression predicted probabilities of structural grade classes for both (a) surface and (b) subsurface horizons for each parent material considered in this study. Intermediate grade classes (e.g., weak to moderate) were removed prior to analyzing the data with mulinomial logistic regression. Width of the boxes corresponds to how many observations fall into the category.

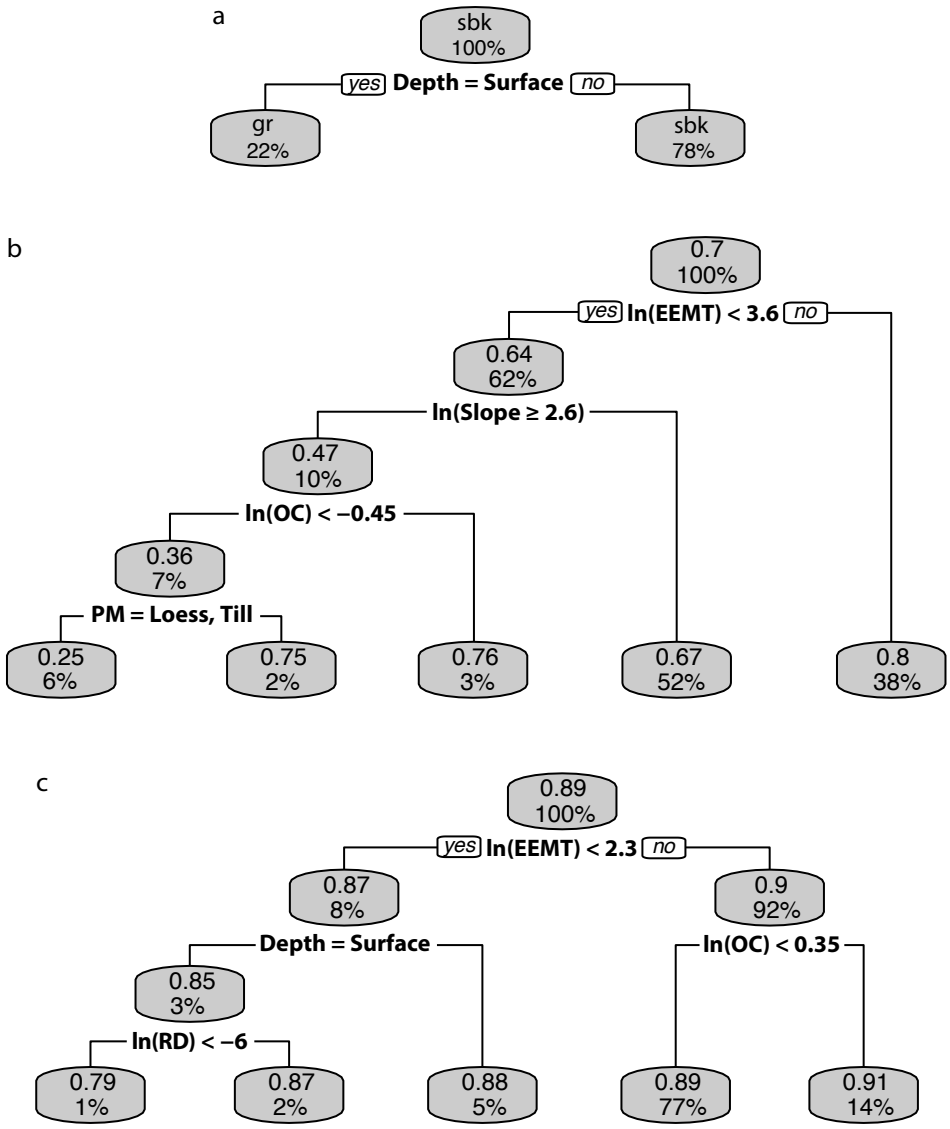

Fig. 11. Pruned decision trees showing predicted (a) ped types (gr = granular; sbk = subangular blocky), (b) ped roundness, and (c) ped solidity across all parent materials (PM) for both surface and subsurface horizons used in this study. All endogenous variables and the exogenous variables—EEMT, slope, and parent material—were included as predictors in these decision trees.

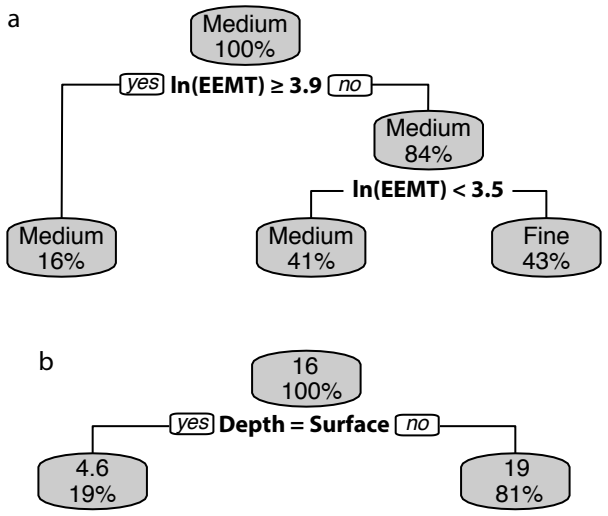

Fig. 12. Pruned decision trees showing predicted (a) ped size (includes only angular and subangular blocky peds) and (b) quantified ped size (includes all ped types) across all parent materials for both surface and subsurface horizons used in this study. All endogenous variables and the exogenous variables—EEMT, slope, and parent material—were included as predictors in these decision trees.

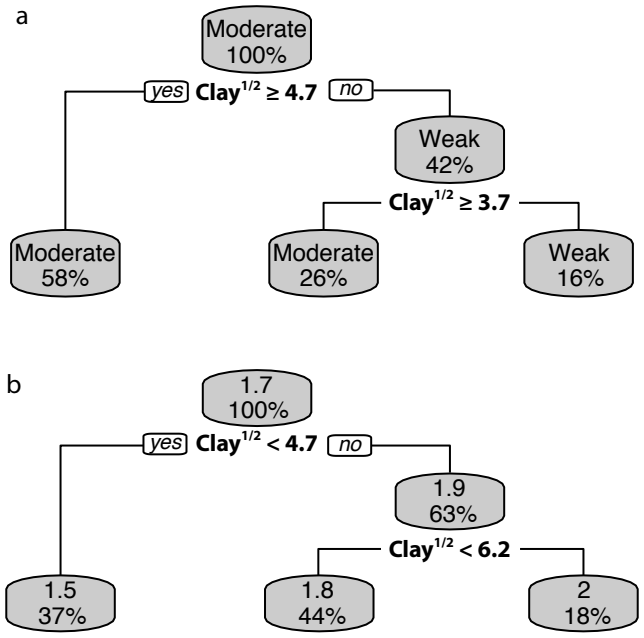

Fig. 13. Pruned decision trees showing predicted (a) grade class and (b) structural grade (ordinal scale) across all parent materials for both surface and subsurface horizons used in this study. All endogenous variables and the exogenous variables—EEMT, slope, and parent material—were included as predictors in these decision trees.

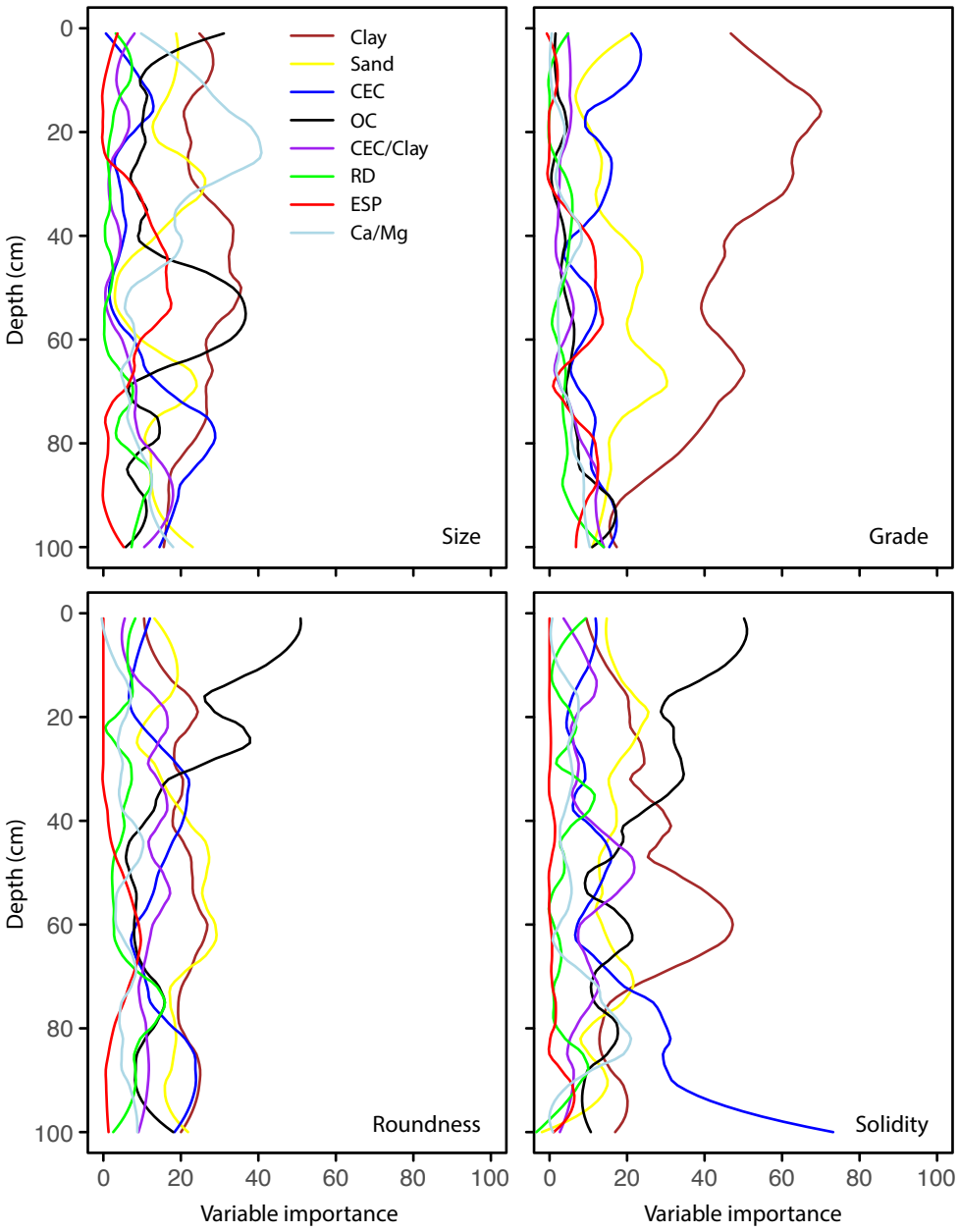

Fig. 14. Plots of the normalized variable importance metric derived from decision tree analysis of each depth interval (1 cm). Decision trees were used to predict quantified ped size, grade, roundness, and solidity separately across all parent materials considered in this study. Only independent variables that varied with depth (i.e., clay, sand, CEC, CEC/clay ratio, root denisty, ESP, and Ca/Mg ratio) were considered in this analysis. Only pedons with contiguous horizons beginning with the surface horizon that met the criteria listed in Table 2 were used in this analysis (N = 1,086). We used an equal-area spline to place all variables on the same scale (i.e., 1 cm) prior to analysis. The resulting variable importance curves were plotted by depth and smoothed using the mean calculated from a 25-cm moving depth window.

CHAPTER 4. CONCLUSIONS

Soil structure is described by three morphological properties: size, shape, and grade. These morphological properties develop as a result of complex interactions between exogenous and endogenous properties and are important because they influence soil hydrological properties and processes through alterations in pore-size distributions. In this work, we develop a new method for quantitatively describing one of these morphological properties—ped shape—in the form of morphometric indices and demonstrate its usefulness in examining continental-scale soil structural development.

We changed typical categorical and subjective descriptions of peds into continuous quantitative shape data in Chapter 2. Shape metrics such as circularity and width to height ratio were examples of the continuous variables allowing significant differences between ped shapes to be detected. We used the intercept of regressed unalikeability coefficients, which account for the quality of each ped, to predict idealized ped shape metrics. The results of the survey used in this study (Appendix A) showed that participant ability to recognize prismatic structure was positively influenced by education and expertise, suggesting that the correct identification of prisms requires more training and experience. The numerical values assigned to each ped shape in this study may open up the opportunity to study soil structure and model hydrologic processes at regional and continental scales without the need to resample (i.e., using photographs of previously sampled soil pits). We argue that digital shape metrics from this study could also be used to consistently convert morphological descriptions of soil structure into numeric shape indices.

In Chapter 3, we assembled a large soil structure database called KURDS. The dataset included a wide range of environmental, morphological, physical, and chemical soil properties

for the USA. We show that exogenous variables such as climate and slope, were the best predictors of ped shape. When the effects of exogenous variables were removed, endogenous variables such as soil organic carbon, clay content, and the mineralogical proxy, CEC, best predicted ped shape. Platy, prismatic, and angular blocky peds decreased in frequency under warmer, more humid conditions, whereas granular peds in surface horizons and subangular blocky peds in subsurface horizons increased under these climates. In cold and/or dry climates, the proportion of anisotropic peds increased. Equidimensional peds increased in warmer, wetter climates. Effective energy and mass transfer (EEMT), a climatological parameter integrating mean annual precipitation (MAP) and mean annual temperature (MAT), was the best predictor for ped size in both surface and subsurface horizons. Warmer and wetter climates developed smaller peds, in general, for a given depth. Clay content was the only important variable affecting ped grade.

The findings in this dissertation suggest that climate affects the development of soil structure by controlling the dominance of either 'breaking down' mechanisms (e.g., freeze/thaw or wet/dry cycles) or 'building up' mechanisms (e.g., fungal hyphae enmeshing or clay cohesion) that ultimately define either a separation or aggregation pedogenic pathway, respectively. The link between climate and the development of soil structure should be explored further, especially given the importance of this morphological property to soil hydrology.

This dissertation demonstrates the importance of analyzing soil structure at a continental scale using quantitative and qualitative descriptions. The combination of field- and laboratory-based observations and measurements with ecological and climatological information provided new insights into broad-scale pedogenic processes.

APPENDIX A. A SURVEY FOR QUANTIFYING PED TYPE FROM SOIL PROFILE PHOTOGRAPHS

Quantifying ped shape from profile photographs

Quantifying ped type from soil profile photographs

In this survey you will see a series of photographs of digitized ped types. The silhouettes linked to each photograph outline recognizable peds. The soil profile photographs you will see throughout the survey are photographs taken of pit excavation walls. No edits have been made to the photos. Silhouettes outline peds within each photograph and are marked by a dashed line that links the silhouette to the location where it was outlined in the photograph.

Each participant will be given (53) questions. Four of these questions will ask about your background and experience with soil structure. The rest of the questions will ask you to classify the ped types represented in the photos. Please use your visual judgment and experience to complete this survey.

The survey is expected to take between 30 and 40 minutes to complete.

Please follow the instructions provided and click next to go to the next page. Please do not forget to click "Done" once you answer all the questions. NOTE: Your answers will not be recorded if you close the browser before clicking "Done."

Please feel free to contact the survey developer, Aoesta Mohammed (aoesta.k@ku.edu), or the PI, Daniel Hirmas (hirmas@ku.edu) if you have any questions regarding this survey.

Thank you for your assistance with this research project.

Quantifying ped shape from profile photographs

Quantifying ped type from soil profile photographs

Information Statement

The Department of Geography at the University of Kansas supports the practice of protection for human subjects participating in research. The following information is provided for you to decide whether you wish to participate in the present study. You should be aware that even if you agree to participate, you are free to withdraw at any time without penalty.

We are conducting this study to better understand the shape of soil structure. This will entail your completion of a survey. Your participation is expected to take approximately 30 minutes to complete. The content of the survey should cause no more discomfort than you would experience in your everyday life.

Although participation may not benefit you directly, we believe that the information obtained from this study will help us gain an ability to better quantify ped shape and understand how ped shape interacts with soil forming processes. Your participation is solicited, although strictly voluntary. Your name will not be associated in any way with the research findings and personally identifiable information will not be collected in this survey. It is possible, however, with internet communications, that through intent or accident someone other than the intended recipient may see your response.

If you would like additional information concerning this study before or after it is completed, please feel free to contact us by phone or mail.

Completion of the survey indicates your willingness to take part in this study and that you are at least 18 years old. If you have any additional questions about your rights as a research participant, you may call (785) 864-7429 or write the Human Subjects Committee Lawrence Campus (HSCL), University of Kansas, 2385 Irving Hill Road, Lawrence, Kansas 66045-7563, email irb@ku.edu.

Sincerely,

Aoesta Mohammed
Ph.D. Candidate
Investigator
Department of Geography
Lindley Hall
University of Kansas
Lawrence, KS 66045
(785) 864-5143
aoesta.k@ku.edu

Daniel Hirmas
Associate Professor
Faculty Supervisor
Department of Geography
Lindley Hall
University of Kansas
Lawrence, KS 66045
(785) 864-5542
hirmas@ku.edu

Quantifying ped shape from profile photographs

Background and Experience

*** 1. Please indicate the highest level of education that you have completed:**

- ○ Doctorate
- ○ Masters
- ○ Bachelors
- ○ Other (please specify)

*** 2. Please indicate the number of years of experience you have describing soils in the field:**

- ○ 0-5 years
- ○ 5-10 years
- ○ 11-25 years
- ○ 26 years or more

*** 3. Which of following best describes your current sector of employment?**

- ○ K-12 Education
- ○ Higher Education (including faculty, post doctoral scholar, or student)
- ○ Government
- ○ Private Sector
- ○ Other (please specify)

4. If you selected Higher Education in the last question, which of the following best describes your current position:

- ◯ Faculty member
- ◯ Graduate student
- ◯ Post doctoral researcher
- ◯ Undergraduate student
- ◯ Other (please specify)

Quantifying ped shape from profile photographs

What is the type of structure for the image bellow

*** 5. Which of the following type categories BEST describes the peds represented in the photo above?**

	platy	angular blocky	subangular blocky	granular	columnar	prism	wedge	N/A
39-1	○	○	○	○	○	○	○	○

Quantifying ped shape from profile photographs

What is the type of structure for the image bellow

*** 6. Which of the following type categories BEST describes the peds represented in the photo above?**

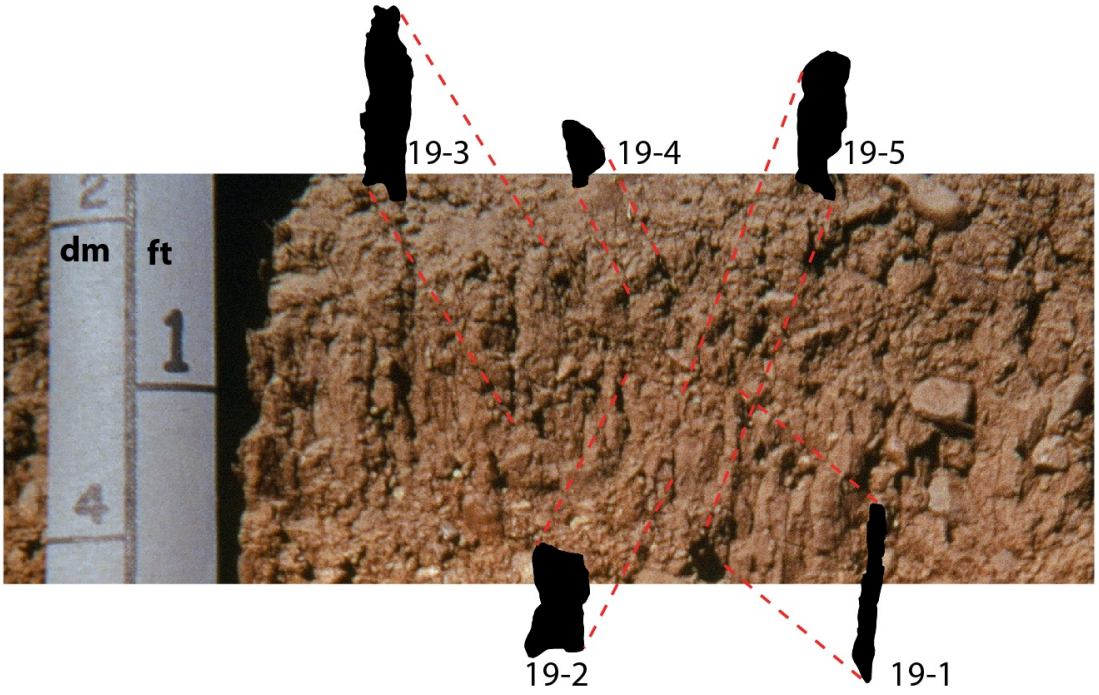

	platy	angular blocky	subangular blocky	granular	columnar	prism	wedge	N/A
19-1	○	○	○	○	○	○	○	○
19-2	○	○	○	○	○	○	○	○
19-3	○	○	○	○	○	○	○	○
19-4	○	○	○	○	○	○	○	○
19-5	○	○	○	○	○	○	○	○

Quantifying ped shape from profile photographs

What is the type of structure for the image bellow

*** 7. Which of the following type categories BEST describes the peds represented in the photo above?**

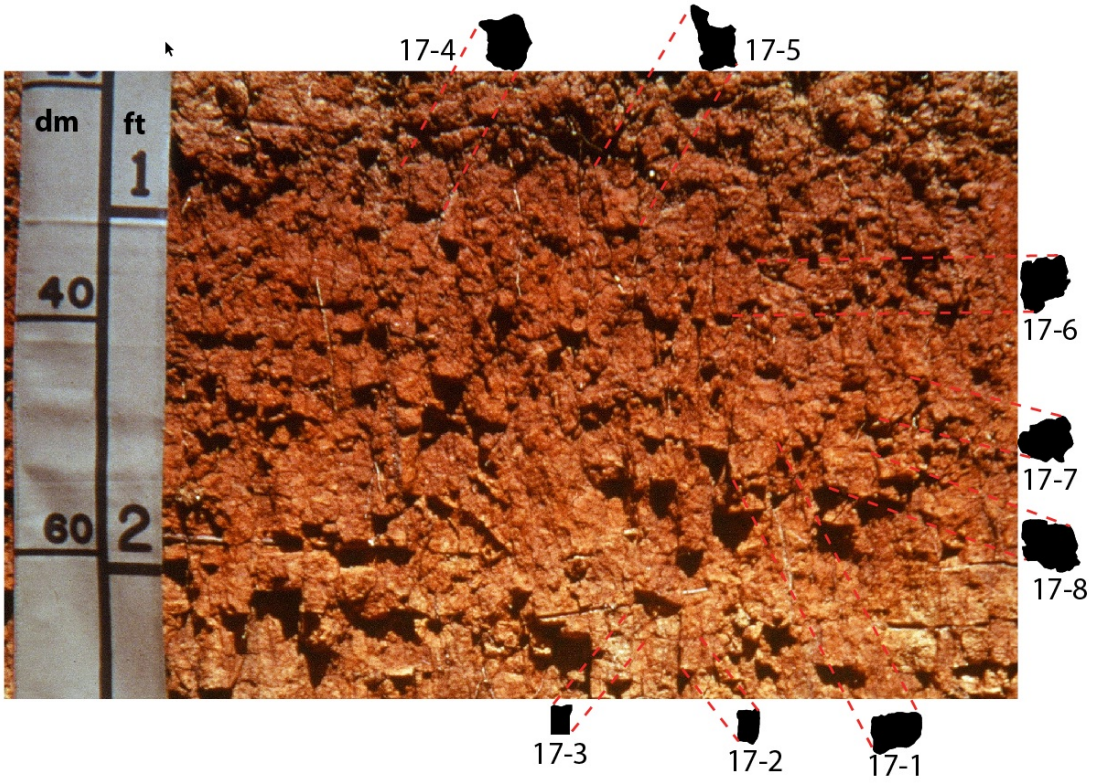

	platy	angular blocky	subangular blocky	granular	columnar	prism	wedge	N/A
17-1	○	○	○	○	○	○	○	○
17-2	○	○	○	○	○	○	○	○
17-3	○	○	○	○	○	○	○	○
17-4	○	○	○	○	○	○	○	○
17-5	○	○	○	○	○	○	○	○
17-6	○	○	○	○	○	○	○	○
17-7	○	○	○	○	○	○	○	○
17-8	○	○	○	○	○	○	○	○

Quantifying ped shape from profile photographs

What is the type of structure for the image bellow

*** 8. Which of the following type categories BEST describes the peds represented in the photo above?**

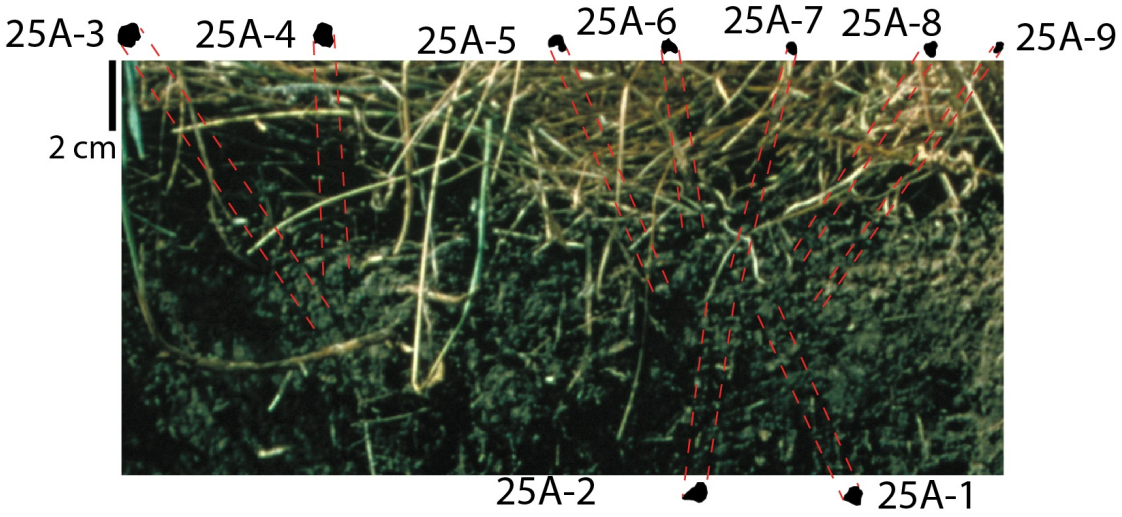

	platy	angular blocky	subangular blocky	granular	columnar	prism	wedge	N/A
25A-1	○	○	○	○	○	○	○	○
25A-2	○	○	○	○	○	○	○	○
25A-3	○	○	○	○	○	○	○	○
25A-4	○	○	○	○	○	○	○	○
25A-5	○	○	○	○	○	○	○	○
25A-6	○	○	○	○	○	○	○	○
25A-7	○	○	○	○	○	○	○	○
25A-8	○	○	○	○	○	○	○	○
25A-9	○	○	○	○	○	○	○	○

Quantifying ped shape from profile photographs

What is the type of structure for the image bellow

*** 9. Which of the following type categories BEST describes the peds represented in the photo above?**

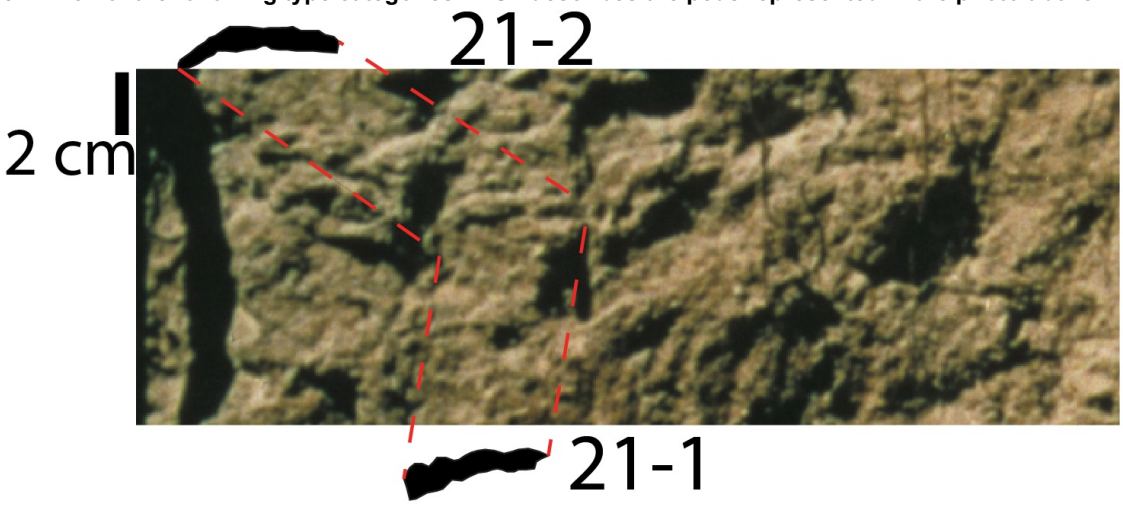

	platy	angular blocky	subangular blocky	granular	columnar	prism	wedge	N/A
21-1	○	○	○	○	○	○	○	○
21-2	○	○	○	○	○	○	○	○

Quantifying ped shape from profile photographs

What is the type of structure for the image bellow

*** 10. Which of the following type categories BEST describes the peds represented in the photo above?**

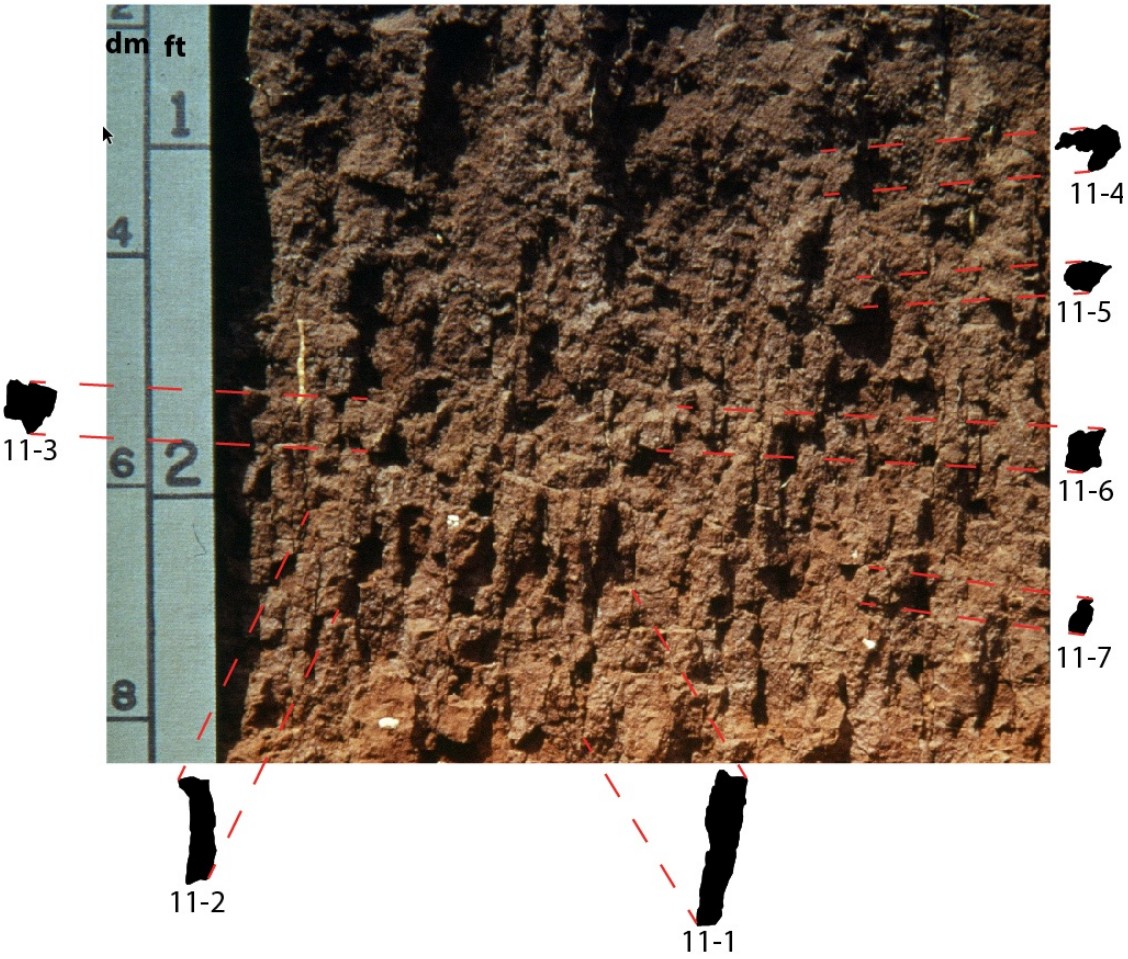

	platy	angular blocky	subangular blocky	granular	columnar	prism	wedge	N/A
11-1	○	○	○	○	○	○	○	○
11-2	○	○	○	○	○	○	○	○
11-3	○	○	○	○	○	○	○	○
11-4	○	○	○	○	○	○	○	○
11-5	○	○	○	○	○	○	○	○
11-6	○	○	○	○	○	○	○	○
11-7	○	○	○	○	○	○	○	○

Quantifying ped shape from profile photographs

Copy of page: What is the type of structure for the image bellow

*** 11. Which of the following type categories BEST describes the peds represented in the photo above?**

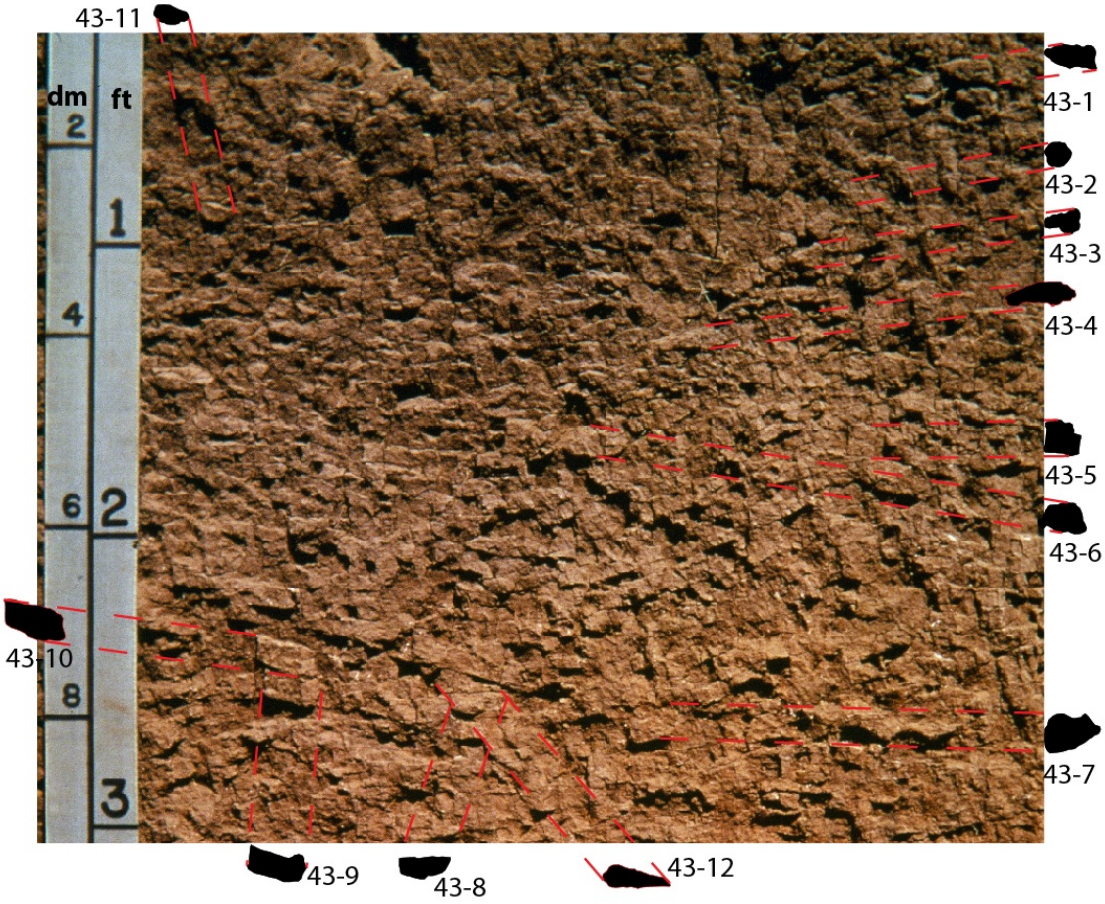

	platy	angular blocky	subangular blocky	granular	columnar	prism	wedge	N/A
43-1	○	○	○	○	○	○	○	○
43-2	○	○	○	○	○	○	○	○
43-3	○	○	○	○	○	○	○	○
43-4	○	○	○	○	○	○	○	○
43-5	○	○	○	○	○	○	○	○
43-6	○	○	○	○	○	○	○	○

	platy	angular blocky	subangular blocky	granular	columnar	prism	wedge	N/A
43-7	◯	◯	◯	◯	◯	◯	◯	◯
43-8	◯	◯	◯	◯	◯	◯	◯	◯
43-9	◯	◯	◯	◯	◯	◯	◯	◯
43-10	◯	◯	◯	◯	◯	◯	◯	◯
43-11	◯	◯	◯	◯	◯	◯	◯	◯
43-12	◯	◯	◯	◯	◯	◯	◯	◯

Quantifying ped shape from profile photographs

What is the type of structure for the image bellow

*** 12. Which of the following type categories BEST describes the peds represented in the photo above?**

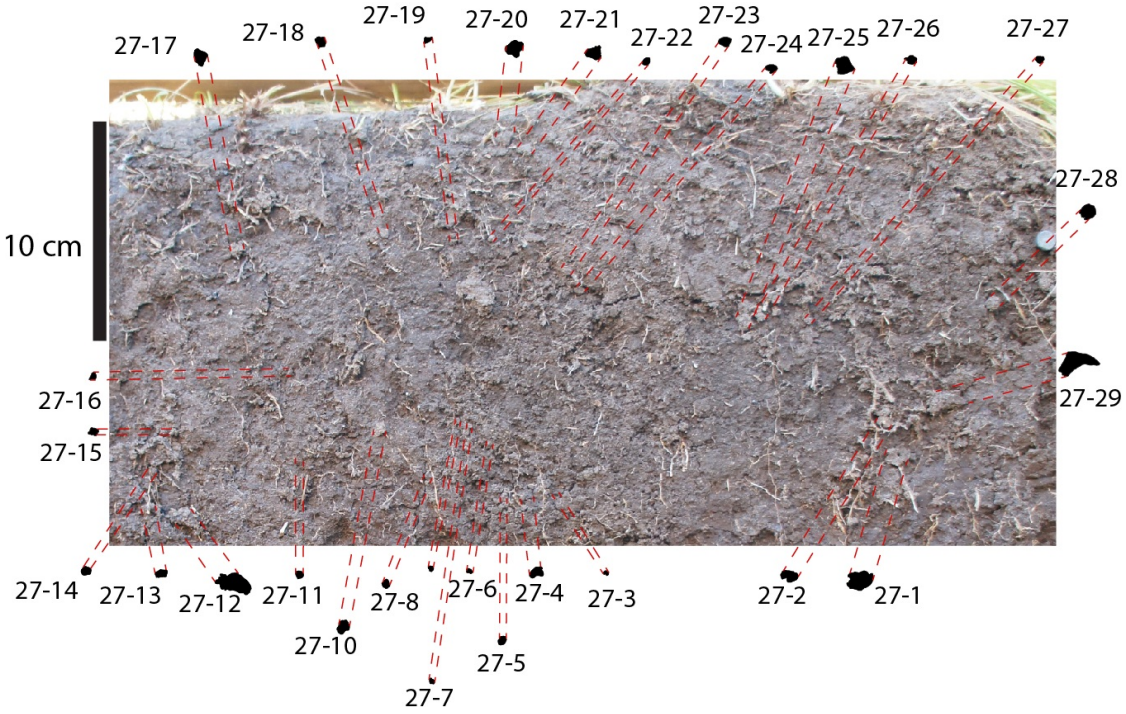

	platy	angular blocky	subangular blocky	granular	columnar	prism	wedge	N/A
27-1	○	○	○	○	○	○	○	○
27-2	○	○	○	○	○	○	○	○
27-3	○	○	○	○	○	○	○	○
27-4	○	○	○	○	○	○	○	○
27-5	○	○	○	○	○	○	○	○
27-6	○	○	○	○	○	○	○	○
27-7	○	○	○	○	○	○	○	○
27-8	○	○	○	○	○	○	○	○
27-9	○	○	○	○	○	○	○	○
27-10	○	○	○	○	○	○	○	○

	platy	angular blocky	subangular blocky	granular	columnar	prism	wedge	N/A
27-11	○	○	○	○	○	○	○	○
27-12	○	○	○	○	○	○	○	○
27-13	○	○	○	○	○	○	○	○
27-14	○	○	○	○	○	○	○	○
27-15	○	○	○	○	○	○	○	○
27-16	○	○	○	○	○	○	○	○
27-17	○	○	○	○	○	○	○	○
27-18	○	○	○	○	○	○	○	○
27-19	○	○	○	○	○	○	○	○
27-20	○	○	○	○	○	○	○	○
27-21	○	○	○	○	○	○	○	○
27-22	○	○	○	○	○	○	○	○
27-23	○	○	○	○	○	○	○	○
27-24	○	○	○	○	○	○	○	○
27-25	○	○	○	○	○	○	○	○
27-26	○	○	○	○	○	○	○	○
27-27	○	○	○	○	○	○	○	○
27-28	○	○	○	○	○	○	○	○
27-29	○	○	○	○	○	○	○	○

Quantifying ped shape from profile photographs

What is the type of structure for the image bellow

*** 13. Which of the following type categories BEST describes the peds represented in the photo above?**

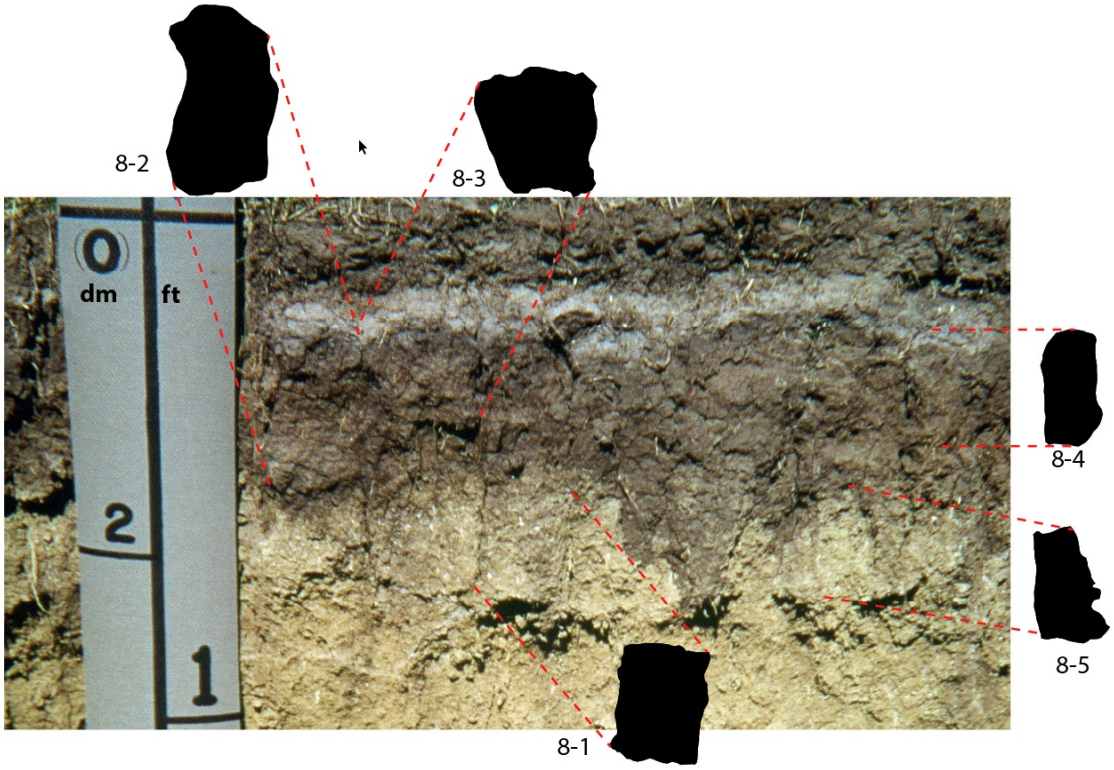

	platy	angular blocky	subangular blocky	granular	columnar	prism	wedge	N/A
8-1	○	○	○	○	○	○	○	○
8-2	○	○	○	○	○	○	○	○
8-3	○	○	○	○	○	○	○	○
8-4	○	○	○	○	○	○	○	○
8-5	○	○	○	○	○	○	○	○

Quantifying ped shape from profile photographs

What is the type of structure for the image bellow

*** 14. Which of the following type categories BEST describes the peds represented in the photo above?**

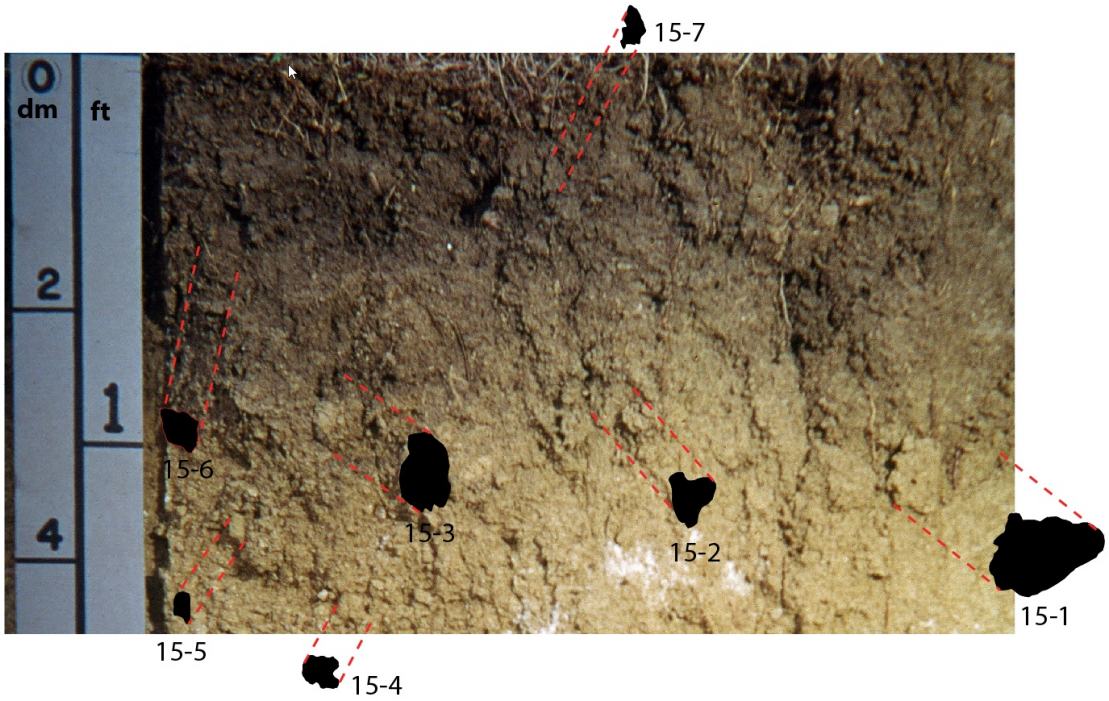

	platy	angular blocky	subangular blocky	granular	columnar	prism	wedge	N/A
15-1	○	○	○	○	○	○	○	○
15-2	○	○	○	○	○	○	○	○
15-3	○	○	○	○	○	○	○	○
15-4	○	○	○	○	○	○	○	○
15-5	○	○	○	○	○	○	○	○
15-6	○	○	○	○	○	○	○	○
15-7	○	○	○	○	○	○	○	○

Quantifying ped shape from profile photographs

What is the type of structure for the image bellow

*** 15. Which of the following type categories BEST describes the peds represented in the photo above?**

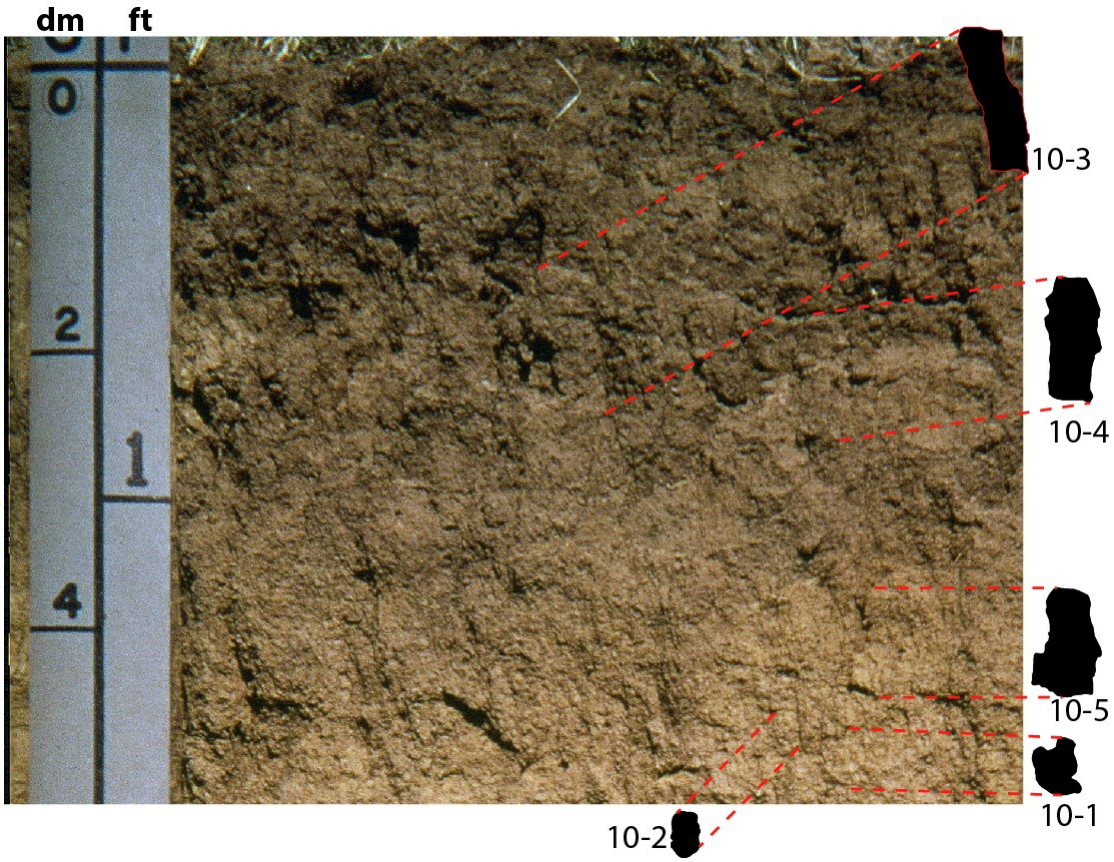

	platy	angular blocky	subangular blocky	granular	columnar	prism	wedge	N/A
10-1	○	○	○	○	○	○	○	○
10-2	○	○	○	○	○	○	○	○
10-3	○	○	○	○	○	○	○	○
10-4	○	○	○	○	○	○	○	○
10-5	○	○	○	○	○	○	○	○

Quantifying ped shape from profile photographs

What is the type of structure for the image bellow

*** 16. Which of the following type categories BEST describes the peds represented in the photo above?**

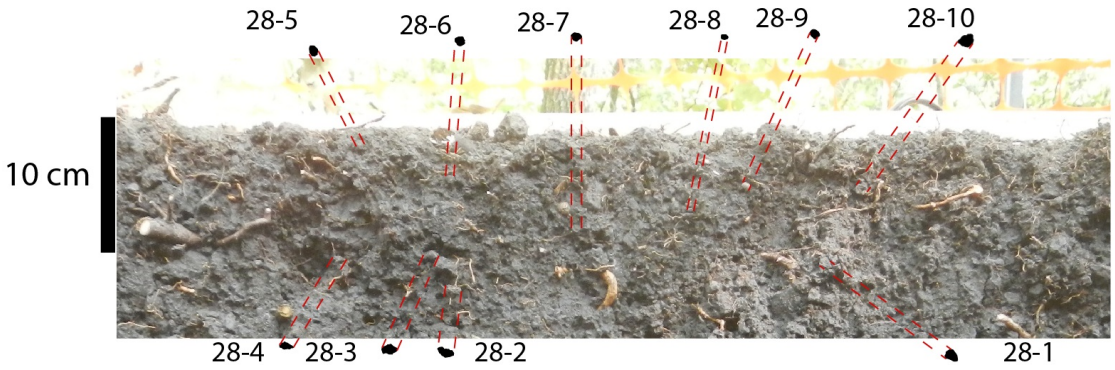

	platy	angular blocky	subangular blocky	granular	columnar	prism	wedge	N/A
28-1	○	○	○	○	○	○	○	○
28-2	○	○	○	○	○	○	○	○
28-3	○	○	○	○	○	○	○	○
28-4	○	○	○	○	○	○	○	○
28-5	○	○	○	○	○	○	○	○
28-6	○	○	○	○	○	○	○	○
28-7	○	○	○	○	○	○	○	○
28-8	○	○	○	○	○	○	○	○
28-9	○	○	○	○	○	○	○	○
28-10	○	○	○	○	○	○	○	○

Quantifying ped shape from profile photographs

What is the type of structure for the image bellow

*** 17. Which of the following type categories BEST describes the peds represented in the photo above?**

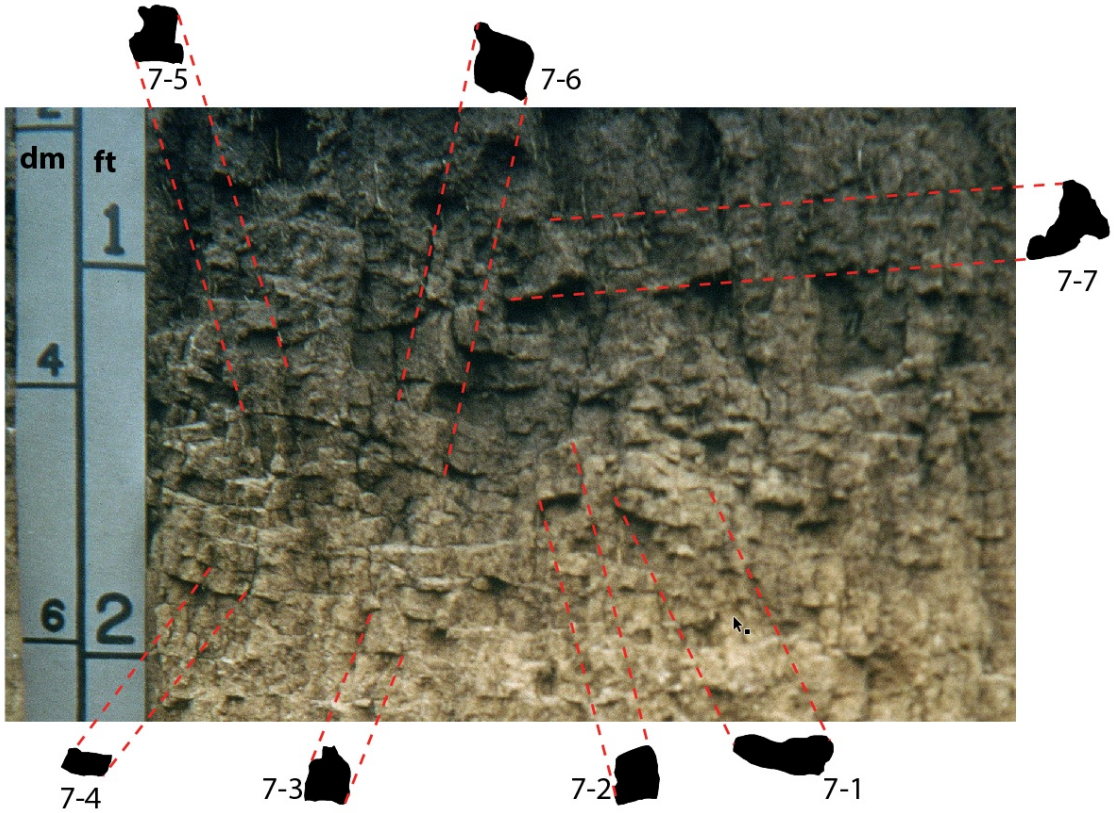

	platy	angular blocky	subangular blocky	granular	columnar	prism	wedge	N/A
7-1	○	○	○	○	○	○	○	○
7-2	○	○	○	○	○	○	○	○
7-3	○	○	○	○	○	○	○	○
7-4	○	○	○	○	○	○	○	○
7-5	○	○	○	○	○	○	○	○
7-6	○	○	○	○	○	○	○	○
7-7	○	○	○	○	○	○	○	○

Quantifying ped shape from profile photographs

What is the type of structure for the image bellow

*** 18. Which of the following type categories BEST describes the peds represented in the photo above?**

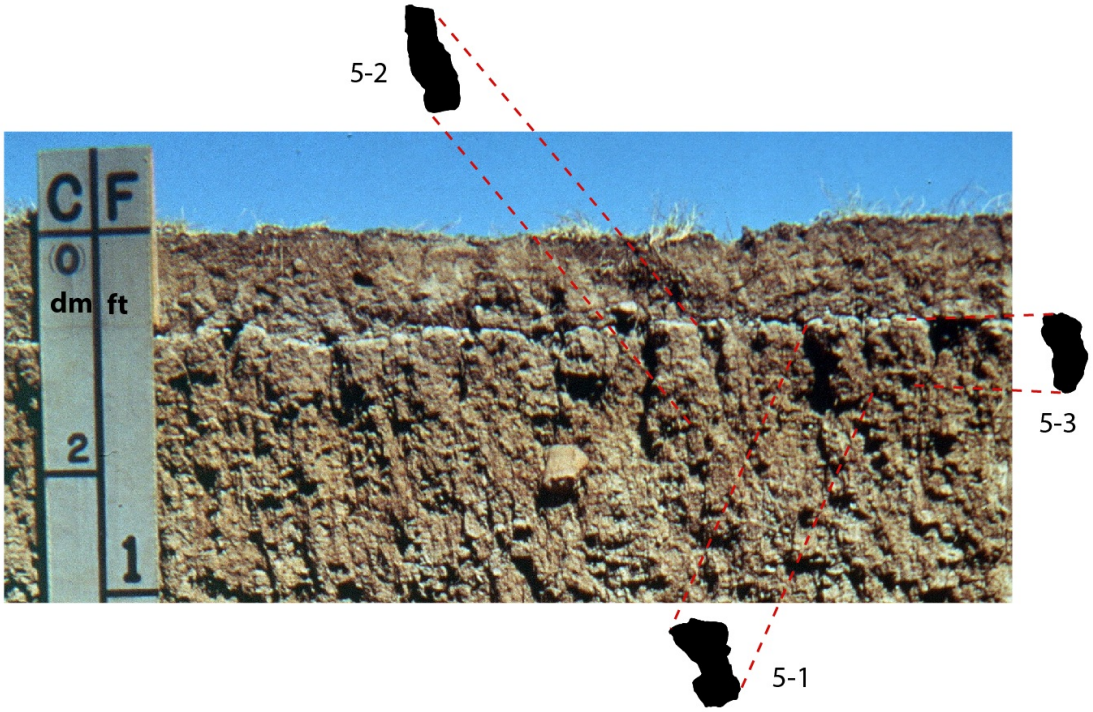

	platy	angular blocky	subangular blocky	granular	columnar	prism	wedge	N/A
5-1	○	○	○	○	○	○	○	○
5-2	○	○	○	○	○	○	○	○
5-3	○	○	○	○	○	○	○	○

Quantifying ped shape from profile photographs

What is the type of structure for the image bellow

*** 19. Which of the following type categories BEST describes the peds represented in the photo above?**

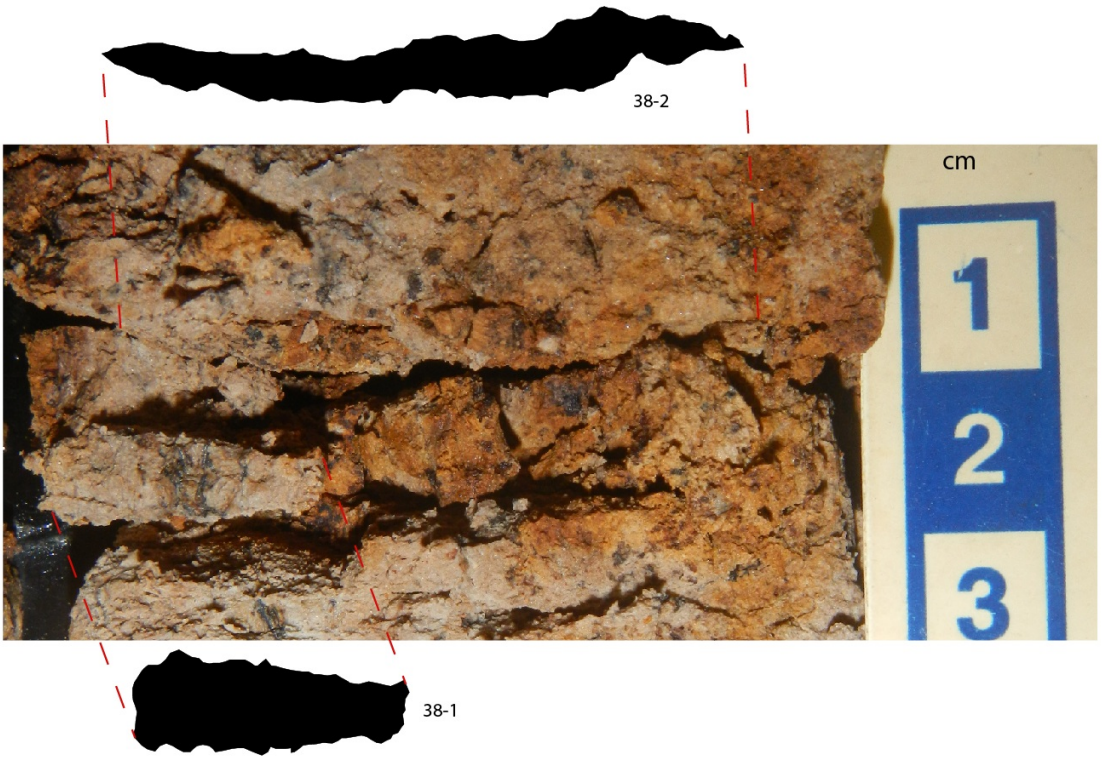

	platy	angular blocky	subangular blocky	granular	columnar	prism	wedge	N/A
38-1	◯	◯	◯	◯	◯	◯	◯	◯
38-2	◯	◯	◯	◯	◯	◯	◯	◯

Quantifying ped shape from profile photographs

What is the type of structure for the image bellow

*** 20. Which of the following type categories BEST describes the peds represented in the photo above?**

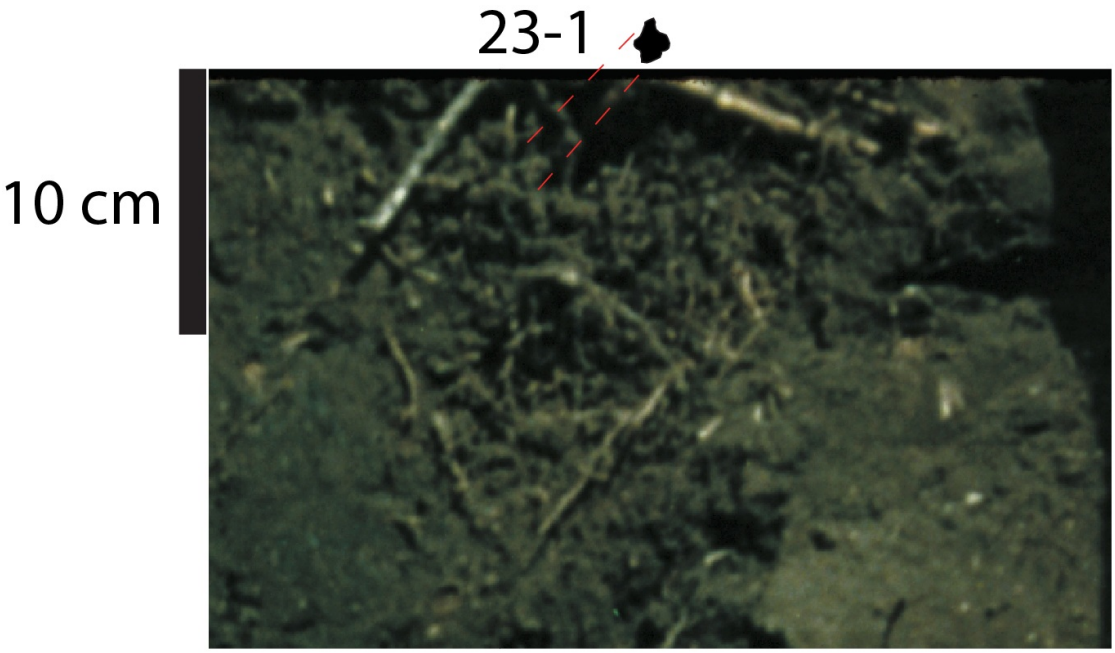

	platy	angular blocky	subangular blocky	granular	columnar	prism	wedge	N/A
23-1	○	○	○	○	○	○	○	○

Quantifying ped shape from profile photographs

What is the type of structure for the image bellow

*** 21. Which of the following type categories BEST describes the peds represented in the photo above?**

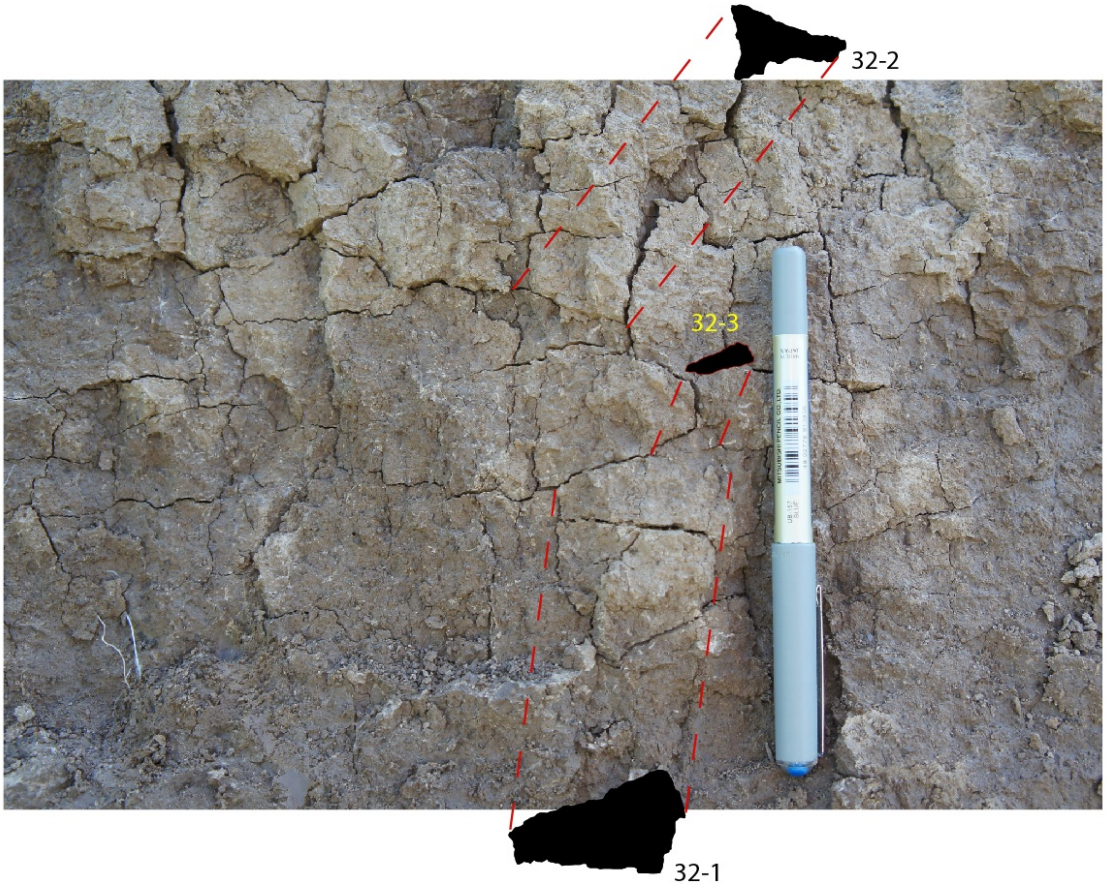

	platy	angular blocky	subangular blocky	granular	columnar	prism	wedge	N/A
32-1	○	○	○	○	○	○	○	○
32-2	○	○	○	○	○	○	○	○
32-3	○	○	○	○	○	○	○	○

Quantifying ped shape from profile photographs

What is the type of structure for the image bellow

*** 22. Which of the following type categories BEST describes the peds represented in the photo above?**

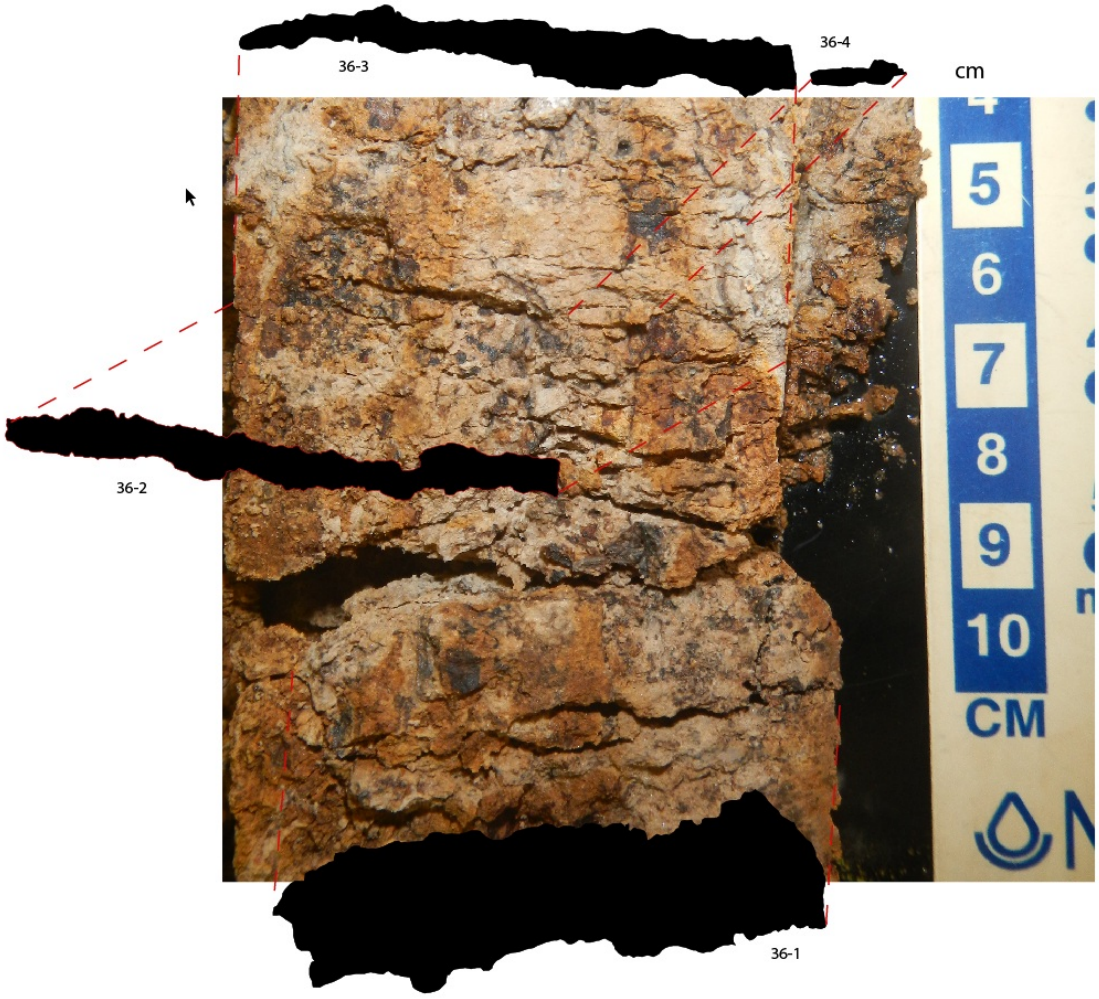

	platy	angular blocky	subangular blocky	granular	columnar	prism	wedge	N/A
36-1	○	○	○	○	○	○	○	○
36-2	○	○	○	○	○	○	○	○
36-3	○	○	○	○	○	○	○	○
36-4	○	○	○	○	○	○	○	○

Quantifying ped shape from profile photographs

What is the type of structure for the image bellow

*** 23. Which of the following type categories BEST describes the peds represented in the photo above?**

	platy	angular blocky	subangular blocky	granular	columnar	prism	wedge	N/A
33-1	◯	◯	◯	◯	◯	◯	◯	◯
33-2	◯	◯	◯	◯	◯	◯	◯	◯
33-3	◯	◯	◯	◯	◯	◯	◯	◯
33-4	◯	◯	◯	◯	◯	◯	◯	◯

Quantifying ped shape from profile photographs

Copy of page: What is the type of structure for the image bellow

*** 24. Which of the following type categories BEST describes the peds represented in the photo above?**

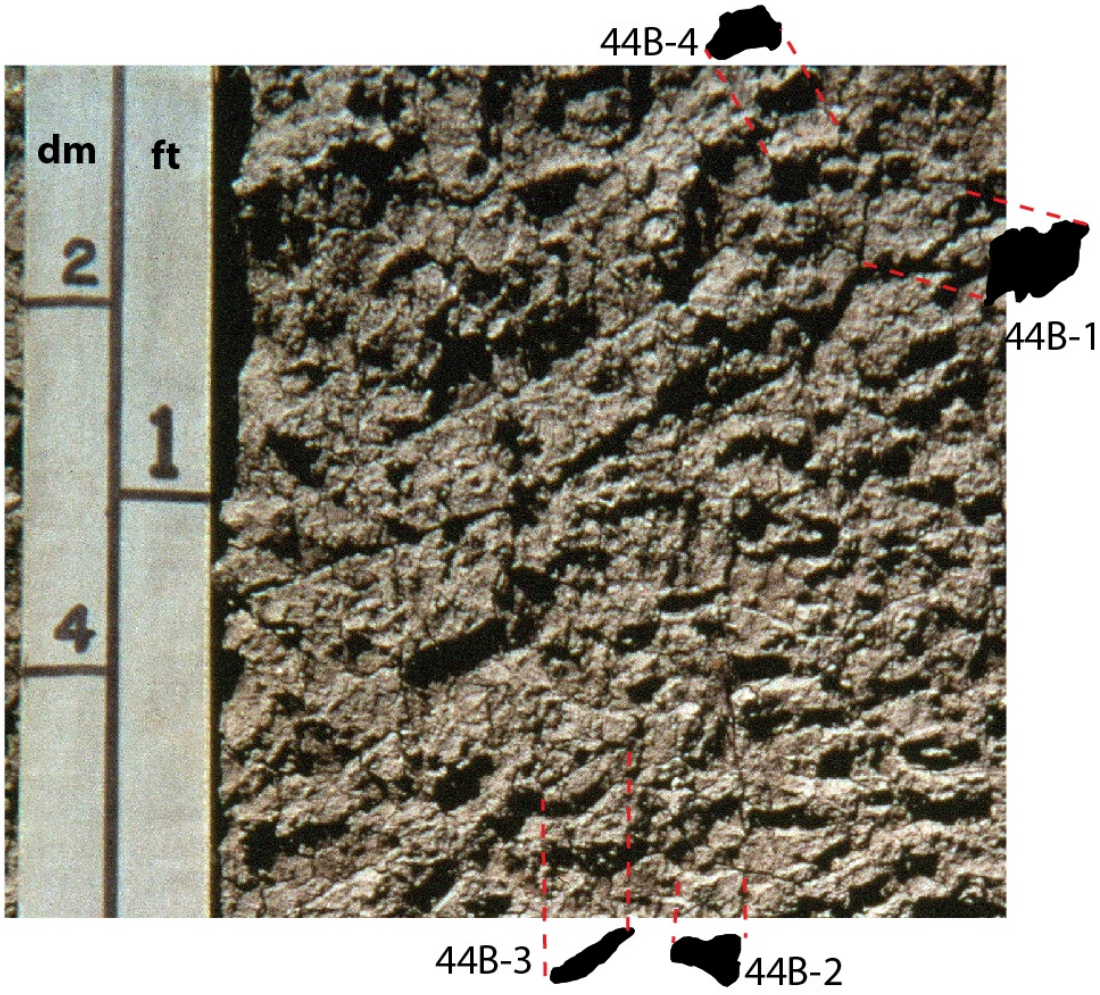

	platy	angular blocky	subangular blocky	granular	columnar	prism	wedge	N/A
44B-1	○	○	○	○	○	○	○	○
44B-2	○	○	○	○	○	○	○	○
44B-3	○	○	○	○	○	○	○	○
44B-4	○	○	○	○	○	○	○	○

Quantifying ped shape from profile photographs

What is the type of structure for the image bellow

*** 25. Which of the following type categories BEST describes the peds represented in the photo above?**

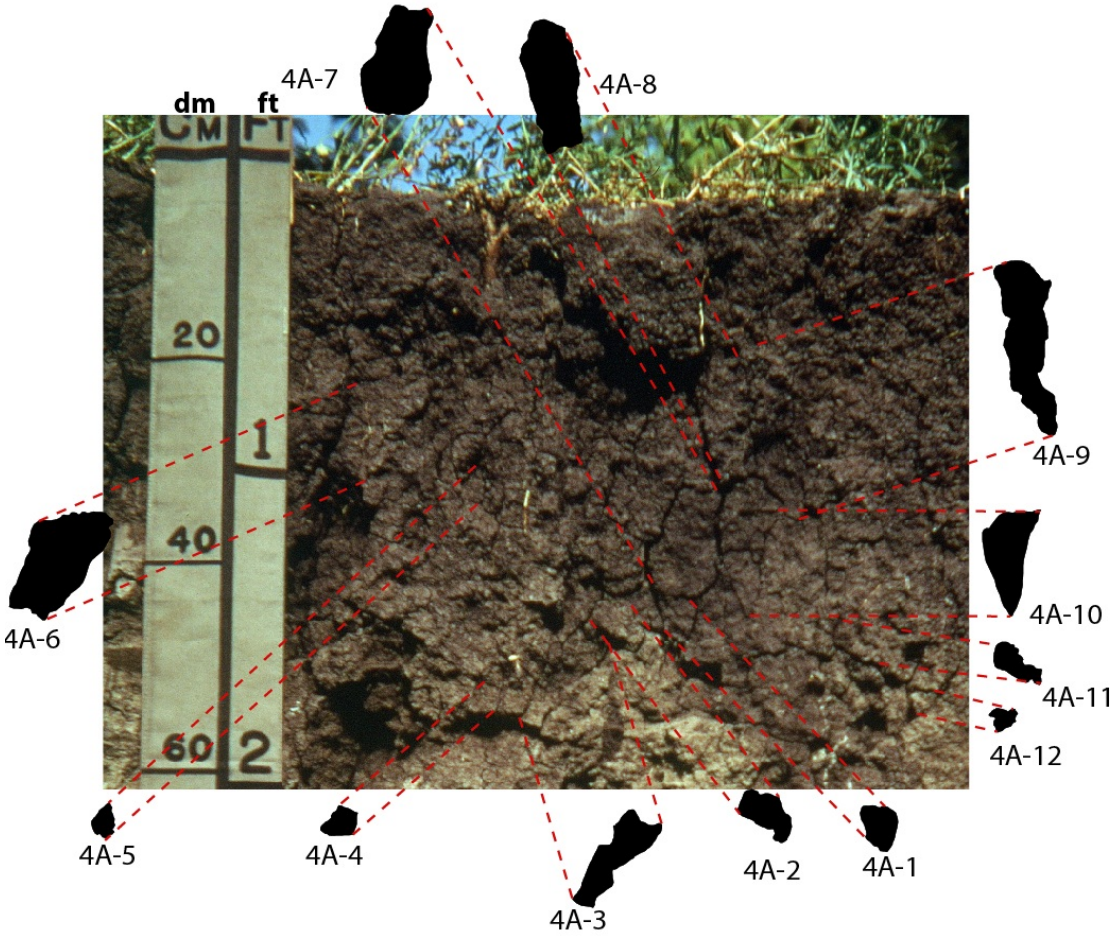

	platy	angular blocky	subangular blocky	granular	columnar	prism	wedge	N/A
4A-1	○	○	○	○	○	○	○	○
4A-2	○	○	○	○	○	○	○	○
4A-3	○	○	○	○	○	○	○	○
4A-4	○	○	○	○	○	○	○	○
4A-5	○	○	○	○	○	○	○	○

	platy	angular blocky	subangular blocky	granular	columnar	prism	wedge	N/A
4A-6	◯	◯	◯	◯	◯	◯	◯	◯
4A-7	◯	◯	◯	◯	◯	◯	◯	◯
4A-8	◯	◯	◯	◯	◯	◯	◯	◯
4A-9	◯	◯	◯	◯	◯	◯	◯	◯
4A-10	◯	◯	◯	◯	◯	◯	◯	◯
4A-11	◯	◯	◯	◯	◯	◯	◯	◯
4A-12	◯	◯	◯	◯	◯	◯	◯	◯

Quantifying ped shape from profile photographs

What is the type of structure for the image bellow

*** 26. Which of the following type categories BEST describes the peds represented in the photo above?**

29-1

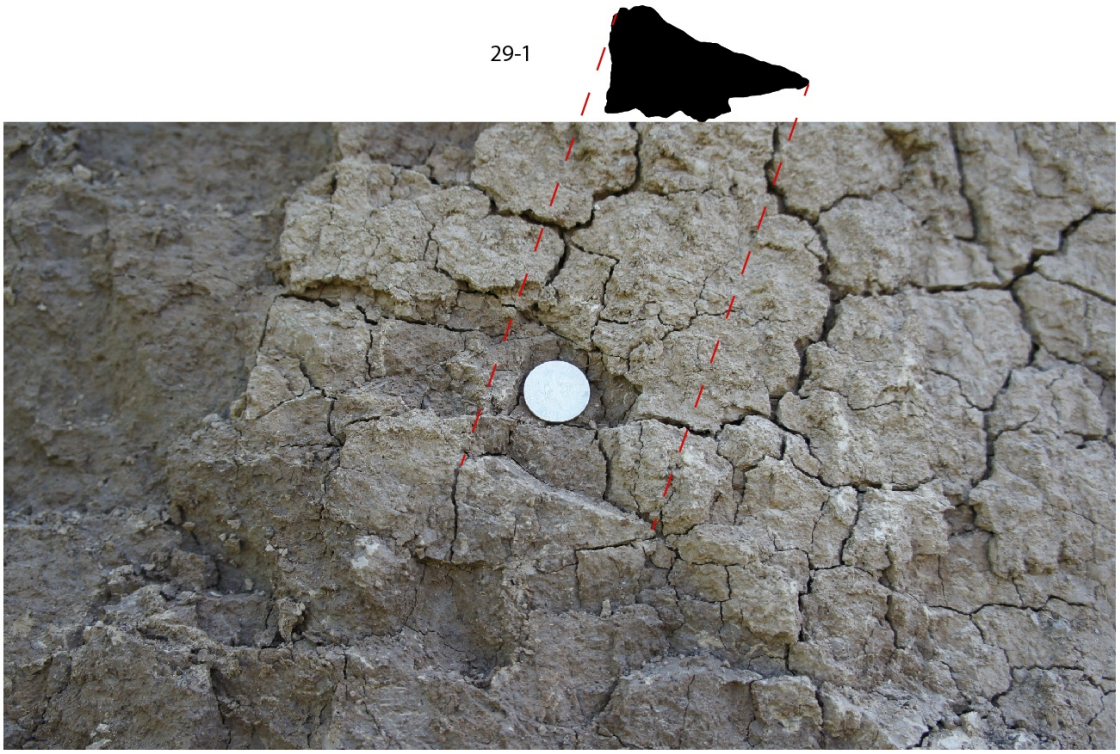

	platy	angular blocky	subangular blocky	granular	columnar	prism	wedge	N/A
29-1	○	○	○	○	○	○	○	○

Quantifying ped shape from profile photographs

What is the type of structure for the image bellow

*** 27. Which of the following type categories BEST describes the peds represented in the photo above?**

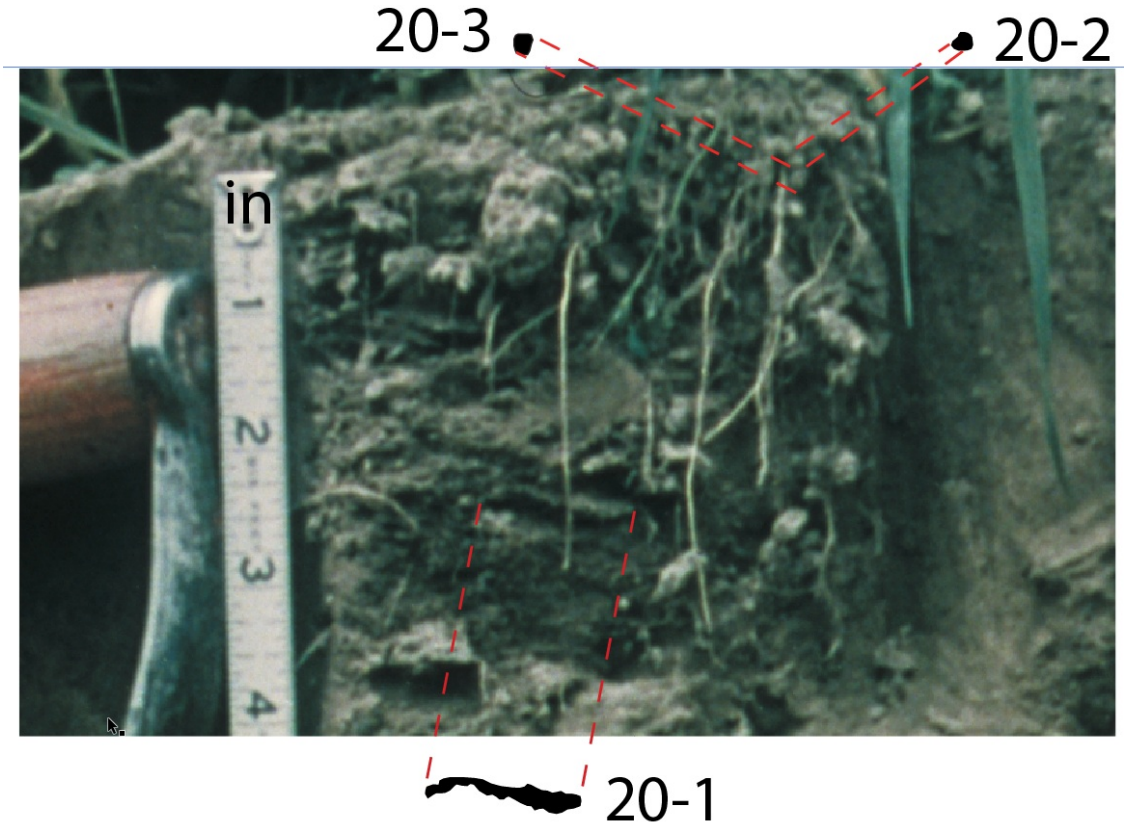

	platy	angular blocky	subangular blocky	granular	columnar	prism	wedge	N/A
20-1	○	○	○	○	○	○	○	○
20-2	○	○	○	○	○	○	○	○
20-3	○	○	○	○	○	○	○	○

Quantifying ped shape from profile photographs

What is the type of structure for the image bellow

*** 28. Which of the following type categories BEST describes the peds represented in the photo above?**

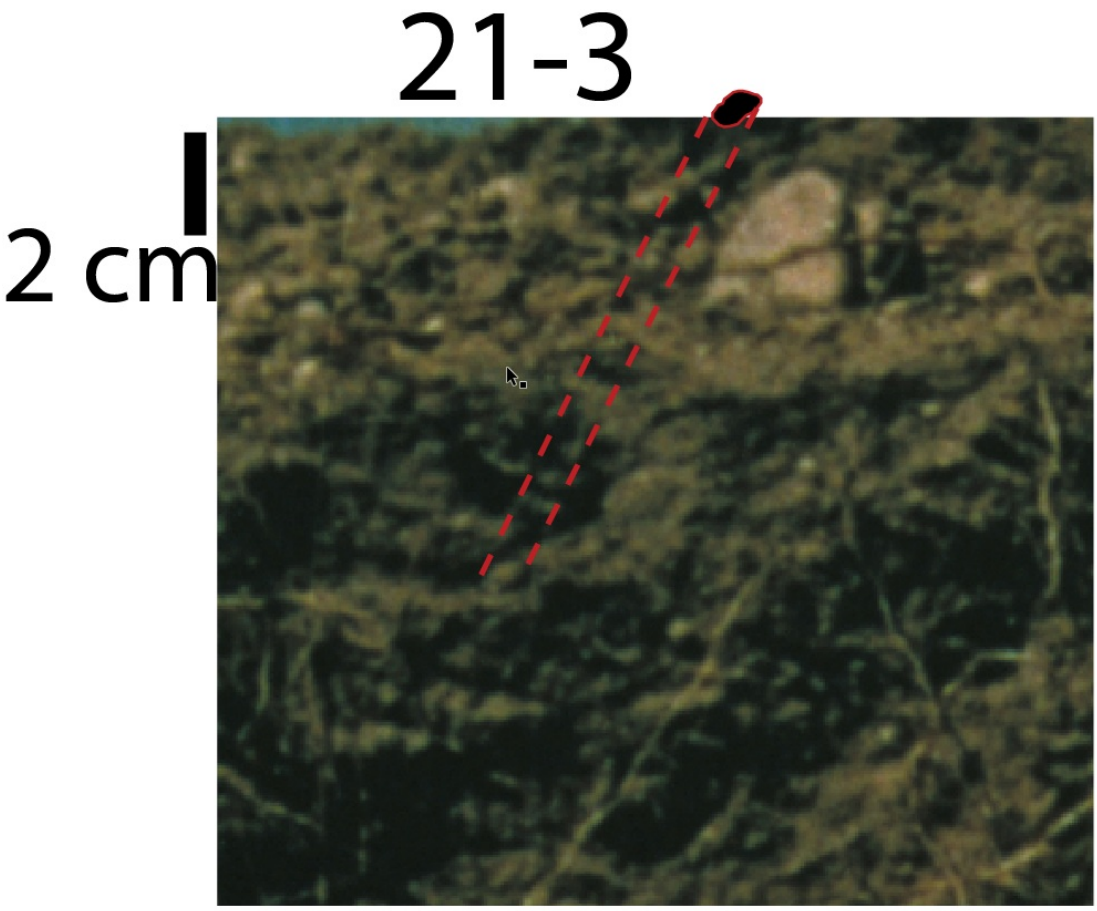

	platy	angular blocky	subangular blocky	granular	columnar	prism	wedge	N/A
21-3	○	○	○	○	○	○	○	○

Quantifying ped shape from profile photographs

What is the type of structure for the image bellow

*** 29. Which of the following type categories BEST describes the peds represented in the photo above?**

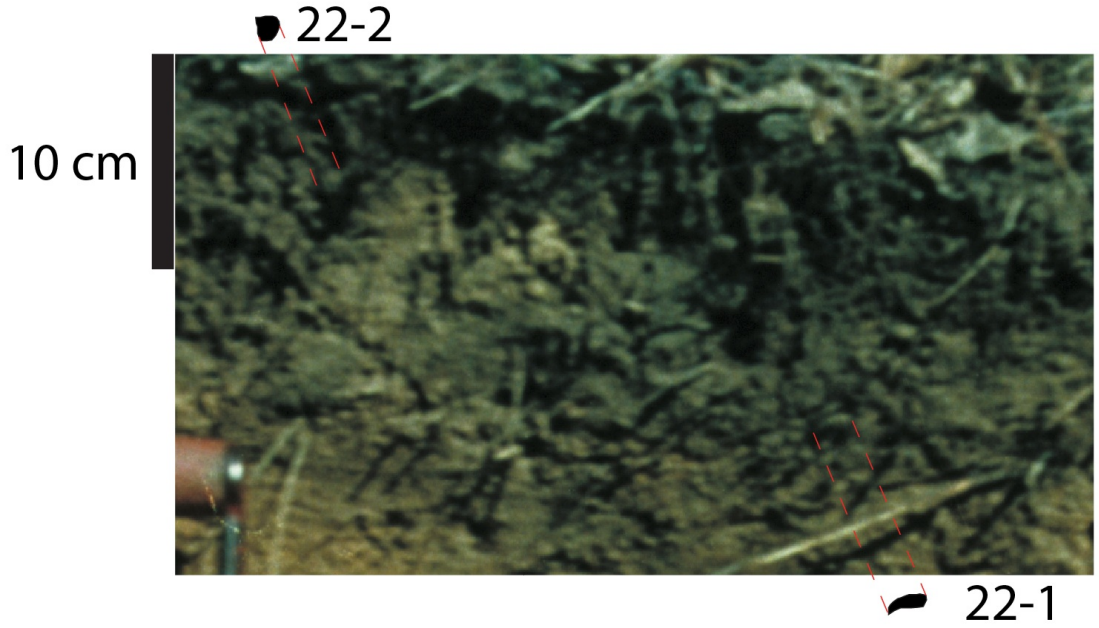

	platy	angular blocky	subangular blocky	granular	columnar	prism	wedge	N/A
22-1	○	○	○	○	○	○	○	○
22-2	○	○	○	○	○	○	○	○

Quantifying ped shape from profile photographs

What is the type of structure for the image bellow

*** 30. Which of the following type categories BEST describes the peds represented in the photo above?**

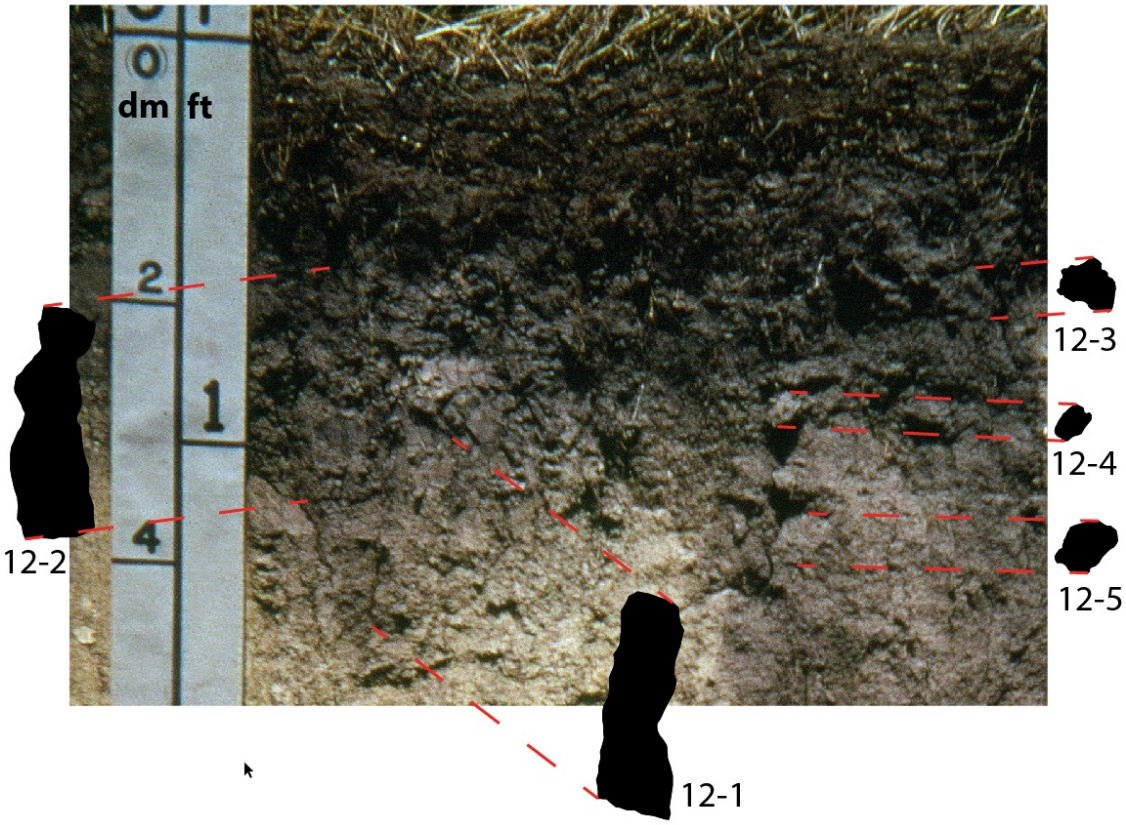

	platy	angular blocky	subangular blocky	granular	columnar	prism	wedge	N/A
12-1	◯	◯	◯	◯	◯	◯	◯	◯
12-2	◯	◯	◯	◯	◯	◯	◯	◯
12-3	◯	◯	◯	◯	◯	◯	◯	◯
12-4	◯	◯	◯	◯	◯	◯	◯	◯
12-5	◯	◯	◯	◯	◯	◯	◯	◯

Quantifying ped shape from profile photographs

What is the type of structure for the image bellow

*** 31. Which of the following type categories BEST describes the peds represented in the photo above?**

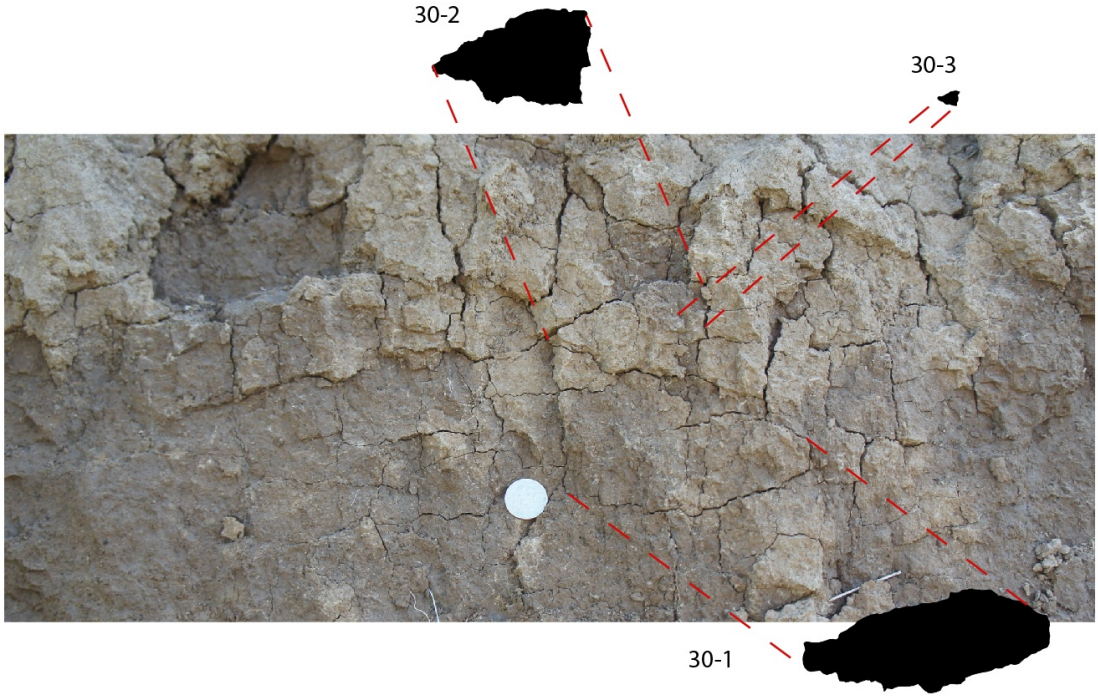

	platy	angular blocky	subangular blocky	granular	columnar	prism	wedge	N/A
30-1	○	○	○	○	○	○	○	○
30-2	○	○	○	○	○	○	○	○
30-3	○	○	○	○	○	○	○	○

Quantifying ped shape from profile photographs

What is the type of structure for the image bellow

*** 32. Which of the following type categories BEST describes the peds represented in the photo above?**

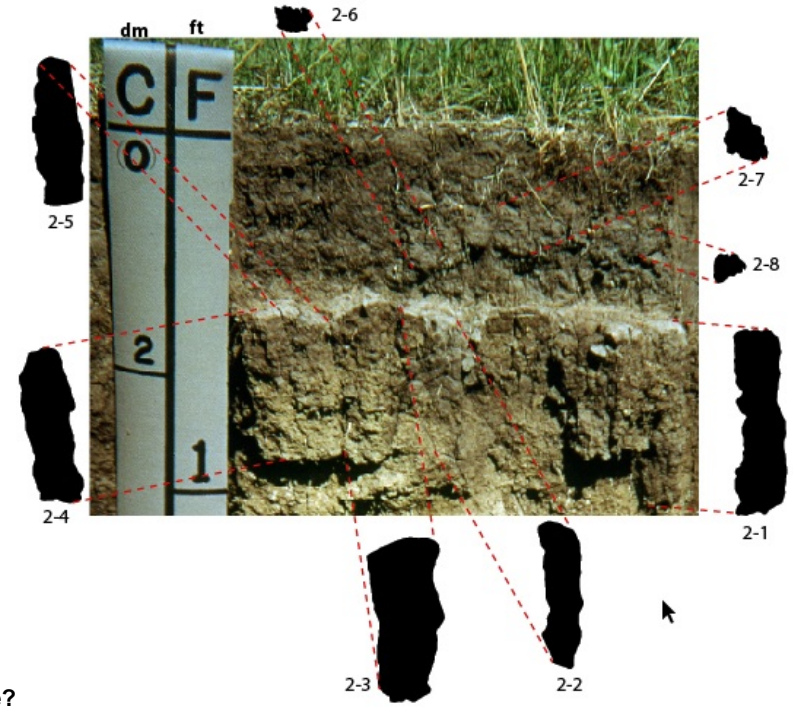

	platy	angular blocky	subangular blocky	granular	columnar	prism	wedge	N/A
2-1	○	○	○	○	○	○	○	○
2-2	○	○	○	○	○	○	○	○
2-3	○	○	○	○	○	○	○	○
2-4	○	○	○	○	○	○	○	○
2-5	○	○	○	○	○	○	○	○
2-6	○	○	○	○	○	○	○	○
2-7	○	○	○	○	○	○	○	○
2-8	○	○	○	○	○	○	○	○

Quantifying ped shape from profile photographs

What is the type of structure for the image bellow

*** 33. Which of the following type categories BEST describes the peds represented in the photo above?**

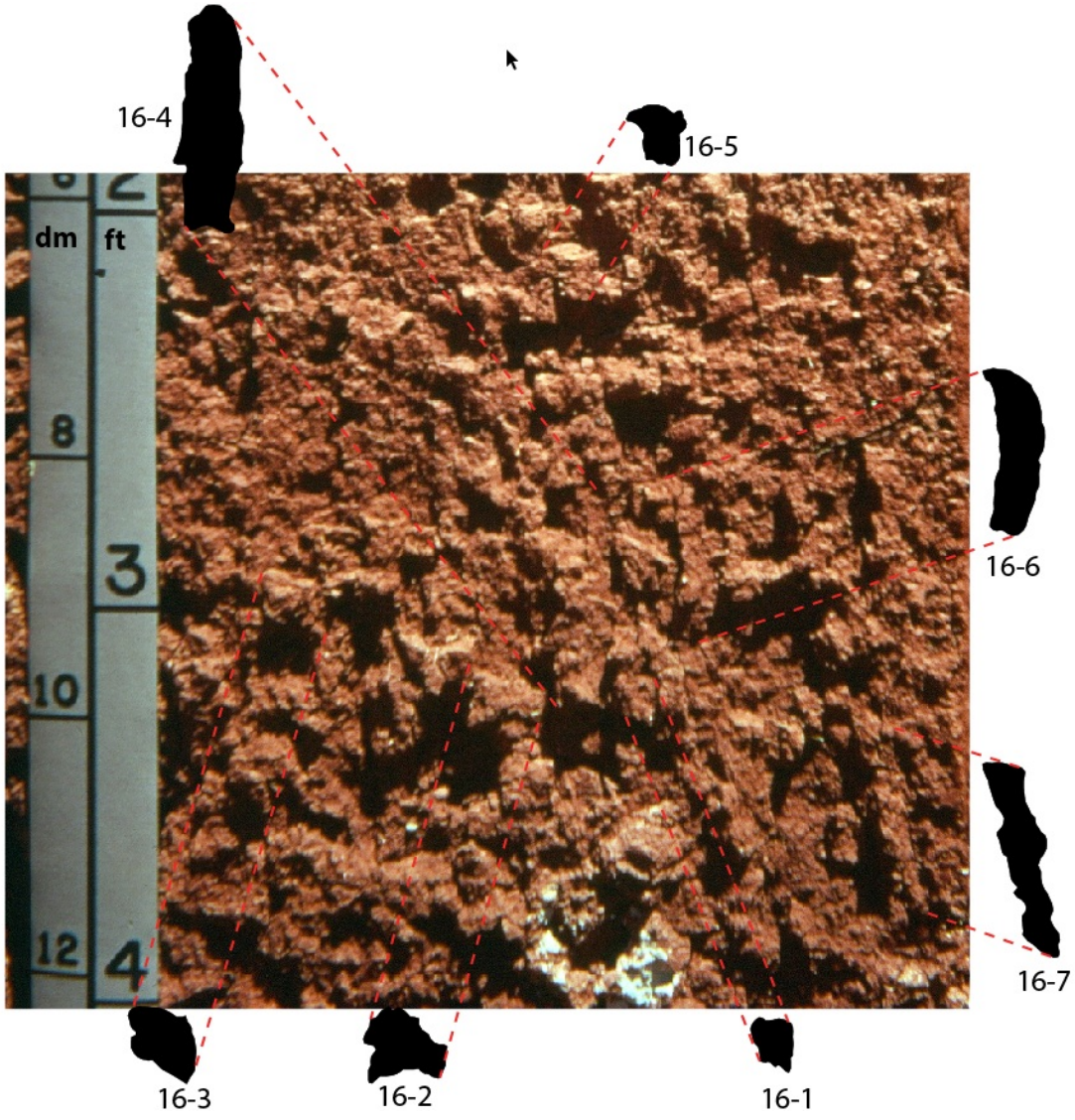

	platy	angular blocky	subangular blocky	granular	columnar	prism	wedge	N/A
16-1	○	○	○	○	○	○	○	○
16-2	○	○	○	○	○	○	○	○

	platy	angular blocky	subangular blocky	granular	columnar	prism	wedge	N/A
16-3	◯	◯	◯	◯	◯	◯	◯	◯
16-4	◯	◯	◯	◯	◯	◯	◯	◯
16-5	◯	◯	◯	◯	◯	◯	◯	◯
16-6	◯	◯	◯	◯	◯	◯	◯	◯
16-7	◯	◯	◯	◯	◯	◯	◯	◯

Quantifying ped shape from profile photographs

What is the type of structure for the image bellow

*** 34. Which of the following type categories BEST describes the peds represented in the photo above?**

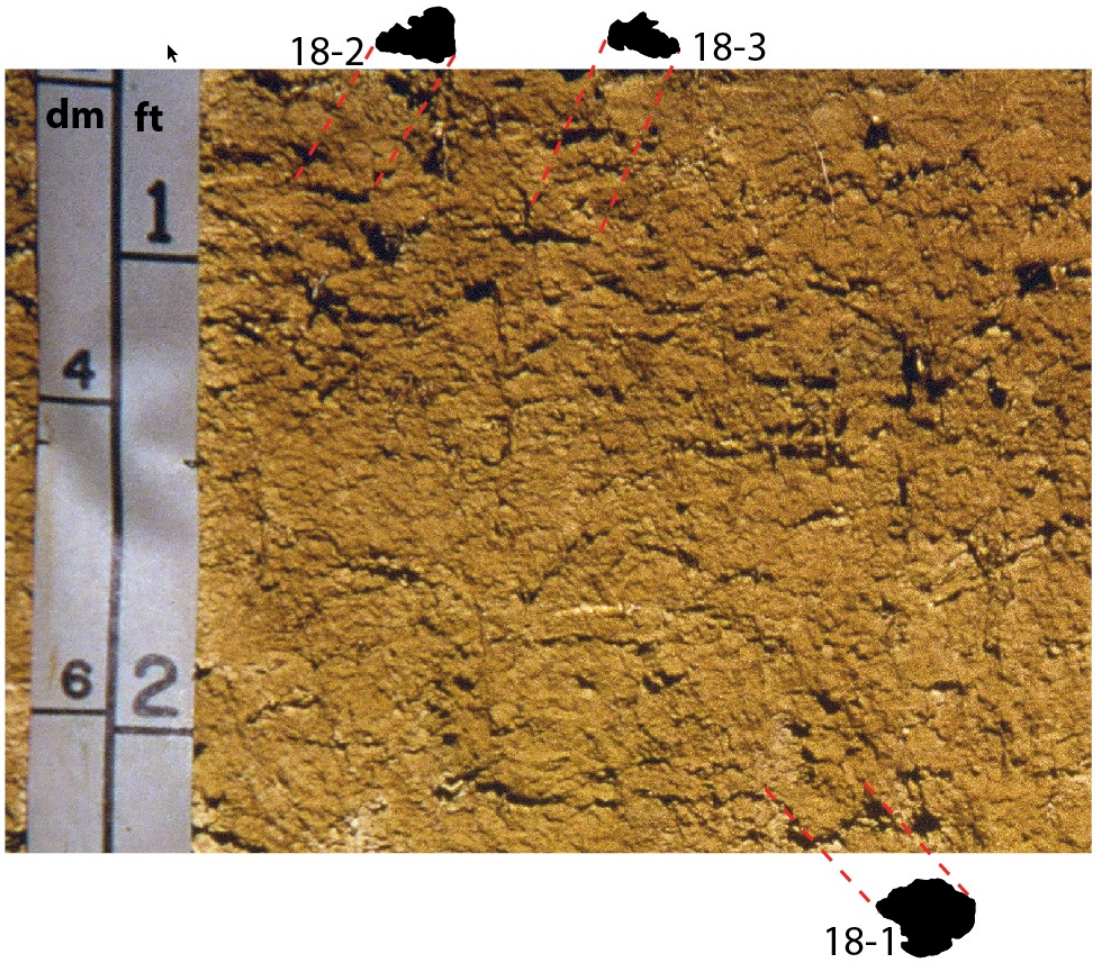

	platy	angular blocky	subangular blocky	granular	columnar	prism	wedge	N/A
18-1	○	○	○	○	○	○	○	○
18-2	○	○	○	○	○	○	○	○
18-3	○	○	○	○	○	○	○	○

Quantifying ped shape from profile photographs

What is the type of structure for the image bellow

*** 35. Which of the following type categories BEST describes the peds represented in the photo above?**

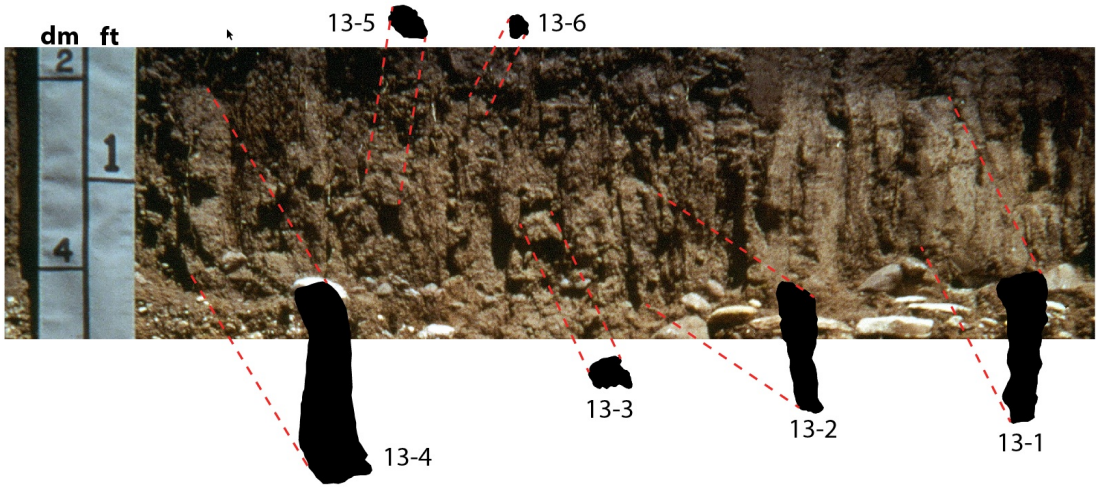

	platy	angular blocky	subangular blocky	granular	columnar	prism	wedge	N/A
13-1	○	○	○	○	○	○	○	○
13-2	○	○	○	○	○	○	○	○
13-3	○	○	○	○	○	○	○	○
13-4	○	○	○	○	○	○	○	○
13-5	○	○	○	○	○	○	○	○
13-6	○	○	○	○	○	○	○	○

Quantifying ped shape from profile photographs

What is the type of structure for the image bellow

*** 36. Which of the following type categories BEST describes the peds represented in the photo above?**

34-1

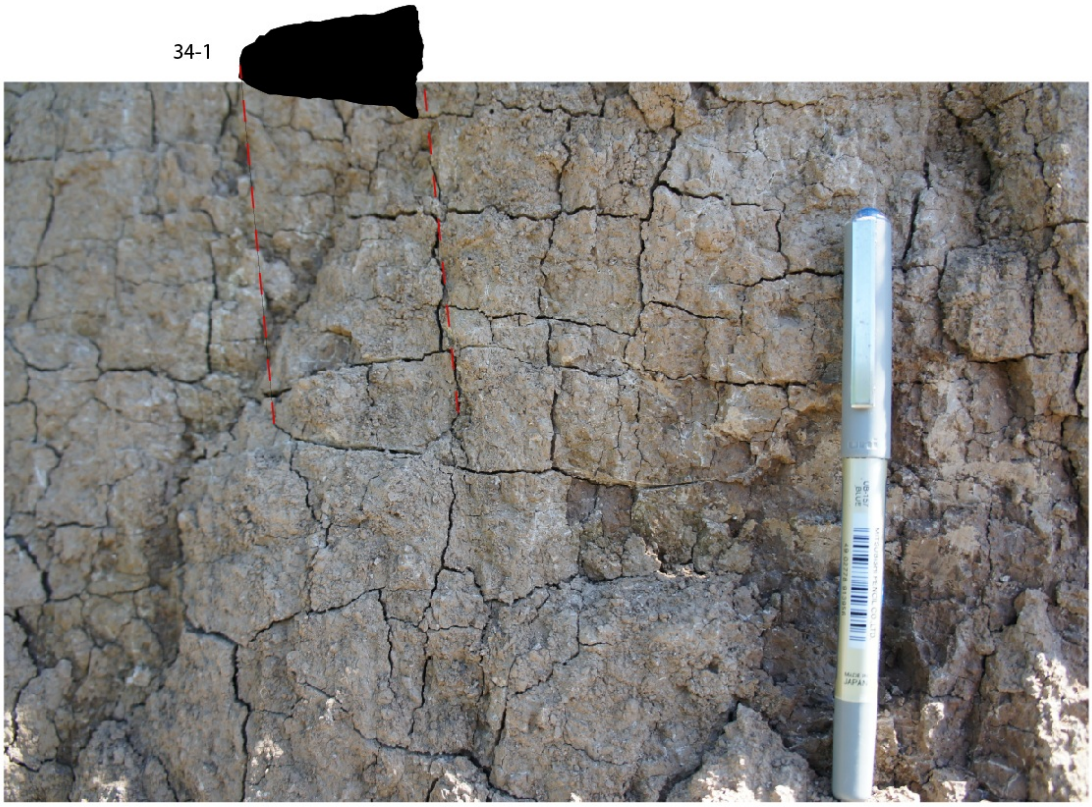

	platy	angular blocky	subangular blocky	granular	columnar	prism	wedge	N/A
34-1	○	○	○	○	○	○	○	○

Quantifying ped shape from profile photographs

Copy of page: What is the type of structure for the image bellow

*** 37. Which of the following type categories BEST describes the peds represented in the photo above?**

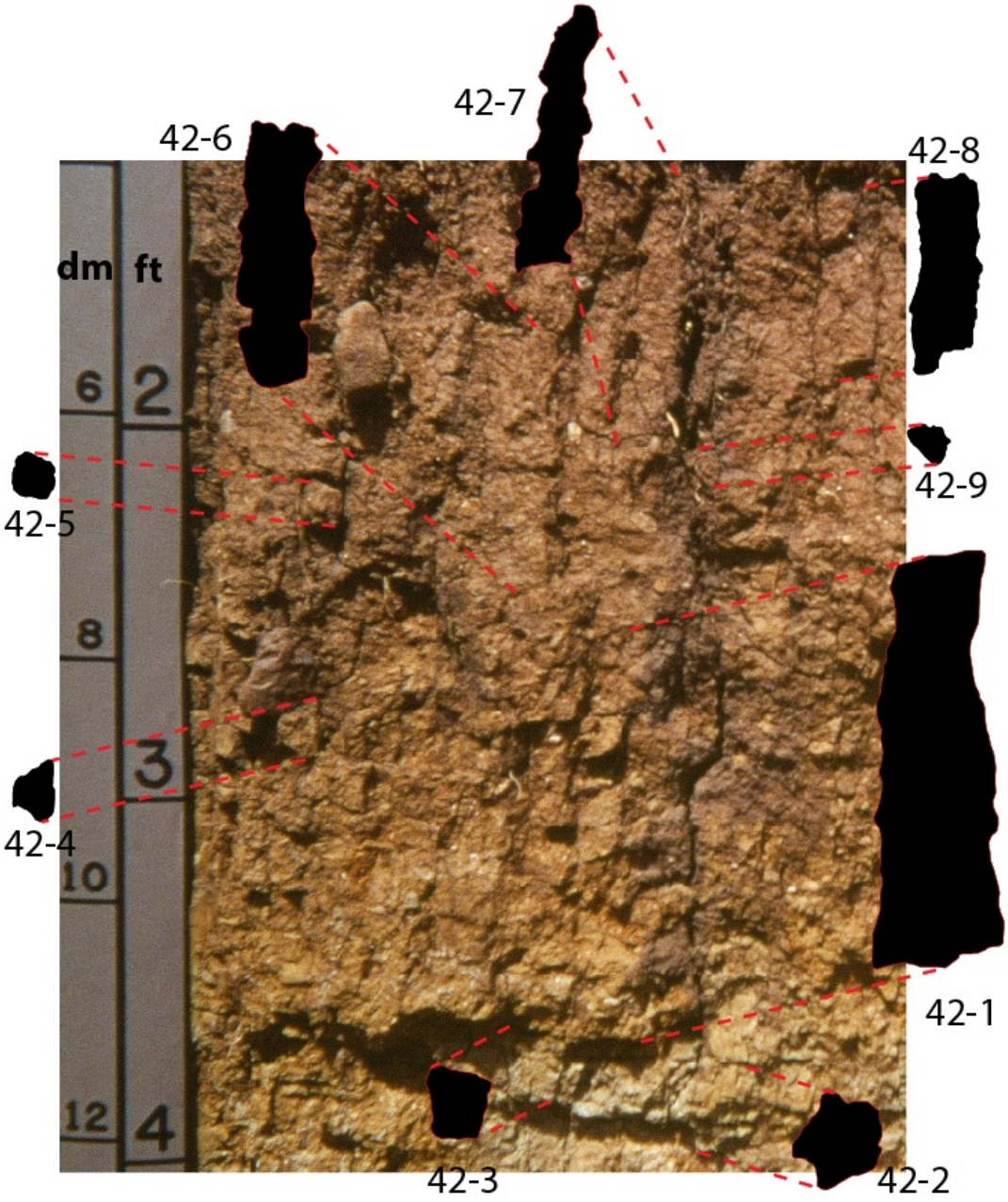

	platy	angular blocky	subangular blocky	granular	columnar	prism	wedge	N/A
42-1	○	○	○	○	○	○	○	○
42-2	○	○	○	○	○	○	○	○
42-3	○	○	○	○	○	○	○	○
42-4	○	○	○	○	○	○	○	○
42-5	○	○	○	○	○	○	○	○
42-6	○	○	○	○	○	○	○	○
42-7	○	○	○	○	○	○	○	○
42-8	○	○	○	○	○	○	○	○
42-9	○	○	○	○	○	○	○	○

Quantifying ped shape from profile photographs

What is the type of structure for the image bellow

*** 38. Which of the following type categories BEST describes the peds represented in the photo above?**

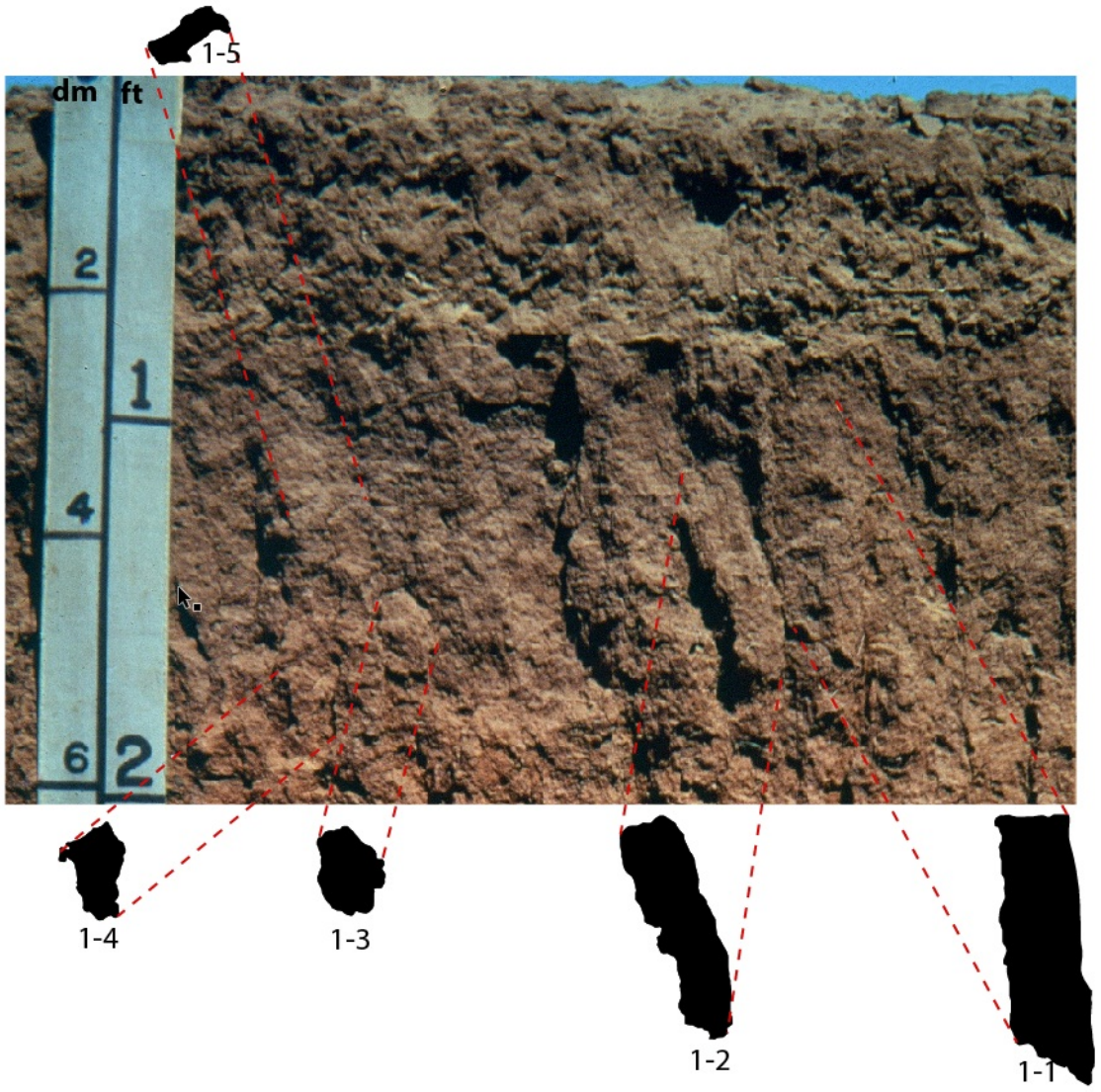

	platy	angular blocky	subangular blocky	granular	columnar	prism	wedge	N/A
1-1	○	○	○	○	○	○	○	○
1-2	○	○	○	○	○	○	○	○
1-3	○	○	○	○	○	○	○	○
1-4	○	○	○	○	○	○	○	○
1-5	○	○	○	○	○	○	○	○

Quantifying ped shape from profile photographs

What is the type of structure for the image bellow

*** 39. Which of the following type categories BEST describes the peds represented in the photo above?**

	platy	angular blocky	subangular blocky	granular	columnar	prism	wedge	N/A
31-1	◯	◯	◯	◯	◯	◯	◯	◯
31-2	◯	◯	◯	◯	◯	◯	◯	◯

Quantifying ped shape from profile photographs

What is the type of structure for the image bellow

*** 40. Which of the following type categories BEST describes the peds represented in the photo above?**

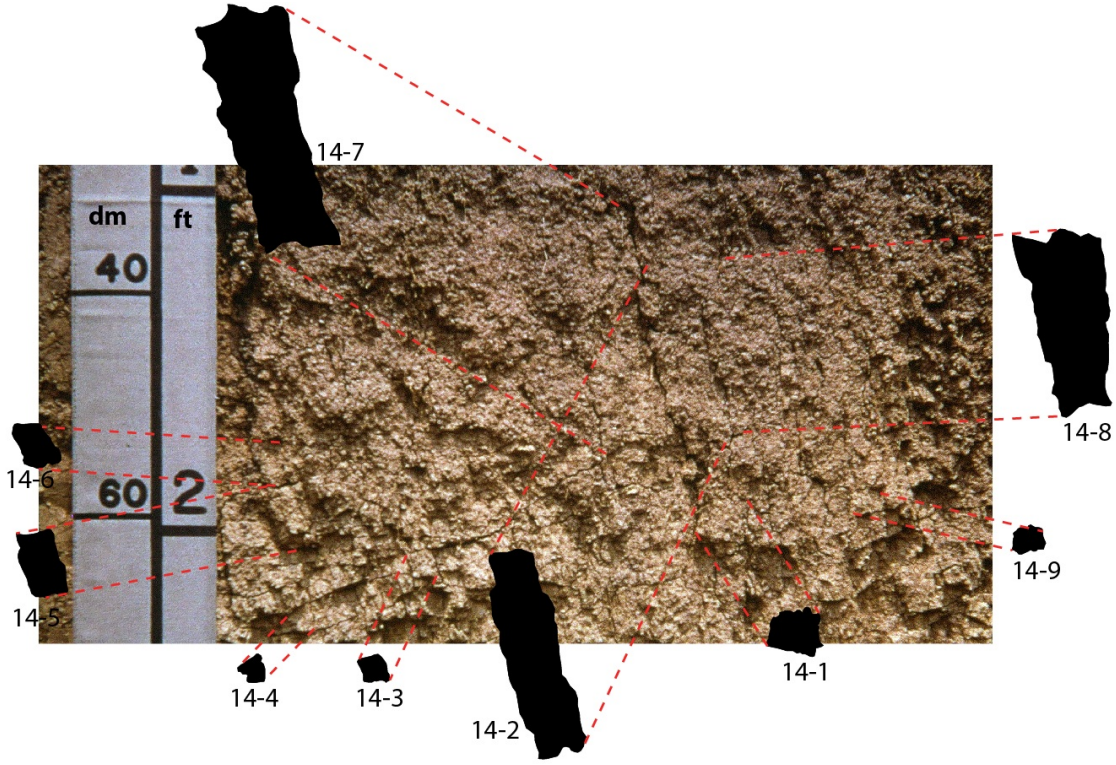

	platy	angular blocky	subangular blocky	granular	columnar	prism	wedge	N/A
14-1	○	○	○	○	○	○	○	○
14-2	○	○	○	○	○	○	○	○
14-3	○	○	○	○	○	○	○	○
14-4	○	○	○	○	○	○	○	○
14-5	○	○	○	○	○	○	○	○
14-6	○	○	○	○	○	○	○	○
14-7	○	○	○	○	○	○	○	○
14-8	○	○	○	○	○	○	○	○
14-9	○	○	○	○	○	○	○	○

Quantifying ped shape from profile photographs

What is the type of structure for the image bellow

*** 41. Which of the following type categories BEST describes the peds represented in the photo above?**

	platy	angular blocky	subangular blocky	granular	columnar	prism	wedge	N/A
25B-1	◯	◯	◯	◯	◯	◯	◯	◯

Quantifying ped shape from profile photographs

What is the type of structure for the image bellow

*** 42. Which of the following type categories BEST describes the peds represented in the photo above?**

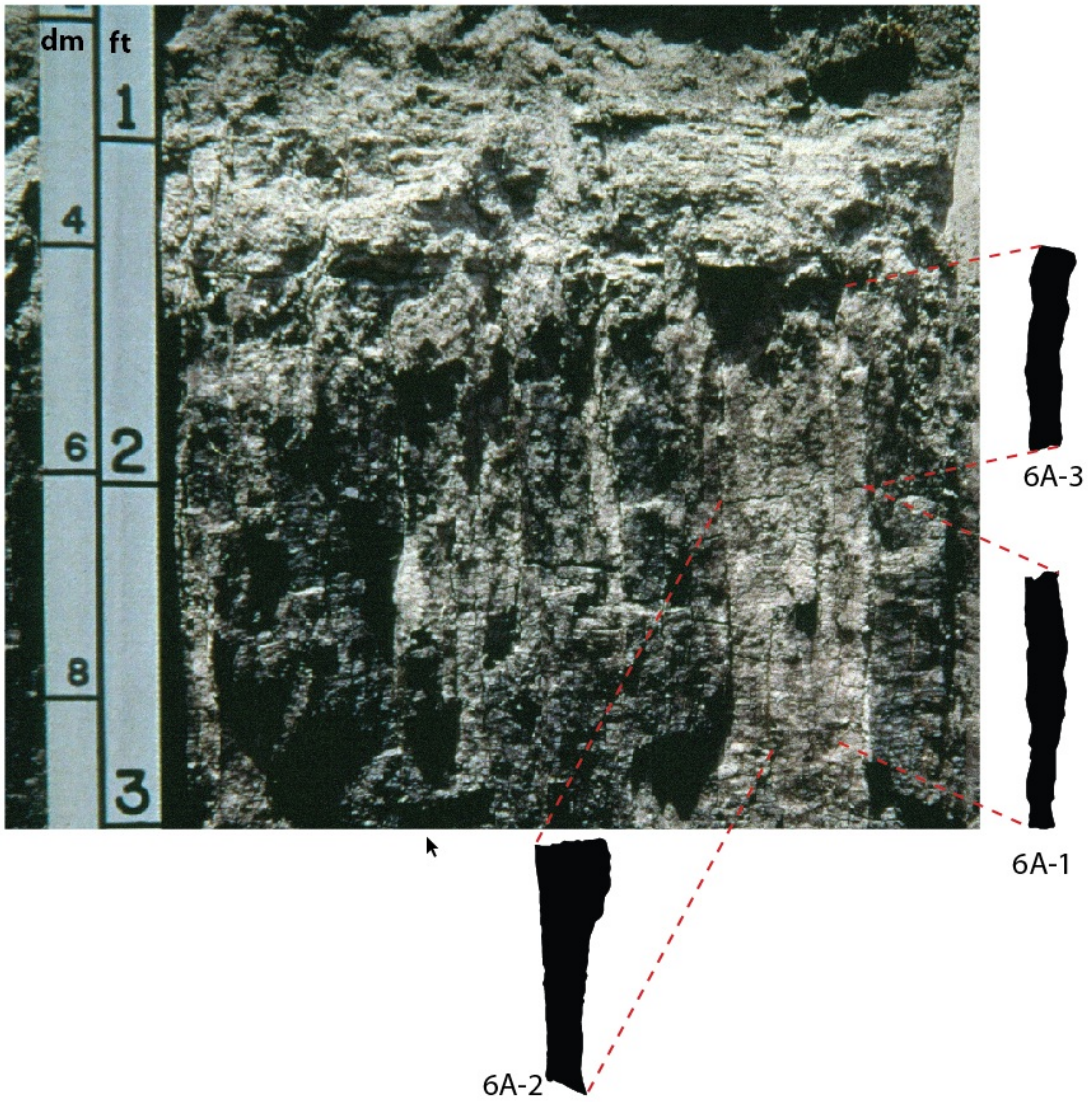

	platy	angular blocky	subangular blocky	granular	columnar	prism	wedge	N/A
6A-1	○	○	○	○	○	○	○	○
6A-2	○	○	○	○	○	○	○	○
6A-3	○	○	○	○	○	○	○	○

Quantifying ped shape from profile photographs

Copy of page: What is the type of structure for the image bellow

*** 43. Which of the following type categories BEST describes the peds represented in the photo above?**

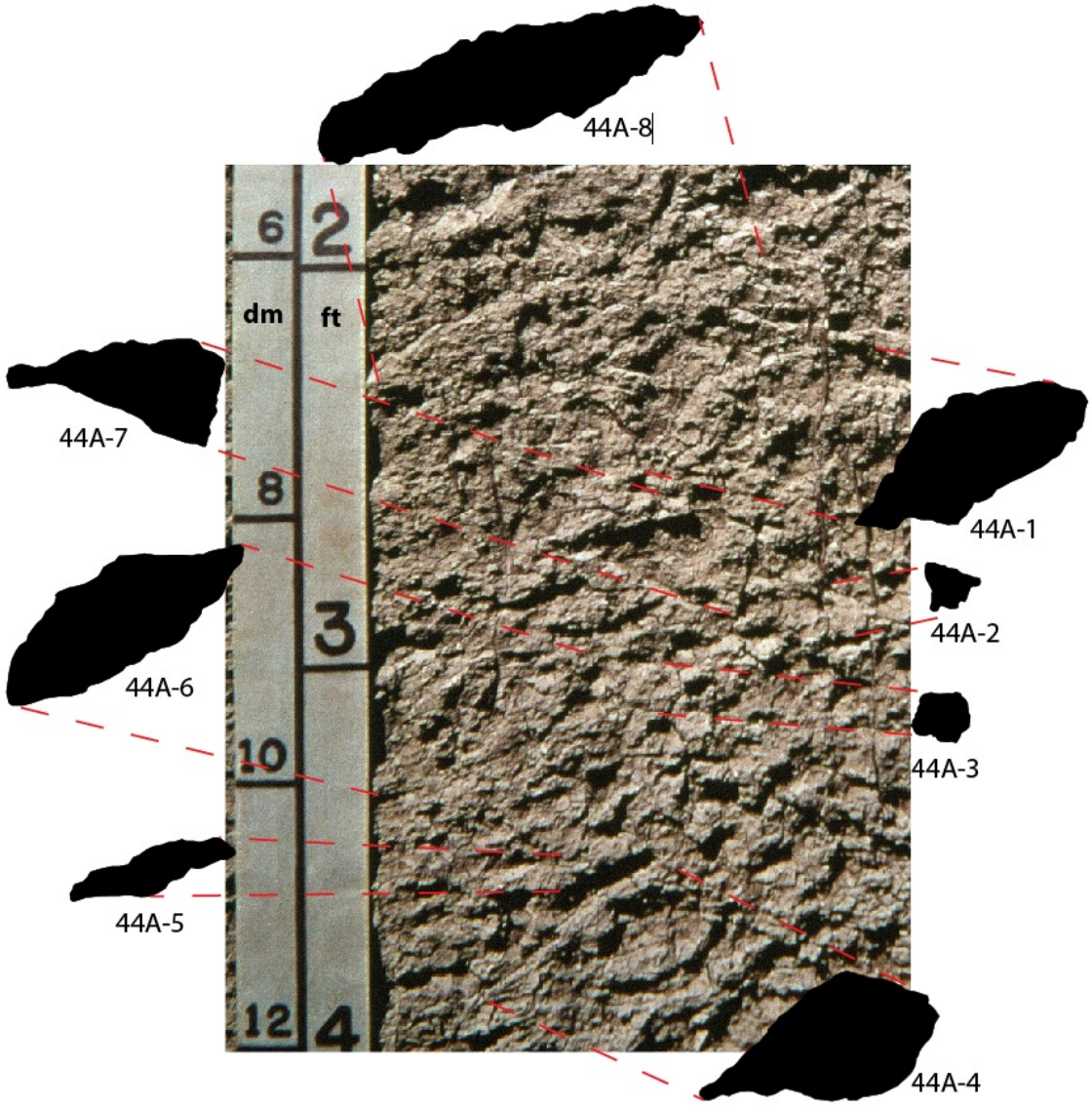

	platy	angular blocky	subangular blocky	granular	columnar	prism	wedge	N/A
44A-1	○	○	○	○	○	○	○	○

	platy	angular blocky	subangular blocky	granular	columnar	prism	wedge	N/A
44A-2	◯	◯	◯	◯	◯	◯	◯	◯
44A-3	◯	◯	◯	◯	◯	◯	◯	◯
44A-4	◯	◯	◯	◯	◯	◯	◯	◯
44A-5	◯	◯	◯	◯	◯	◯	◯	◯
44A-6	◯	◯	◯	◯	◯	◯	◯	◯
44A-7	◯	◯	◯	◯	◯	◯	◯	◯
44A-8	◯	◯	◯	◯	◯	◯	◯	◯

Quantifying ped shape from profile photographs

What is the type of structure for the image bellow

*** 44. Which of the following type categories BEST describes the peds represented in the photo above?**

	platy	angular blocky	subangular blocky	granular	columnar	prism	wedge	N/A
24-1	○	○	○	○	○	○	○	○
24-2	○	○	○	○	○	○	○	○
24-3	○	○	○	○	○	○	○	○

Quantifying ped shape from profile photographs

What is the type of structure for the image bellow

*** 45. Which of the following type categories BEST describes the peds represented in the photo above?**

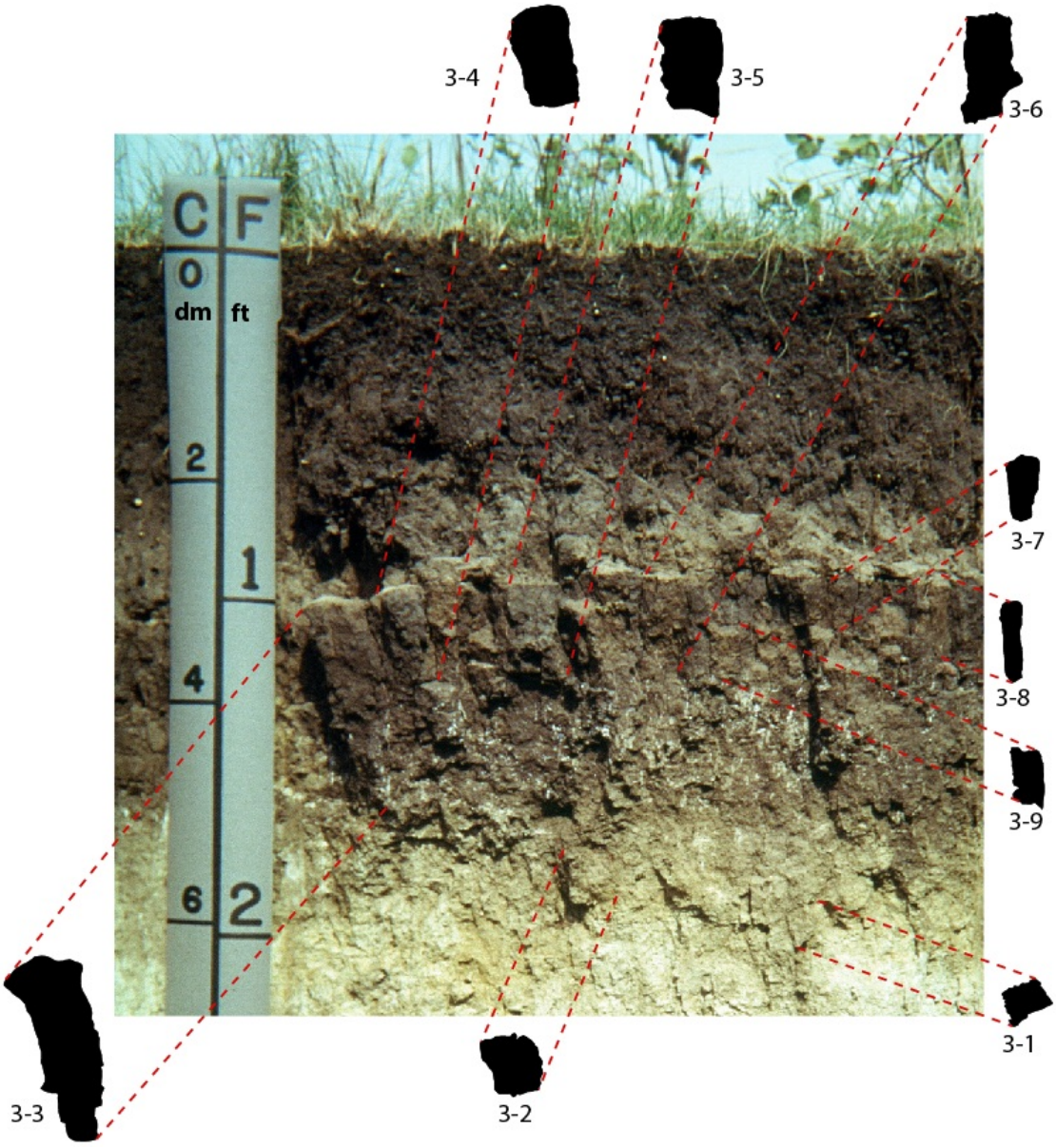

	platy	angular blocky	subangular blocky	granular	columnar	prism	wedge	N/A
3-1	○	○	○	○	○	○	○	○
3-2	○	○	○	○	○	○	○	○
3-3	○	○	○	○	○	○	○	○
3-4	○	○	○	○	○	○	○	○
3-5	○	○	○	○	○	○	○	○
3-6	○	○	○	○	○	○	○	○
3-7	○	○	○	○	○	○	○	○
3-8	○	○	○	○	○	○	○	○
3-9	○	○	○	○	○	○	○	○

Quantifying ped shape from profile photographs

What is the type of structure for the image bellow

*** 46. Which of the following type categories BEST describes the peds represented in the photo above?**

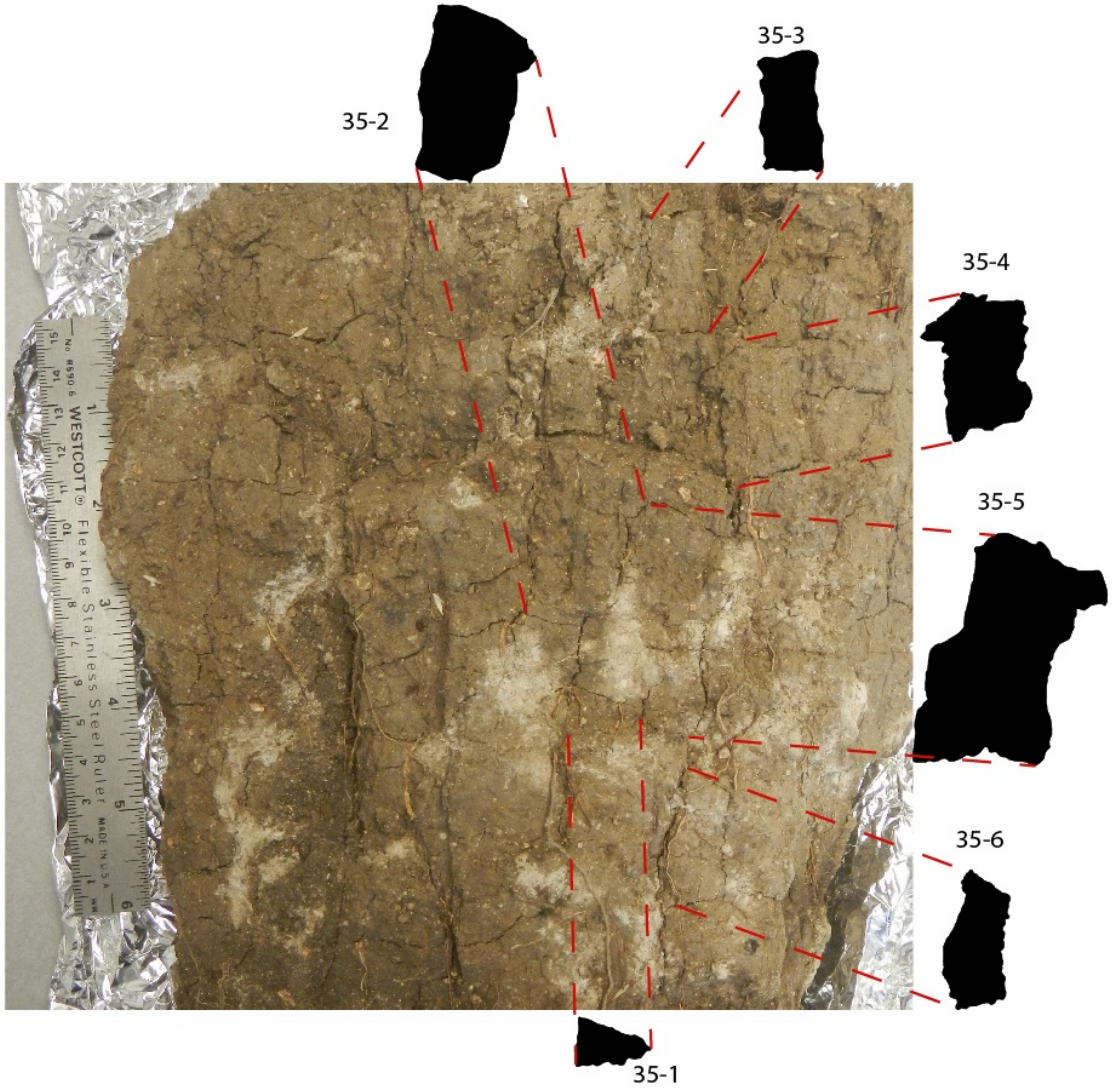

	platy	angular blocky	subangular blocky	granular	columnar	prism	wedge	N/A
35-1	◯	◯	◯	◯	◯	◯	◯	◯
35-2	◯	◯	◯	◯	◯	◯	◯	◯

	platy	angular blocky	subangular blocky	granular	columnar	prism	wedge	N/A
35-3	◯	◯	◯	◯	◯	◯	◯	◯
35-4	◯	◯	◯	◯	◯	◯	◯	◯
35-5	◯	◯	◯	◯	◯	◯	◯	◯
35-6	◯	◯	◯	◯	◯	◯	◯	◯

Quantifying ped shape from profile photographs

What is the type of structure for the image bellow

*** 47. Which of the following type categories BEST describes the peds represented in the photo above?**

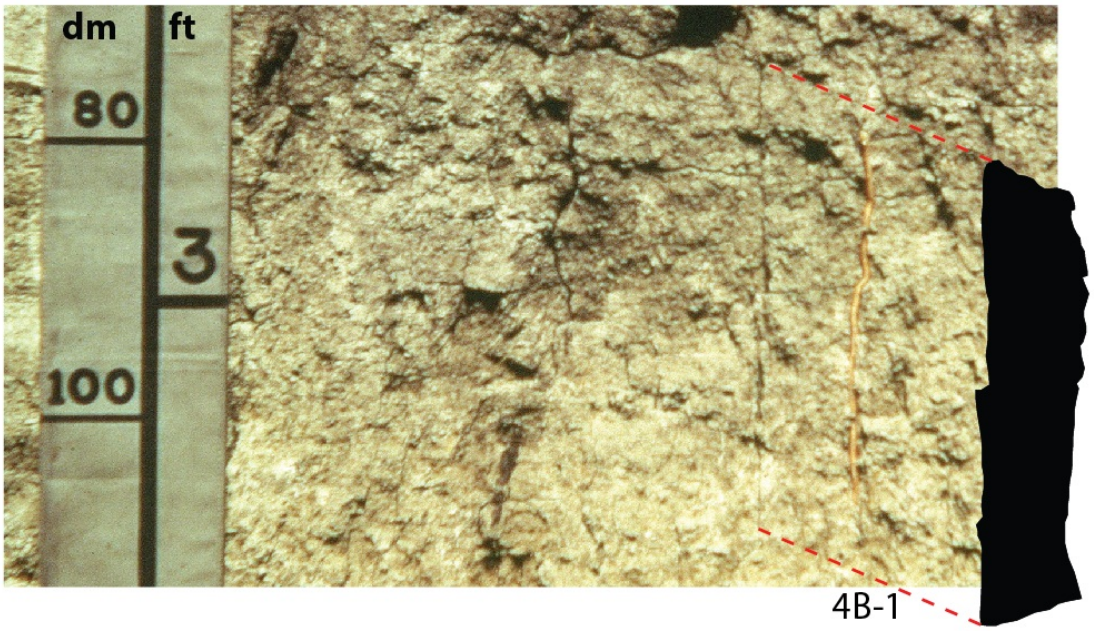

	platy	angular blocky	subangular blocky	granular	columnar	prism	wedge	N/A
4B-1	○	○	○	○	○	○	○	○

Quantifying ped shape from profile photographs

What is the type of structure for the image bellow

*** 48. Which of the following type categories BEST describes the peds represented in the photo above?**

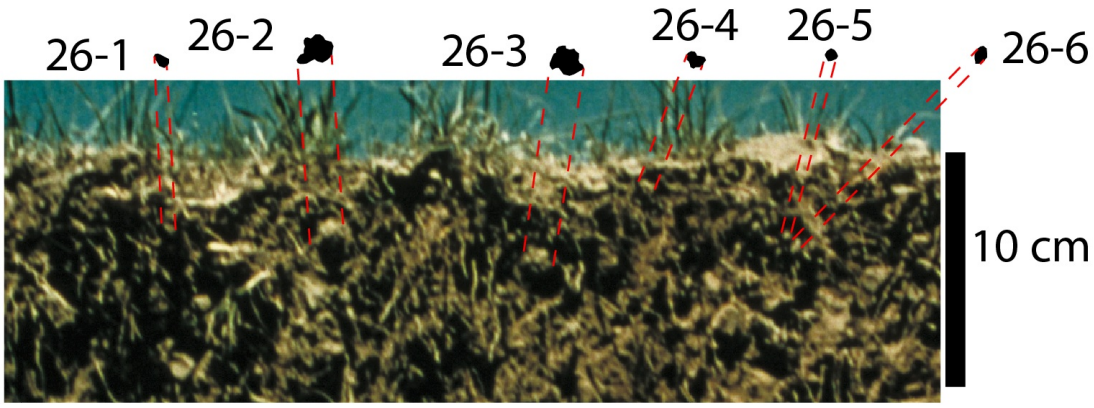

	platy	angular blocky	subangular blocky	granular	columnar	prism	wedge	N/A
26-1	○	○	○	○	○	○	○	○
26-2	○	○	○	○	○	○	○	○
26-3	○	○	○	○	○	○	○	○
26-4	○	○	○	○	○	○	○	○
26-5	○	○	○	○	○	○	○	○
26-6	○	○	○	○	○	○	○	○

Quantifying ped shape from profile photographs

What is the type of structure for the image bellow

*** 49. Which of the following type categories BEST describes the peds represented in the photo above?**

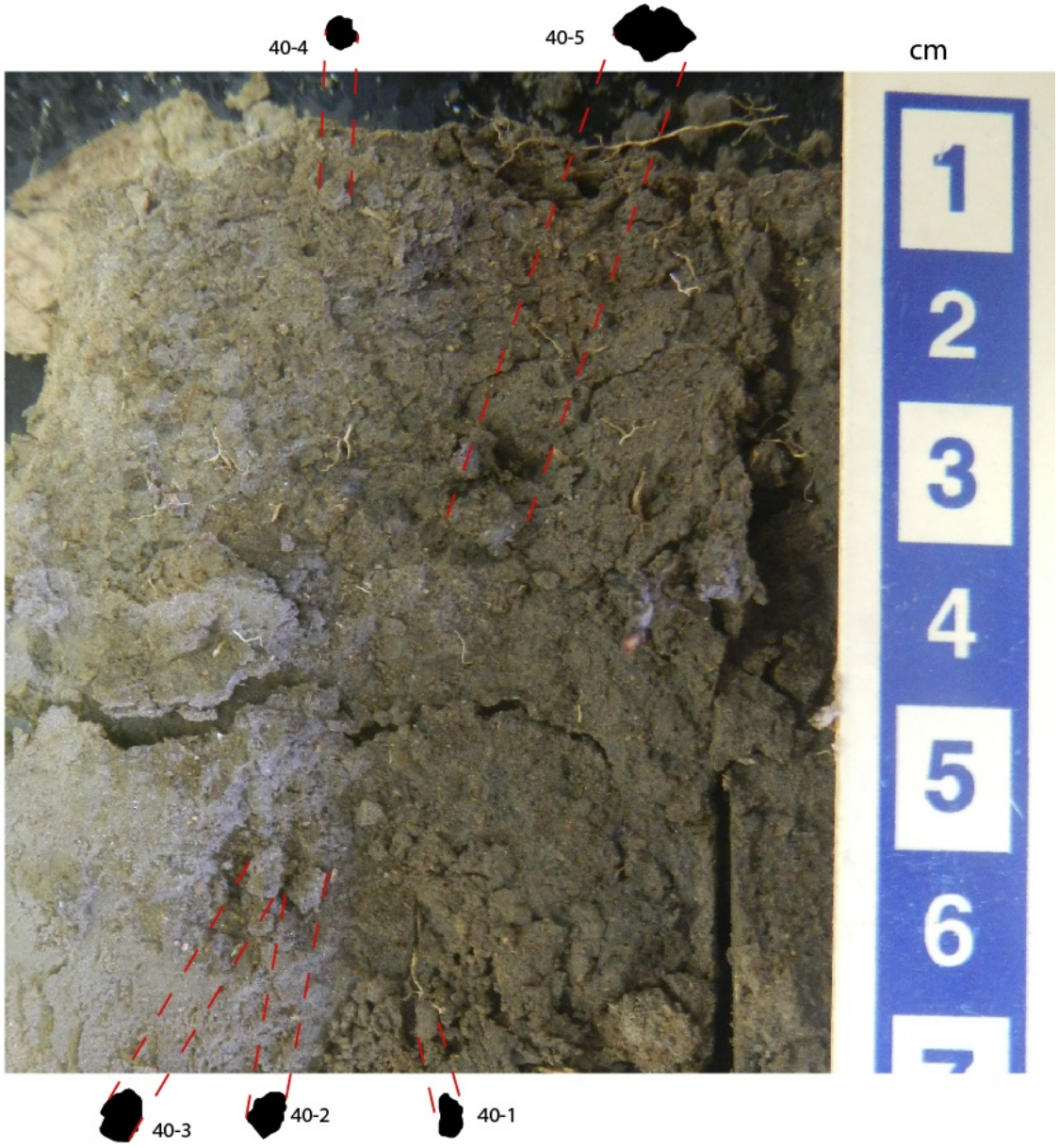

	platy	angular blocky	subangular blocky	granular	columnar	prism	wedge	N/A
40-1	◯	◯	◯	◯	◯	◯	◯	◯
40-2	◯	◯	◯	◯	◯	◯	◯	◯
40-3	◯	◯	◯	◯	◯	◯	◯	◯
40-4	◯	◯	◯	◯	◯	◯	◯	◯
40-5	◯	◯	◯	◯	◯	◯	◯	◯

Quantifying ped shape from profile photographs

What is the type of structure for the image bellow

*** 50. Which of the following type categories BEST describes the peds represented in the photo above?**

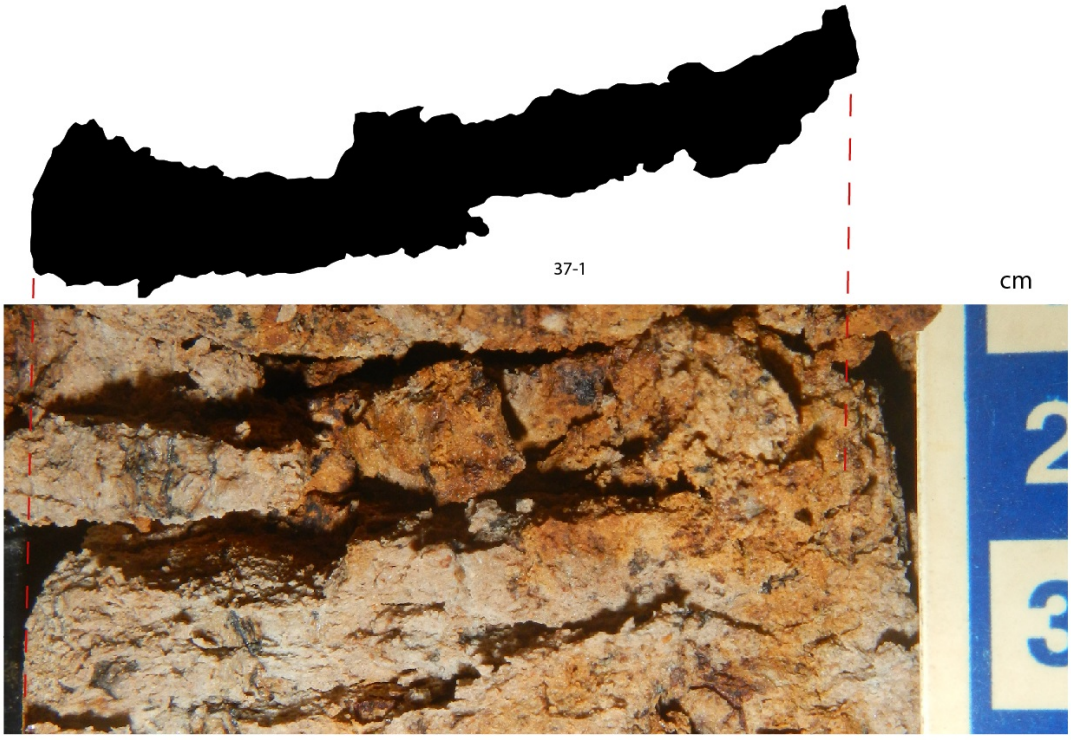

	platy	angular blocky	subangular blocky	granular	columnar	prism	wedge	N/A
37-1	○	○	○	○	○	○	○	○

Quantifying ped shape from profile photographs

What is the type of structure for the image bellow

*** 51. Which of the following type categories BEST describes the peds represented in the photo above?**

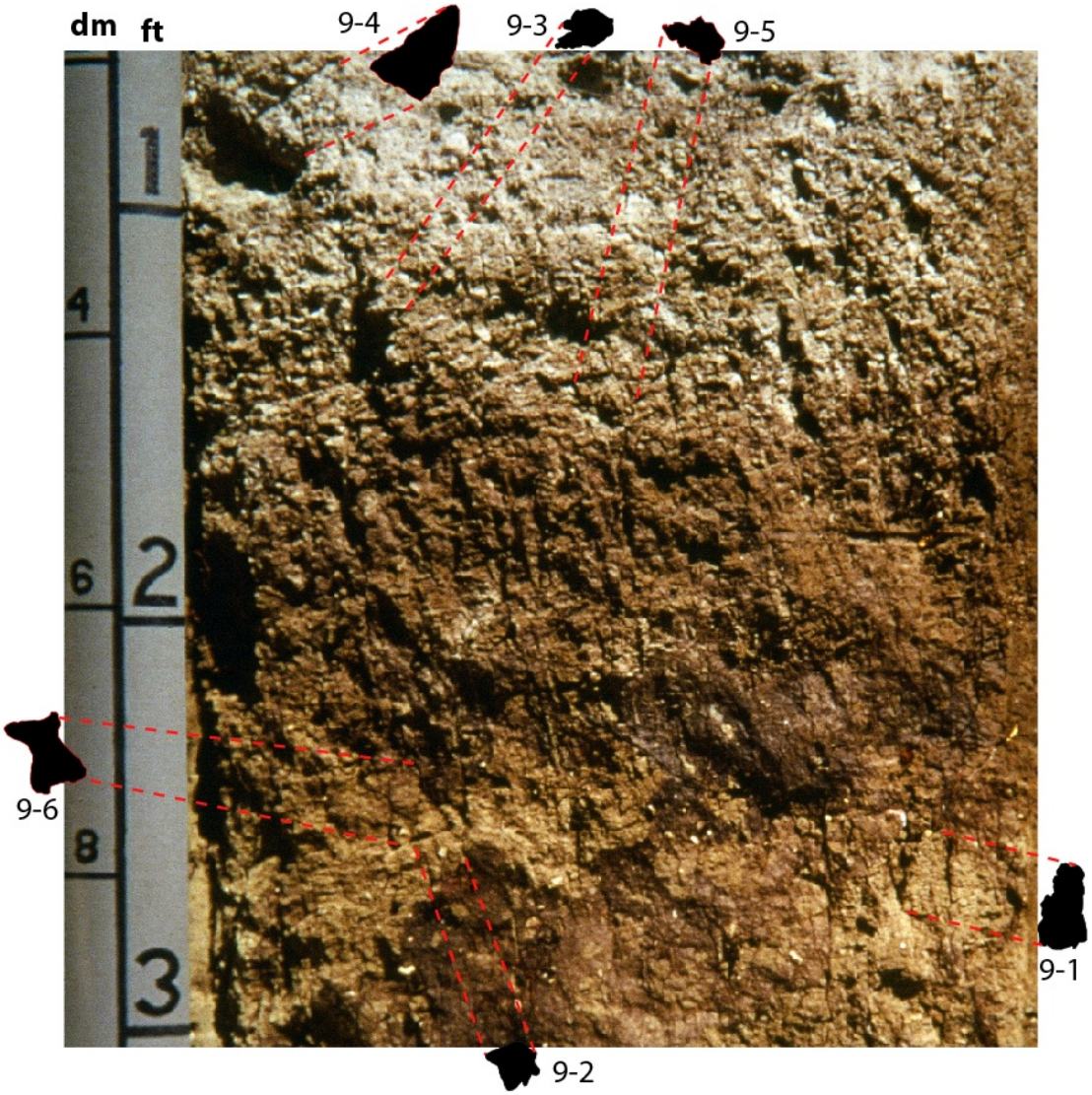

	platy	angular blocky	subangular blocky	granular	columnar	prism	wedge	N/A
9-1	○	○	○	○	○	○	○	○
9-2	○	○	○	○	○	○	○	○

	platy	angular blocky	subangular blocky	granular	columnar	prism	wedge	N/A
9-3	◯	◯	◯	◯	◯	◯	◯	◯
9-4	◯	◯	◯	◯	◯	◯	◯	◯
9-5	◯	◯	◯	◯	◯	◯	◯	◯
9-6	◯	◯	◯	◯	◯	◯	◯	◯

Quantifying ped shape from profile photographs

Copy of page: What is the type of structure for the image bellow

*** 52. Which of the following type categories BEST describes the peds represented in the photo above?**

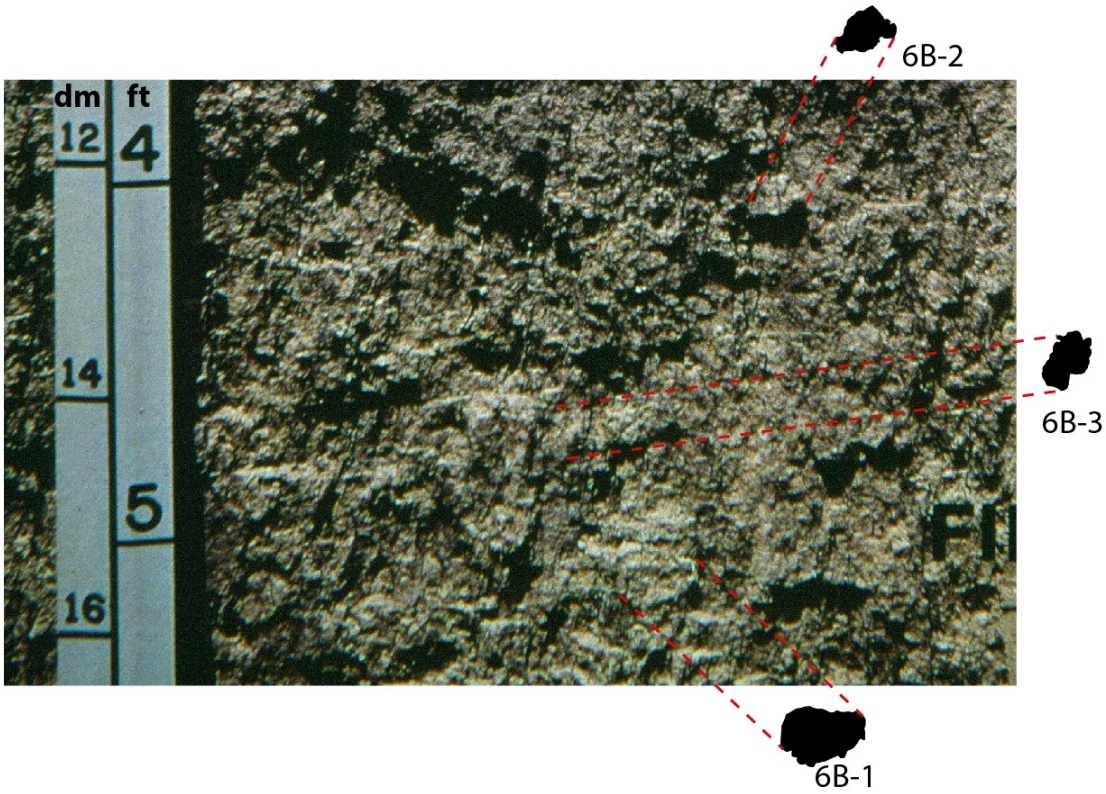

	platy	angular blocky	subangular blocky	granular	columnar	prism	wedge	N/A
6B-1	○	○	○	○	○	○	○	○
6B-2	○	○	○	○	○	○	○	○
6B-3	○	○	○	○	○	○	○	○

Quantifying ped shape from profile photographs

Copy of page: What is the type of structure for the image bellow

*** 53. Which of the following type categories BEST describes the peds represented in the photo above?**

	platy	angular blocky	subangular blocky	granular	columnar	prism	wedge	N/A
41-1	○	○	○	○	○	○	○	○
41-2	○	○	○	○	○	○	○	○
41-3	○	○	○	○	○	○	○	○
41-4	○	○	○	○	○	○	○	○
41-5	○	○	○	○	○	○	○	○

APPENDIX B. MULTINOMIAL LOGISTIC REGRESSION RESULTS FOR SOIL STRUCTURE WITHIN EACH KÖPPEN-GEIGER CLIMATE REGION AND ECOREGION PROVINCE FOR BOTH SURFACE AND SUBSURFACE HORIZONS

Table B1. Distribution of ped type class probabilities determined by multinomial logistic regression within each Köppen-Geiger (KG) climate regions for surface and subsurface horizons, separately. (Row probabilities within either the surface or subsurface columns sum to 1.) Zero probabilities represent values < 0.01.

	Surface†					Subsurface†						
KG	**Abk**	**Gr**	**Pl**	**Pr**	**Sbk**	**Abk**	**Col**	**Gr**	**Pl**	**Pr**	**Sbk**	**Weg**
Aw						0.00	0.00	0.00	0.00	0.00	1.00	0.00
BSh	0.00	0.09	0.64	0.00	0.27	0.08	0.15	0.00	0.00	0.08	0.69	0.00
BSk	0.01	0.43	0.24	0.00	0.32	0.10	0.00	0.09	0.03	0.13	0.64	0.00
BWh	0.09	0.00	0.45	0.00	0.45	0.17	0.00	0.00	0.00	0.00	0.83	0.00
BWk	0.00	0.00	0.75	0.06	0.19	0.28	0.00	0.00	0.00	0.28	0.44	0.00
Cfa	0.00	0.71	0.00	0.00	0.29	0.12	0.00	0.01	0.00	0.04	0.82	0.00
Cfb	0.00	1.00	0.00	0.00	0.00	0.00	0.00	0.00	0.00	0.00	1.00	0.00
Csa	0.00	0.50	0.00	0.00	0.50	0.00	0.00	0.00	0.00	0.00	1.00	0.00
Csb	0.04	0.30	0.00	0.00	0.67	0.29	0.00	0.04	0.00	0.00	0.67	0.00
Dfa	0.01	0.69	0.03	0.00	0.28	0.09	0.00	0.01	0.00	0.09	0.80	0.00
Dfb	0.03	0.76	0.07	0.00	0.14	0.13	0.01	0.02	0.01	0.05	0.77	0.00
Dfc	0.00	0.75	0.00	0.00	0.25	0.14	0.00	0.00	0.00	0.43	0.43	0.00
Dsa						0.25	0.00	0.00	0.00	0.00	0.75	0.00
Dsb	0.00	0.31	0.24	0.00	0.45	0.45	0.00	0.00	0.00	0.10	0.45	0.00
ET	0.00	1.00	0.00	0.00	0.00	0.00	0.00	0.00	0.00	0.00	1.00	0.00

† Abk, Angular Blocky; Col, Columnar; Gr, Granular; Platy, Pl; Pr, Prismatic; Sbk, Subangular Blocky; Weg, Wedge.

Table B2. Distribution of ped type class probabilities determined by multinomial logistic regression within each Köppen-Geiger (KG) climate regions for surface and subsurface horizons, separately. (Column probabilities sum to 1.) Zero probabilities represent values < 0.01.

	Surface†					Subsurface†						
KG	**Abk**	**Gr**	**Pl**	**Pr**	**Sbk**	**Abk**	**Col**	**Gr**	**Pl**	**Pr**	**Sbk**	**Weg**
Aw						0.00	0.00	0.00	0.00	0.00	0.00	0.00
BSh	0.00	0.00	0.12	0.00	0.02	0.00	0.33	0.00	0.00	0.01	0.00	0.00
BSk	0.17	0.09	0.32	0.00	0.13	0.06	0.00	0.41	0.42	0.12	0.05	0.00
BWh	0.17	0.00	0.08	0.00	0.03	0.00	0.00	0.00	0.00	0.00	0.00	0.00
BWk	0.00	0.00	0.20	1.00	0.02	0.02	0.00	0.00	0.00	0.03	0.00	0.00
Cfa	0.00	0.38	0.02	0.00	0.31	0.43	0.00	0.25	0.00	0.26	0.42	1.00
Cfb	0.00	0.01	0.00	0.00	0.00	0.00	0.00	0.00	0.00	0.00	0.01	0.00
Csa	0.00	0.01	0.00	0.00	0.03	0.00	0.00	0.00	0.00	0.00	0.02	0.00
Csb	0.17	0.02	0.00	0.00	0.09	0.05	0.00	0.06	0.00	0.00	0.02	0.00
Dfa	0.17	0.34	0.08	0.00	0.28	0.30	0.33	0.16	0.33	0.48	0.37	0.00
Dfb	0.33	0.11	0.07	0.00	0.04	0.10	0.33	0.13	0.25	0.07	0.08	0.00
Dfc	0.00	0.01	0.00	0.00	0.01	0.00	0.00	0.00	0.00	0.02	0.00	0.00
Dsa						0.00	0.00	0.00	0.00	0.00	0.00	0.00
Dsb	0.00	0.02	0.12	0.00	0.07	0.03	0.00	0.00	0.00	0.01	0.00	0.00
ET	0.00	0.01	0.00	0.00	0.00	0.00	0.00	0.00	0.00	0.00	0.00	0.00

† Abk, Angular Blocky; Col, Columnar; Gr, Granular; Platy, Pl; Pr, Prismatic; Sbk, Subangular Blocky; Weg, Wedge.

Table B3. Distribution of ped size class probabilities determined by multinomial logistic regression within each Köppen-Geiger (KG) climate regions for both surface and subsurface, separately. (Row probabilities within either the surface or subsurface columns sum to 1.) Horizons containing structures with intermediate size classes (e.g., fine to medium) or where multiple ped types, sizes, or grades were recorded were removed prior to data analysis. Zero probabilities represent values < 0.01.

	Surface†					Subsurface†					
KG	**VF**	**F**	**M**	**C**	**VC**	**VF**	**F**	**M**	**C**	**VC**	**EC**
Aw						0.50	0.00	0.50	0.00	0.00	0.00
BSh	0.00	0.13	0.50	0.37	0.00	0.00	0.00	0.50	0.42	0.08	0.00
BSk	0.18	0.41	0.34	0.07	0.00	0.09	0.19	0.52	0.16	0.03	0.00
BWh	0.00	0.00	0.73	0.27	0.00	0.00	0.00	0.67	0.33	0.00	0.00
BWk	0.08	0.31	0.23	0.31	0.08	0.14	0.00	0.50	0.36	0.00	0.00
Cfa	0.09	0.68	0.21	0.01	0.00	0.07	0.22	0.62	0.07	0.02	0.00
Cfb	0.00	0.33	0.00	0.00	0.67	0.00	0.00	0.62	0.38	0.00	0.00
Csa	0.00	0.57	0.43	0.00	0.00	0.00	0.19	0.78	0.00	0.04	0.00
Csb	0.08	0.38	0.54	0.00	0.00	0.00	0.17	0.73	0.10	0.00	0.00
Dfa	0.15	0.70	0.15	0.01	0.00	0.09	0.36	0.48	0.06	0.01	0.00
Dfb	0.13	0.48	0.35	0.04	0.00	0.03	0.22	0.59	0.14	0.00	0.01
Dfc	0.00	0.75	0.00	0.25	0.00	0.00	0.00	0.43	0.43	0.14	0.00
Dsa						0.00	0.00	1.00	0.00	0.00	0.00
Dsb	0.11	0.63	0.16	0.11	0.00	0.00	0.29	0.57	0.14	0.00	0.00
ET	0.00	1.00	0.00	0.00	0.00	0.00	0.00	1.00	0.00	0.00	0.00

†VF, Very Fine; F, Fine; M, Medium; C, Coarse; VC, Very Coarse; EC, Extremely Coarse.

Table B4. Distribution of ped size class probabilities determined by multinomial logistic regression with each Köppen-Geiger (KG) climate regions for both surface and subsurface horizons, separately. (Column probabilities sum to 1.) Horizons containing structures with intermediate size classes (e.g., fine to medium) or where multiple ped types, sizes, or grades were recorded were removed prior to data analysis. Zero probabilities represent values < 0.01.

	Surface†					Subsurface†					
KG	**VF**	**F**	**M**	**C**	**VC**	**VF**	**F**	**M**	**C**	**VC**	**EC**
Aw						0.01	0.00	0.00	0.00	0.00	0.00
BSh	0.00	0.00	0.03	0.12	0.00	0.00	0.00	0.01	0.03	0.04	0.00
BSk	0.19	0.09	0.17	0.21	0.00	0.08	0.05	0.06	0.11	0.14	0.00
BWh	0.00	0.00	0.06	0.13	0.00	0.00	0.00	0.00	0.01	0.00	0.00
BWk	0.01	0.01	0.02	0.17	0.33	0.01	0.00	0.01	0.03	0.00	0.00
Cfa	0.25	0.37	0.28	0.08	0.00	0.40	0.34	0.46	0.34	0.57	0.00
Cfb	0.00	0.00	0.00	0.00	0.67	0.00	0.00	0.01	0.03	0.00	0.00
Csa	0.00	0.01	0.02	0.00	0.00	0.00	0.01	0.02	0.00	0.04	0.00
Csb	0.03	0.03	0.10	0.00	0.00	0.00	0.01	0.03	0.02	0.00	0.00
Dfa	0.38	0.36	0.18	0.08	0.00	0.45	0.50	0.31	0.25	0.18	0.00
Dfb	0.10	0.07	0.13	0.08	0.00	0.04	0.08	0.09	0.15	0.00	1.00
Dfc	0.00	0.01	0.00	0.04	0.00	0.00	0.00	0.00	0.02	0.04	0.00
Dsa						0.00	0.00	0.00	0.00	0.00	0.00
Dsb	0.03	0.03	0.02	0.08	0.00	0.00	0.01	0.01	0.01	0.00	0.00
ET	0.00	0.00	0.00	0.00	0.00	0.00	0.00	0.00	0.00	0.00	0.00

†VF, Very Fine; F, Fine; M, Medium; C, Coarse; VC, Very Coarse; EC, Extremely Coarse.

Table B5. Distribution of ped grade class probabilities determined by multinomial logistic regression within each Köppen-Geiger (KG) climate regions for both surface and subsurface horizons, separately. (Row probabilities within either the surface or subsurface columns sum to 1.) Horizons containing structures with intermediate grade classes (e.g., weak to moderate) or where multiple ped types, sizes, or grades were recorded were removed prior to data analysis. Zero probabilities represent values < 0.01.

	Surface†			**Subsurface†**		
KG	**W**	**M**	**S**	**W**	**M**	**S**
Aw				0.00	1.00	0.00
BSh	0.55	0.36	0.09	0.31	0.46	0.23
BSk	0.53	0.44	0.03	0.51	0.40	0.09
BWh	0.73	0.27	0.00	0.67	0.17	0.17
BWk	0.50	0.31	0.19	0.44	0.39	0.17
Cfa	0.51	0.47	0.01	0.28	0.67	0.05
Cfb	1.00	0.00	0.00	0.33	0.67	0.00
Csa	0.40	0.40	0.20	0.16	0.81	0.03
Csb	0.26	0.63	0.11	0.37	0.52	0.10
Dfa	0.52	0.41	0.06	0.36	0.54	0.10
Dfb	0.57	0.33	0.10	0.35	0.57	0.08
Dfc	0.75	0.25	0.00	0.00	0.86	0.14
Dsa				0.00	0.75	0.25
Dsb	0.55	0.45	0.00	0.35	0.50	0.15
ET	0.50	0.50	0.00	0.33	0.67	0.00

† W, Weak; M, Moderate; S, Strong.

Table B6. Distribution of ped grade class probabilities determined by multinomial logistic regression within each Köppen-Geiger (KG) climate regions for both surface and subsurface horizons, separately. (Column probabilities sum to 1.) Horizons containing structures with intermediate grade classes (e.g., weak to moderate) or where multiple ped types, sizes, or grades were recorded were removed prior to data analysis. Zero probabilities represent values < 0.01.

	Surface†			Subsurface†		
KG	**W**	**M**	**S**	**W**	**M**	**S**
Aw				0.00	0.00	0.00
BSh	0.02	0.01	0.03	0.01	0.00	0.02
BSk	0.13	0.13	0.06	0.10	0.04	0.07
BWh	0.02	0.01	0.00	0.01	0.00	0.01
BWk	0.02	0.02	0.09	0.01	0.01	0.02
Cfa	0.32	0.35	0.09	0.35	0.46	0.27
Cfb	0.00	0.00	0.00	0.00	0.00	0.00
Csa	0.01	0.01	0.06	0.01	0.02	0.01
Csb	0.02	0.06	0.09	0.02	0.02	0.03
Dfa	0.29	0.28	0.38	0.40	0.34	0.47
Dfb	0.10	0.07	0.19	0.09	0.08	0.09
Dfc	0.01	0.00	0.00	0.00	0.00	0.01
Dsa				0.00	0.00	0.01
Dsb	0.05	0.05	0.00	0.01	0.01	0.02
ET	0.00	0.00	0.00	0.00	0.00	0.00

† W, Weak; M, Moderate; S, Strong.

Table B7. Distribution of ped type class probabilities determined by multinomial logistic regression within each ecoregion province for surface and subsurface horizons, separately. (Row probabilities within either the surface or subsurface columns sum to 1.) Ecoregion provinces not well represented by observations in the dataset ($N \leq 5$ horizons) were not considered in this analysis. Zero probabilities represent values < 0.01.

		Surface‡					Subsurface‡						
Ecoregion Province	**PC†**	**Abk**	**Gr**	**Pl**	**Pr**	**Sbk**	**Abk**	**Col**	**Gr**	**Pl**	**Pr**	**Sbk**	**Weg**
Laurentian Mixed Forest	212	0.08	0.83	0.00	0.00	0.08	0.24	0.00	0.00	0.08	0.12	0.56	0.00
Central Appalachian Broadleaf Forest – Coniferous Forest – Meadow	M221	0.00	0.90	0.00	0.00	0.10	0.10	0.00	0.02	0.02	0.02	0.85	0.00
Eastern Broadleaf Forest (Oceanic)	221	0.00	0.76	0.05	0.00	0.19	0.02	0.00	0.00	0.00	0.05	0.93	0.00
Eastern Broadleaf Forest (Continental)	222	0.00	0.80	0.01	0.00	0.18	0.12	0.00	0.01	0.00	0.06	0.81	0.00
Southeastern Mixed Forest	231	0.00	0.89	0.00	0.00	0.11	0.05	0.00	0.00	0.00	0.02	0.93	0.00
Outer Coastal Plain Mixed Forest	232						0.09	0.00	0.00	0.00	0.04	0.87	0.00
Lower Mississippi Riverine Forest	234	0.00	0.42	0.00	0.00	0.58	0.00	0.00	0.02	0.00	0.08	0.90	0.00
Pacific Lowland Mixed Forest	242	0.00	0.33	0.00	0.00	0.67	0.11	0.00	0.00	0.00	0.00	0.89	0.00
Prairie Parkland (Temperate)	251	0.00	0.58	0.01	0.00	0.41	0.05	0.00	0.01	0.00	0.10	0.84	0.00
Prairie Parkland (Subtropical)	255	0.00	0.33	0.00	0.00	0.67	0.60	0.00	0.00	0.00	0.00	0.38	0.01
Sierran Steppe – Mixed Forest – Coniferous Forest – Alpine Meadow	M261	0.00	0.33	0.13	0.00	0.54	0.17	0.00	0.00	0.00	0.02	0.81	0.00
California Coastal Chaparral Forest and Shrub	261	0.10	0.10	0.20	0.00	0.60	0.40	0.00	0.00	0.00	0.10	0.50	0.00
California Coastal Range Open Woodland – Shrub – Coniferous Forest – Meadow	M262	0.00	0.25	0.00	0.00	0.75	0.33	0.00	0.00	0.00	0.00	0.67	0.00
California Dry Steppe	262						0.00	0.00	0.00	0.00	0.18	0.82	0.00
California Coastal Steppe, Mixed Forest, and Redwood Forest	263	0.00	0.33	0.00	0.00	0.67	0.40	0.00	0.00	0.00	0.00	0.60	0.00
Colorado Plateau Semi-Desert	313	0.00	0.50	0.25	0.00	0.25	0.00	0.00	0.00	0.00	0.00	1.00	0.00
Southwest Plateau and Plains Dry Steppe and Shrub	315	0.00	0.21	0.04	0.00	0.75	0.10	0.03	0.01	0.00	0.15	0.71	0.00
American Semi-Desert and Desert	322	0.05	0.05	0.65	0.00	0.25	0.14	0.00	0.00	0.00	0.21	0.64	0.00
Southern Rocky Mountains Steppe – Open Woodland – Coniferous Forest – Alpine Meadow	M331	0.00	0.88	0.00	0.00	0.12	0.03	0.09	0.06	0.00	0.00	0.82	0.00
Great Plains-Palouse Dry Steppe	331	0.00	0.75	0.04	0.00	0.21	0.11	0.00	0.00	0.00	0.18	0.72	0.00
Middle Rocky Mountains Steppe – Coniferous Forest – Alpine Meadow	M332	0.00	0.43	0.29	0.00	0.29	0.56	0.00	0.00	0.00	0.11	0.33	0.00
Great Plains Steppe	332						0.06	0.06	0.00	0.00	0.19	0.69	0.00
Nevada-Utah Mountains Semi-Desert – Coniferous Forest – Alpine Meadow	M341	0.06	0.11	0.50	0.00	0.33	0.06	0.00	0.00	0.00	0.53	0.41	0.00
Intermountain Semi-Desert and Desert	341	0.00	0.12	0.46	0.04	0.37	0.09	0.00	0.00	0.05	0.18	0.68	0.00
Intermountain Semi-Desert	342	0.02	0.35	0.28	0.00	0.35	0.12	0.00	0.17	0.05	0.07	0.59	0.00

† PC, Province Code.

‡ Abk; Angular Blocky, Col; Columnar, Gr; Granular, Platy; Pl, Pr; Prismatic, Sbk; Subangular Blocky, Weg; Wedge.

Table B8. Distribution of ped type class probabilities determined by multinomial logistic regression within each ecoregion province for surface and subsurface horizons, separately. (Column probabilities sum to 1.) Ecoregion provinces not well represented by observations in the dataset ($N \leq 5$ horizons) were not considered in this analysis. Zero probabilities represent values < 0.01.

		Surface‡					Subsurface‡						
Ecoregion Province	**PC†**	**Abk**	**Gr**	**Pl**	**Pr**	**Sbk**	**Abk**	**Col**	**Gr**	**Pl**	**Pr**	**Sbk**	**Weg**
Laurentian Mixed Forest	212	0.17	0.03	0.00	0.00	0.01	0.02	0.00	0.00	0.17	0.02	0.01	0.00
Central Appalachian Broadleaf Forest – Coniferous Forest – Meadow	M221	0.00	0.07	0.00	0.00	0.02	0.04	0.00	0.06	0.17	0.01	0.06	0.00
Eastern Broadleaf Forest (Oceanic)	221	0.17	0.43	0.05	0.00	0.19	0.42	0.00	0.34	0.25	0.35	0.43	0.00
Eastern Broadleaf Forest (Continental)	222						0.01	0.00	0.00	0.00	0.01	0.01	0.00
Southeastern Mixed Forest	231	0.00	0.01	0.02	0.00	0.01	0.00	0.00	0.00	0.00	0.00	0.00	0.00
Outer Coastal Plain Mixed Forest	232	0.00	0.04	0.02	0.00	0.02	0.01	0.00	0.00	0.00	0.03	0.04	0.00
Lower Mississippi Riverine Forest	234	0.00	0.01	0.00	0.00	0.04	0.00	0.00	0.03	0.00	0.03	0.03	0.00
Pacific Lowland Mixed Forest	242	0.00	0.01	0.00	0.00	0.02	0.00	0.00	0.00	0.00	0.00	0.00	0.00
Prairie Parkland (Temperate)	251	0.00	0.15	0.02	0.00	0.21	0.06	0.00	0.06	0.00	0.20	0.14	0.00
Prairie Parkland (Subtropical)	255	0.00	0.00	0.00	0.00	0.01	0.19	0.00	0.00	0.00	0.00	0.02	1.00
Sierran Steppe – Mixed Forest – Coniferous Forest – Alpine Meadow	M261	0.00	0.02	0.05	0.00	0.07	0.03	0.00	0.00	0.00	0.01	0.02	0.00
California Coastal Chaparral Forest and Shrub	261	0.17	0.00	0.03	0.00	0.03	0.01	0.00	0.00	0.00	0.01	0.00	0.00
California Coastal Range Open Woodland – Shrub – Coniferous Forest – Meadow	M262	0.00	0.01	0.00	0.00	0.03	0.01	0.00	0.00	0.00	0.00	0.00	0.00
California Dry Steppe	262	0.00	0.05	0.02	0.00	0.03	0.00	0.00	0.00	0.00	0.02	0.01	0.00
California Coastal Steppe, Mixed Forest, and Redwood Forest	263	0.00	0.00	0.00	0.00	0.01	0.02	0.00	0.00	0.00	0.00	0.00	0.00
Colorado Plateau Semi-Desert	313	0.00	0.06	0.00	0.00	0.02	0.04	0.00	0.00	0.00	0.03	0.11	0.00
Southwest Plateau and Plains Dry Steppe and Shrub	315	0.00	0.02	0.02	0.00	0.11	0.03	0.33	0.03	0.00	0.06	0.03	0.00
American Semi-Desert and Desert	322	0.17	0.00	0.22	0.00	0.03	0.01	0.00	0.00	0.00	0.02	0.00	0.00
Southern Rocky Mountains Steppe – Open Woodland – Coniferous Forest – Alpine Meadow	M331	0.00	0.04	0.00	0.00	0.01	0.00	0.50	0.06	0.00	0.00	0.02	0.00
Great Plains-Palouse Dry Steppe	331						0.02	0.00	0.00	0.00	0.06	0.02	0.00
Middle Rocky Mountains Steppe – Coniferous Forest – Alpine Meadow	M332	0.00	0.01	0.03	0.00	0.01	0.02	0.00	0.00	0.00	0.01	0.00	0.00
Great Plains Steppe	332						0.00	0.17	0.00	0.00	0.02	0.01	0.00
Nevada-Utah Mountains Semi-Desert – Coniferous Forest – Alpine Meadow	M341	0.17	0.01	0.15	0.00	0.03	0.00	0.00	0.00	0.00	0.06	0.00	0.00
Intermountain Semi-Desert and Desert	341	0.00	0.01	0.18	1.00	0.05	0.01	0.00	0.00	0.08	0.03	0.01	0.00
Intermountain Semi-Desert	342	0.17	0.04	0.20	0.00	0.08	0.03	0.00	0.41	0.33	0.03	0.02	0.00

† PC, Province Code.

‡ Abk; Angular Blocky, Col; Columnar, Gr; Granular, Platy; Pl, Pr; Prismatic, Sbk; Subangular Blocky, Weg; Wedge.

Table B9. Distribution of ped size class probabilities determined by multinomial logistic regression within each ecoregion province for surface and subsurface horizons, separately. (Row probabilities within either the surface or subsurface columns sum to 1.) Horizons containing structures with intermediate size classes (e.g., fine to medium) or where multiple ped types, sizes, or grades were recorded were removed prior to data analysis. Ecoregion provinces not well represented by observations in the dataset ($N \leq 5$ horizons) were not considered in this analysis. Zero probabilities represent values < 0.01.

		Surface‡					Subsurface‡					
Ecoregion Province	**PC†**	**VF**	**F**	**M**	**C**	**VC**	**VF**	**F**	**M**	**C**	**VC**	**EC**
Laurentian Mixed Forest	212	0.00	0.82	0.18	0.00	0.00	0.00	0.18	0.73	0.09	0.00	0.00
Central Appalachian Broadleaf Forest – Coniferous Forest – Meadow	M221	0.23	0.62	0.08	0.00	0.08	0.00	0.16	0.71	0.11	0.01	0.00
Eastern Broadleaf Forest (Oceanic)	221	0.05	0.47	0.42	0.05	0.00	0.01	0.11	0.70	0.11	0.06	0.00
Eastern Broadleaf Forest (Continental)	222	0.12	0.76	0.11	0.01	0.00	0.14	0.36	0.43	0.06	0.01	0.00
Southeastern Mixed Forest	231	0.00	0.61	0.39	0.00	0.00	0.00	0.02	0.93	0.03	0.02	0.00
Outer Coastal Plain Mixed Forest	232						0.00	0.00	0.86	0.09	0.05	0.00
Lower Mississippi Riverine Forest	234	0.08	0.75	0.17	0.00	0.00	0.02	0.49	0.44	0.04	0.00	0.00
Pacific Lowland Mixed Forest	242	0.00	0.50	0.50	0.00	0.00	0.00	0.00	0.89	0.11	0.00	0.00
Prairie Parkland (Temperate)	251	0.18	0.65	0.17	0.00	0.00	0.06	0.45	0.42	0.07	0.00	0.00
Prairie Parkland (Subtropical)	255	0.00	0.33	0.67	0.00	0.00	0.00	0.03	0.81	0.15	0.00	0.00
Sierran Steppe – Mixed Forest – Coniferous Forest – Alpine Meadow	M261	0.00	0.42	0.58	0.00	0.00	0.00	0.21	0.70	0.09	0.00	0.00
California Coastal Chaparral Forest and Shrub	261	0.00	0.00	1.00	0.00	0.00	0.00	0.00	0.80	0.10	0.10	0.00
California Coastal Range Open Woodland – Shrub – Coniferous Forest – Meadow	M262	0.12	0.63	0.25	0.00	0.00	0.00	0.00	0.78	0.22	0.00	0.00
California Dry Steppe	262						0.00	0.00	0.57	0.29	0.14	0.00
California Coastal Steppe, Mixed Forest, and Redwood Forest	263	0.00	0.50	0.50	0.00	0.00	0.00	0.50	0.38	0.12	0.00	0.00
Colorado Plateau Semi-Desert	313	0.00	1.00	0.00	0.00	0.00	0.00	0.00	1.00	0.00	0.00	0.00
Southwest Plateau and Plains Dry Steppe and Shrub	315	0.11	0.41	0.41	0.07	0.00	0.03	0.09	0.61	0.22	0.05	0.00
American Semi-Desert and Desert	322	0.00	0.13	0.50	0.37	0.00	0.00	0.00	0.64	0.36	0.00	0.00
Southern Rocky Mountains Steppe – Open Woodland – Coniferous Forest – Alpine Meadow	M331	0.00	0.57	0.43	0.00	0.00	0.03	0.06	0.58	0.23	0.03	0.06
Great Plains-Palouse Dry Steppe	331	0.09	0.41	0.50	0.00	0.00	0.00	0.08	0.69	0.20	0.02	0.00
Middle Rocky Mountains Steppe – Coniferous Forest – Alpine Meadow	M332	0.00	0.86	0.14	0.00	0.00	0.00	0.83	0.00	0.17	0.00	0.00
Great Plains Steppe	332						0.00	0.20	0.67	0.00	0.13	0.00
Nevada-Utah Mountains Semi-Desert – Coniferous Forest – Alpine Meadow	M341	0.25	0.44	0.13	0.19	0.00	0.00	0.25	0.42	0.25	0.08	0.00
Intermountain Semi-Desert and Desert	341	0.09	0.27	0.32	0.32	0.00	0.13	0.33	0.47	0.07	0.00	0.00
Intermountain Semi-Desert	342	0.23	0.37	0.28	0.10	0.03	0.19	0.16	0.48	0.16	0.02	0.00

† PC, Province Code.

‡ VF; Very Fine, F; Fine, M; Medium, C; Coarse, VC; Very Coarse, EC; Extremely Coarse.

Table B10. Distribution of ped size class probabilities determined by multinomial logistic regression within each ecoregion province for surface and subsurface horizons, separately. (Column probabilities sum to 1.) Horizons containing structures with intermediate size classes (e.g., fine to medium) or where multiple ped types, sizes, or grades were recorded were removed prior to data analysis. Ecoregion provinces not well represented by observations in the dataset ($N \leq 5$ horizons) were not considered in this analysis. Zero probabilities represent values < 0.01.

		Surface‡					Subsurface‡					
Ecoregion Province	**PC†**	**VF**	**F**	**M**	**C**	**VC**	**VF**	**F**	**M**	**C**	**VC**	**EC**
Laurentian Mixed Forest	212	0.00	0.03	0.01	0.00	0.00	0.00	0.02	0.01	0.01	0.00	0.00
Central Appalachian Broadleaf Forest – Coniferous Forest – Meadow	M221	0.09	0.05	0.01	0.00	0.67	0.03	0.04	0.05	0.05	0.10	0.00
Eastern Broadleaf Forest (Oceanic)	221	0.32	0.41	0.15	0.04	0.00	0.62	0.49	0.28	0.23	0.16	0.00
Eastern Broadleaf Forest (Continental)	222						0.00	0.00	0.02	0.01	0.03	0.00
Southeastern Mixed Forest	231	0.00	0.01	0.00	0.00	0.00	0.00	0.00	0.00	0.00	0.00	0.00
Outer Coastal Plain Mixed Forest	232	0.01	0.03	0.06	0.04	0.00	0.01	0.02	0.05	0.05	0.13	0.00
Lower Mississippi Riverine Forest	234	0.01	0.03	0.01	0.00	0.00	0.01	0.04	0.02	0.01	0.00	0.00
Pacific Lowland Mixed Forest	242	0.00	0.01	0.02	0.00	0.00	0.00	0.00	0.01	0.01	0.00	0.00
Prairie Parkland (Temperate)	251	0.25	0.18	0.11	0.00	0.00	0.15	0.22	0.11	0.09	0.00	0.00
Prairie Parkland (Subtropical)	255	0.00	0.00	0.01	0.00	0.00	0.00	0.00	0.06	0.07	0.00	0.00
Sierran Steppe – Mixed Forest – Coniferous Forest – Alpine Meadow	M261	0.00	0.01	0.05	0.00	0.00	0.00	0.01	0.02	0.02	0.00	0.00
California Coastal Chaparral Forest and Shrub	261	0.00	0.00	0.07	0.00	0.00	0.00	0.00	0.01	0.01	0.03	0.00
California Coastal Range Open Woodland – Shrub – Coniferous Forest – Meadow	M262	0.01	0.01	0.01	0.00	0.00	0.00	0.01	0.01	0.01	0.00	0.00
California Dry Steppe	262	0.03	0.03	0.08	0.00	0.00	0.00	0.00	0.01	0.02	0.06	0.00
California Coastal Steppe, Mixed Forest, and Redwood Forest	263	0.00	0.00	0.01	0.00	0.00	0.00	0.01	0.00	0.01	0.00	0.00
Colorado Plateau Semi-Desert	313	0.00	0.05	0.08	0.00	0.00	0.00	0.03	0.17	0.03	0.16	0.00
Southwest Plateau and Plains Dry Steppe and Shrub	315	0.04	0.03	0.08	0.08	0.00	0.02	0.02	0.04	0.08	0.10	0.00
American Semi-Desert and Desert	322	0.00	0.01	0.06	0.25	0.00	0.00	0.00	0.01	0.06	0.00	0.00
Southern Rocky Mountains Steppe – Open Woodland – Coniferous Forest – Alpine Meadow	M331	0.00	0.02	0.04	0.00	0.00	0.00	0.01	0.02	0.04	0.03	1.00
Great Plains-Palouse Dry Steppe	331						0.01	0.02	0.04	0.05	0.03	0.00
Middle Rocky Mountains Steppe – Coniferous Forest – Alpine Meadow	M332	0.00	0.02	0.01	0.00	0.00	0.00	0.01	0.00	0.01	0.00	0.00
Great Plains Steppe	332						0.00	0.00	0.01	0.00	0.06	0.00
Nevada-Utah Mountains Semi-Desert – Coniferous Forest – Alpine Meadow	M341	0.06	0.02	0.01	0.13	0.00	0.02	0.01	0.01	0.03	0.03	0.00
Intermountain Semi-Desert and Desert	341	0.03	0.02	0.05	0.29	0.00	0.02	0.01	0.01	0.04	0.00	0.00
Intermountain Semi-Desert	342	0.13	0.04	0.08	0.17	0.33	0.10	0.03	0.03	0.07	0.06	0.00

† PC, Province Code.

‡ VF; Very Fine, F; Fine, M; Medium, C; Coarse, VC; Very Coarse, EC; Extremely Coarse.

Table B11. Distribution of ped grade class probabilities determined by multinomial logistic regression within each ecoregion province for surface and subsurface horizons, separately. (Row probabilities within either the surface or subsurface columns sum to 1.) Horizons containing structures with intermediate grade classes (e.g., weak to moderate) or where multiple ped types, sizes, or grades were recorded were removed prior to data analysis. Ecoregion provinces not well represented by observations in the dataset ($N \leq 5$ horizons) were also not considered in this analysis. Zero probabilities represent values < 0.01.

		Surface‡			Subsurface‡		
Ecoregion Province	**PC†**	**W**	**M**	**S**	**W**	**M**	**S**
Laurentian Mixed Forest	212	0.83	0.17	0.00	0.28	0.60	0.12
Central Appalachian Broadleaf Forest – Coniferous Forest – Meadow	M221	0.50	0.29	0.21	0.35	0.54	0.12
Eastern Broadleaf Forest (Oceanic)	221	0.62	0.38	0.00	0.23	0.67	0.10
Eastern Broadleaf Forest (Continental)	222	0.52	0.44	0.04	0.33	0.59	0.08
Southeastern Mixed Forest	231	0.96	0.04	0.00	0.25	0.70	0.05
Outer Coastal Plain Mixed Forest	232				0.39	0.52	0.09
Lower Mississippi Riverine Forest	234	0.33	0.67	0.00	0.36	0.63	0.02
Pacific Lowland Mixed Forest	242	0.33	0.67	0.00	0.00	0.89	0.11
Prairie Parkland (Temperate)	251	0.43	0.49	0.07	0.38	0.57	0.05
Prairie Parkland (Subtropical)	255	0.33	0.67	0.00	0.21	0.78	0.01
Sierran Steppe – Mixed Forest – Coniferous Forest – Alpine Meadow	M261	0.50	0.38	0.13	0.24	0.66	0.10
California Coastal Chaparral Forest and Shrub	261	0.30	0.60	0.10	0.20	0.70	0.10
California Coastal Range Open Woodland – Shrub – Coniferous Forest – Meadow	M262	0.50	0.50	0.00	0.44	0.33	0.22
California Dry Steppe	262				0.24	0.76	0.00
California Coastal Steppe, Mixed Forest, and Redwood Forest	263	0.00	0.67	0.33	0.80	0.20	0.00
Colorado Plateau Semi-Desert	313	1.00	0.00	0.00	0.00	1.00	0.00
Southwest Plateau and Plains Dry Steppe and Shrub	315	0.43	0.57	0.00	0.34	0.50	0.16
American Semi-Desert and Desert	322	0.70	0.25	0.05	0.57	0.14	0.29
Southern Rocky Mountains Steppe – Open Woodland – Coniferous Forest – Alpine Meadow	M331	0.25	0.69	0.06	0.32	0.50	0.18
Great Plains-Palouse Dry Steppe	331	0.46	0.46	0.08	0.32	0.56	0.12
Middle Rocky Mountains Steppe – Coniferous Forest – Alpine Meadow	M332	0.57	0.43	0.00	0.67	0.33	0.00
Great Plains Steppe	332				0.37	0.63	0.00
Nevada-Utah Mountains Semi-Desert – Coniferous Forest – Alpine Meadow	M341	0.72	0.28	0.00	0.35	0.41	0.24
Intermountain Semi-Desert and Desert	341	0.54	0.42	0.04	0.52	0.38	0.10
Intermountain Semi-Desert	342	0.44	0.53	0.02	0.49	0.41	0.09

† PC, Province Code.

‡ W, Weak; M, Moderate; S, Strong.

Table B12. Distribution of ped grade class probabilities determined by multinomial logistic regression within each ecoregion province for surface and subsurface horizons, separately. (Column probabilities sum to 1.) Horizons containing structures with intermediate grade classes (e.g., weak to moderate) or where multiple ped types, sizes, or grades were recorded were removed prior to data analysis. Ecoregion provinces not well represented by observations in the dataset ($N \leq 5$ horizons) were not considered in this analysis. Zero probabilities represent values < 0.01.

		Surface‡			Subsurface‡		
Ecoregion Province	**PC†**	**W**	**M**	**S**	**W**	**M**	**S**
Laurentian Mixed Forest	212	0.03	0.01	0.00	0.02	0.01	0.01
Central Appalachian Broadleaf Forest – Coniferous Forest – Meadow	M221	0.04	0.03	0.19	0.05	0.04	0.09
Eastern Broadleaf Forest (Oceanic)	221	0.32	0.33	0.25	0.39	0.40	0.40
Eastern Broadleaf Forest (Continental)	222				0.01	0.01	0.01
Southeastern Mixed Forest	231	0.01	0.00	0.00	0.00	0.00	0.00
Outer Coastal Plain Mixed Forest	232	0.04	0.03	0.00	0.03	0.04	0.04
Lower Mississippi Riverine Forest	234	0.01	0.03	0.00	0.02	0.03	0.00
Pacific Lowland Mixed Forest	242	0.01	0.01	0.00	0.00	0.01	0.00
Prairie Parkland (Temperate)	251	0.13	0.17	0.22	0.15	0.14	0.10
Prairie Parkland (Subtropical)	255	0.00	0.01	0.00	0.02	0.04	0.00
Sierran Steppe – Mixed Forest – Coniferous Forest – Alpine Meadow	M261	0.04	0.03	0.09	0.02	0.02	0.03
California Coastal Chaparral Forest and Shrub	261	0.01	0.02	0.03	0.00	0.01	0.01
California Coastal Range Open Woodland – Shrub – Coniferous Forest – Meadow	M262	0.01	0.01	0.00	0.01	0.00	0.01
California Dry Steppe	262				0.00	0.01	0.00
California Coastal Steppe, Mixed Forest, and Redwood Forest	263	0.00	0.01	0.03	0.01	0.00	0.00
Colorado Plateau Semi-Desert	313	0.08	0.00	0.00	0.07	0.10	0.05
Southwest Plateau and Plains Dry Steppe and Shrub	315	0.04	0.06	0.00	0.03	0.03	0.05
American Semi-Desert and Desert	322	0.04	0.02	0.03	0.02	0.00	0.02
Southern Rocky Mountains Steppe – Open Woodland – Coniferous Forest – Alpine Meadow	M331	0.01	0.04	0.03	0.01	0.02	0.03
Great Plains-Palouse Dry Steppe	331	0.03	0.04	0.06	0.03	0.03	0.04
Middle Rocky Mountains Steppe – Coniferous Forest – Alpine Meadow	M332	0.01	0.01	0.00	0.01	0.00	0.00
Great Plains Steppe	332				0.01	0.01	0.00
Nevada-Utah Mountains Semi-Desert – Coniferous Forest – Alpine Meadow	M341	0.04	0.02	0.00	0.02	0.01	0.02
Intermountain Semi-Desert and Desert	341	0.04	0.04	0.03	0.02	0.01	0.01
Intermountain Semi-Desert	342	0.06	0.08	0.03	0.05	0.03	0.04

† PC, Province Code.

‡ W, Weak; M, Moderate; S, Strong.

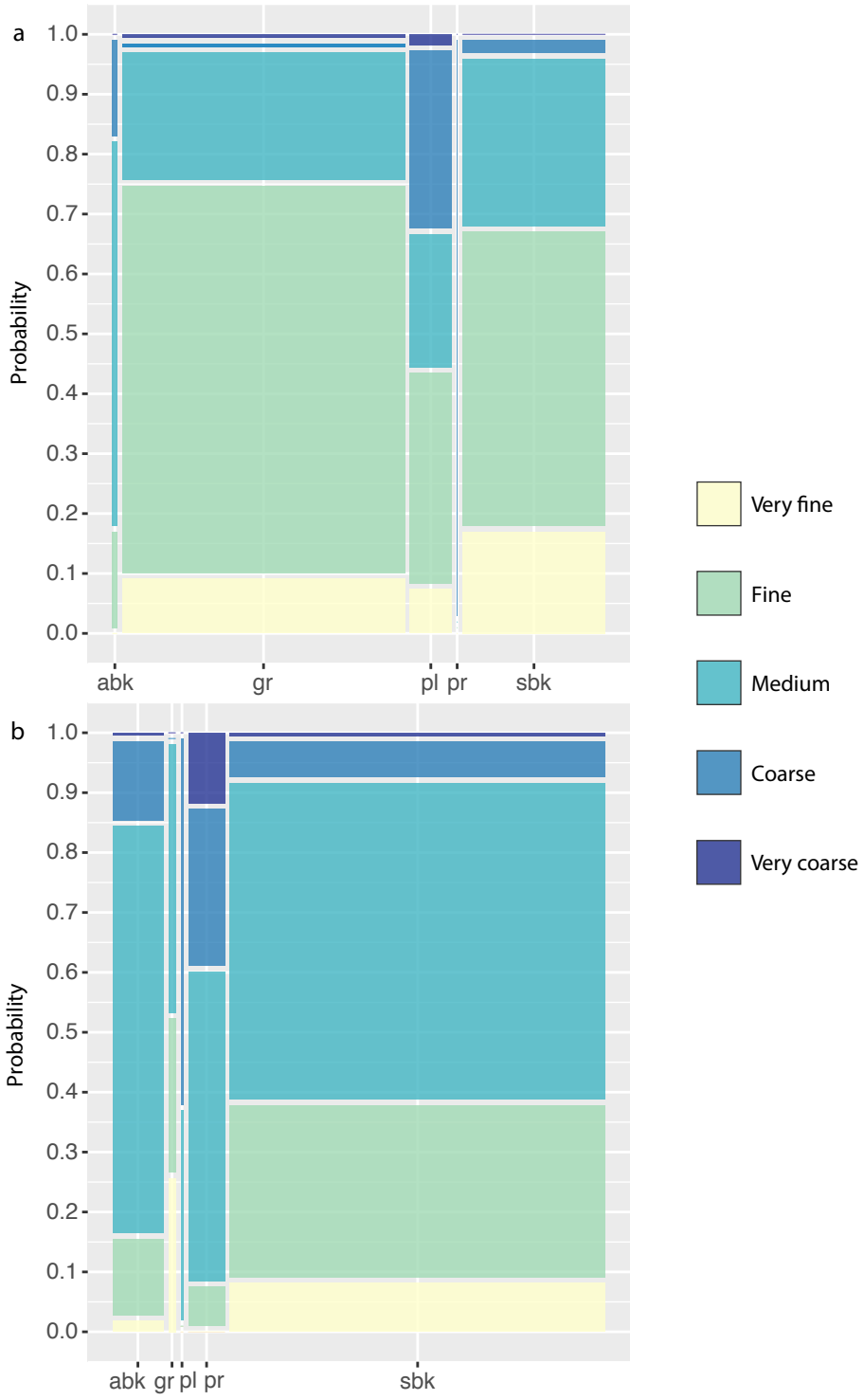

Fig. B1. Mosaic plots showing the multinomial logistic regression predicted probabilities of ped type (abk = angular blocky; gr = granular; pl = platy; pr = prismatic; sbk = subangular blocky) for both (a) surface and (b) subsurface horizons. Intermediate size classes (e.g., very fine to fine) were removed prior to analyzing the data with multinomial logistic regression. Width of the boxes corresponds to how many observations fall into the category.